CHALMERS
UNIVERSITY OF TECHNOLOGY

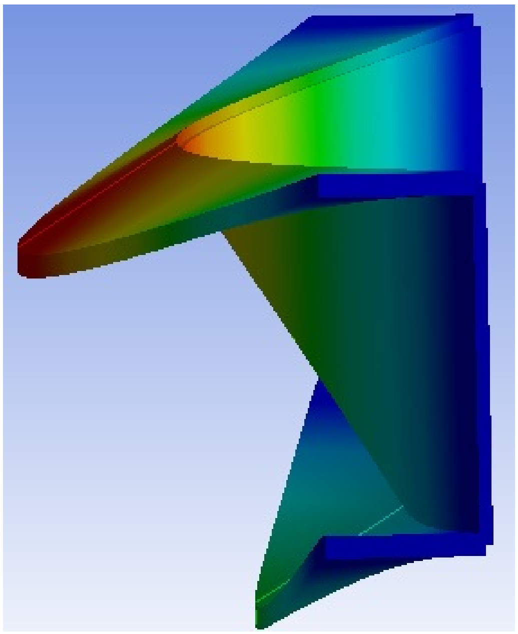

Lateral-torsional Buckling of Steel Channel Beams

A parametric study through FE-analysis

Master's Thesis in the Master's Programme Structural Engineering and Building Technology

CARL-MARCUS EKSTRÖM
DAVID WESLEY

Department of Civil and Environmental Engineering
Division of Structural Engineering
CHALMERS UNIVERSITY OF TECHNOLOGY
Gothenburg, Sweden 2017
Master's Thesis 2017:52

MASTER'S THESIS 2017:52

Lateral-torsional Buckling of Steel Channel Beams

A parametric study through FE-analysis

Master's Thesis in the Master's Programme Structural Engineering and Building Technology

CARL-MARCUS EKSTRÖM
DAVID WESLEY

Department of Civil and Environmental Engineering
Division of Structural Engineering
CHALMERS UNIVERSITY OF TECHNOLOGY

Gothenburg, Sweden 2017

Lateral-torsional Buckling of Steel Channel Beams
A parametric study through FE-analysis

Master's Thesis in the Master's Programme Structural Engineering and Building Technology

CARL-MARCUS EKSTRÖM
DAVID WESLEY

Examensarbete 2017:52/ Institutionen för bygg- och miljöteknik,

Chalmers tekniska högskola 2017

Department of Civil and Environmental Engineering
Division of Structural Engineering
Chalmers University of Technology
SE-412 96 Gothenburg
Sweden
Telephone: +46 (0)31-772 1000

Cover:
Screen shot from free software LTBeam

Chalmers Reproservice
Gothenburg, Sweden 2017

Lateral-torsional Buckling of Steel Channel Beams
A parametric study through FE-analysis

Master's Thesis in the Master's Programme Structural Engineering and Building Technology

CARL-MARCUS EKSTRÖM
DAVID WESLEY
Department of Civil and Environmental Engineering
Division of Structural Engineering
Chalmers University of Technology

ABSTRACT

When a vertical load acts on the web of a channel beam, a torsional moment which twists the cross-section is introduced, leading to an uncertain capacity with regards to lateral-torsional buckling. The general method in Eurocode 3 states that buckling curve d should be used in channel beam design, but the definition of the elastic critical bending moment in the so called "3-factor formula" is in fact only valid for cross-sections that are symmetric around the minor axis, which is not true for channel sections.

In this parametric study the load-carrying capacity of single span steel channel beams of various sizes, lengths and load configurations, with fork support boundary conditions has been made using Finite Element (FE) Modelling in ANSYS. The GMNIA-approach was utilized, which takes geometric imperfections and material non-linearity into account. An initial equivalent geometric imperfection was applied from the lateral-torsional buckling mode with the magnitude of the beam length divided by 150. For the end moment load case, the imperfection was additionally modelled as L/1000 and with residual stresses included in the beam cross-section. The stress and deformation patterns were studied as well.

The results from the FE-analyses show that when load eccentricity is introduced, the normal stresses from restrained warping limits the load-carrying capacity for beams with low slenderness. A size effect was noticed regarding the relationship between the size of the cross-section and the capacity as reducing the size resulted in increased capacity. Additionally, it was observed that the point of load application had a larger effect when load eccentricity was involved. Both of these observations can also be explained by the effect of warping stresses.

The channel beam design curve proposed by (Snijder et al., 2008) seems to be a good choice, taking torsional effects into account, although it does not claim to be correct for beams with a ratio $L/h < 15$. For these cases extra caution should be taken, perhaps limiting the reduction factor χ_{LT} to 0.5.

Stocky beams have a higher post-yielding strength than slender beams. Finally, the GMNIA-method with geometric imperfection of L/150 leads to a clearly lower capacity than the L/1000 method including residual stresses.

Keywords: Lateral-torsional buckling, Eurocode 3, buckling curves, channel section, Finite Element Method, GMNIA, elastic critical bending moment

Vippning av u-balkar i stål
En parametrisk studie genom FE-analys

Examensarbete inom Masterprogrammet Structural Engineering and Building Technology

CARL-MARCUS EKSTRÖM
DAVID WESLEY
Institutionen för bygg- och miljöteknik
Avdelningen för konstruktionsteknik
Chalmers tekniska högskola

SAMMANFATTNING

När en u-balk belastas vertikalt i sitt liv uppstår samtidigt ett vridmoment, som leder till en osäkerhet gällande bärkapaciteten med hänsyn till vippning. Enligt metoden med generella vippnigskurvor i Eurokod 3 ska kurva d användas för u-balkar, men definitionen av elastisk kritisk vippning i den s.k. "3-faktorsformeln" är endast giltig för tvärsektioner som är symmetriska runt sin svaga axel, vilket ej är sant för u-balkar.

I denna parametriska studie har bärförmågan för gaffellagrade enfacksstålbalkar av u-tvärsnitt analyserats, med varierande storlek, längd och lastfall, genom finita elementmetoden i programvaran ANSYS. GMNIA-tekniken, som beaktar geometriska imperfektioner och icke-linjäritet i materialegenskaper, användes. En initial ekvivalent geometrisk imperfektion applicerades i form av vippningsmoden med en maximal deformation av balkens längd delat med 150. För lastfallet med pålagda ändmoment modellerades balkarna även med en maximal deformation av L/1000, samtidigt som egenspänningar infördes. Förutom bärförmåga studerades även spännings- och deformationsmönster.

Resultaten från FE-analyserna visar att normalspänningar från förhindrad välvning begränsar bärförmågan för oslanka balkar då lasteccentricitet föreligger. En storlekseffekt noterades gällande tvärsektionens storlek och bärfömågan på så vis att mindre tvärsektion ledde till en ökad bärförmåga. Vidare observerades att lastappliceringspunkten hade större effekt då lasteccentricitet förelåg. Alla dessa observationer kan förklaras av normalspänningar från välvning.

Designkurvan för u-balkar föreslagen av (Snijder m. fl., 2008) verkar vara ett bra val som beaktar vridningseffekten, även om den ej är giltig för balkar då L/h < 15. För dessa fall bör extra försiktighet vidtas, och reduktionsfaktorn χ_{LT} eventuellt sänkas till 0.5.

Balkar med låg slankhet har en större förmåga att bära ytterligare last efter att stålet har flutit vid någon punkt i balken. Slutligen leder GMNIA-metoden med en geometrisk imperfektion av L/150 till en avsevärt lägre bärförmåga än då L/1000 samt egenspänningar appliceras.

Nyckelord: Vippning, Eurokod 3, vippningskurvor, u-tvärsnitt, finit elementmetod, GMNIA, elastiskt kritiskt böjmoment

CONTENTS

PREFACE

This Master's thesis project was carried out in 2015 at engineering company Reinertsen Sweden AB in cooperation with the Department of Civil and Environmental Engineering, Steel and Timber structures, Chalmers University of Technology. Examiner of the thesis was associate professor Mohammad Al-Emrani at the Department of Structural Engineering.

The supervisors for the project were Martin Gustafsson from Reinertsen and Professor emeritus Bo Edlund at Chalmers. We would like to thank them all for support and help along the way. We are also thankful to Reinertsen for providing the interesting idea for a master thesis project and the tools to carry it out.

Finally, we would like to thank our opponents Jesús Armesto Barros and Andrés Serena Gómez for valuable thoughts concerning the master thesis project.

Gothenburg, December 2016 Carl-Marcus Ekström and David Wesley

NOMENCLATURE

Greek letters

α	[ ]	Imperfection factor for flexural buckling
$\alpha_{cr,op}$	[ ]	Load increase factor according to the general method in Eurocode 3, with regards to buckling
α_{LT}	[ ]	Imperfection factor for lateral-torsional buckling
$\alpha_{ult,k}$	[ ]	Load increase factor according to the general method in Eurocode 3, disregarding buckling
$\alpha_{1/2/3/4/5}$	[ ]	Factor for end warping and lateral restraint conditions
γ_{M1}	[ ]	Partial factor steel, resistance of members to instability
ε	[ ]	Strain
η	[ ]	Generalized initial imperfection for column buckling
η_{LT}	[ ]	Generalized initial imperfection for lateral-torsional buckling
κ_M	[ ]	Reduction factor with regards to lateral-torsional buckling, κ_M design method
λ	[ ]	Load multiplication factor for linear buckling analysis
$\bar{\lambda}$	[ ]	Non-dimensionless slenderness, column buckling
$\bar{\lambda}_{LT}$	[ ]	Non-dimensionless slenderness, lateral-torsional buckling
$\bar{\lambda}_{MT}$	[ ]	Non-dimensionless slenderness with torsional effect included, lateral-torsional buckling
$\bar{\lambda}_{op}$	[ ]	Non-dimensionless slenderness according to the general method in Eurocode 3
$\bar{\lambda}_T$	[ ]	Additional contribution to slenderness from torsional effect on channel beam
μ	[ ]	Factor influencing the C_1-factor
ν	[ ]	Poisson's ratio
σ_{VM}	[N/m^2]	Yield stress criterion according to Von-Mises
$\sigma_{x,\omega}$	[N/m^2]	Normal stresses from restrained warping
$\sigma_{x,My}$	[N/m^2]	Normal stress from major axis bending
τ	[N/m^2]	Shear stress
$\varphi_{x,y,z}$	[rad]	Angle of twist around x-, y- and z-axes
φ_0	[rad]	Maximum initial imperfection angle of twist, lateral-torsional buckling
χ	[ ]	Reduction factor with regards to column buckling
χ_{LT}	[ ]	Reduction factor with regards to lateral-torsional buckling
$\chi_{LT,mod}$	[ ]	Additional reduction factor with regards to lateral-torsional buckling, taking moment distribution into account
χ_{op}	[ ]	Reduction factor according to the general method in Eurocode 3

Ψ	[ ]	Fraction between applied end moments at the two ends of a beam
ψ	[ ]	Eigenvector for linear buckling analysis

Roman letters

A	[m^2]	Cross-section area
A_1,A_2	[ ]	Factors for the shape of the moment diagram
C	[Nm^2]	Torsional stiffness, same as GI_t
C_w	[Nm^4]	Warping stiffness, same as EI_w
C_1	[ ]	Moment diagram factor in the 3-factor formula
C_2	[ ]	Point of load application factor in 3-factor formula
C_3	[ ]	Degree of monosymmetry factor in the 3-factor-formula
E	[N/m^2]	Young's modulus
E_T	[N/m^2]	Tangent modulus
F	[N]	Force
G	[N/m^2]	Shear modulus
H	[J]	Total potential energy
H_i	[J]	Potential energy from external loads
H_y	[J]	Internal and elastically stored potential energy
$H_{deflected}$	[J]	Potential energy for a beam just after buckling
$H_{straight}$	[J]	Potential energy for a beam just before buckling
I	[m^4]	Moment of inertia
I_t	[m^4]	Torsional cross-section constant
I_w	[m^6]	Warping cross-section constant
I_x	[m^4]	Moment of inertia around x-axis
I_y	[m^4]	Moment of inertia around y-axis
I_z	[m^4]	Moment of inertia around z-axis
K	[ ]	Stiffness matrix
K^T	[ ]	Stiffness matrix in the Newton-Raphson integration method
K_v	[m^4]	See I_t
K_w	[m^6]	See I_w
L	[m]	Length of structural element
L_{cr}	[m]	Effective critical buckling length of structural element
$M_{b,Rd}$	[Nm]	Bending moment design resistance
M_{cr}	[Nm]	Elastic critical bending moment
$M_{cr,FEM}$	[Nm]	Elastic critical bending moment from FE-analysis
$M_{cr,0}$	[Nm]	Elastic critical bending moment for referance load case
$M_{cr,3ff}$	[Nm]	Elastic critical bending moment according to the 3-factor formula
M_{max}	[Nm]	Maximum bending moment along a beam

M_{pl}	[Nm]	Plastic moment resistance
$M_{x,tot}$	[Nm]	Torsional moment from Saint-Venant and restrained warping combined
$M_{x,SV}$	[Nm]	Saint-Venant torsional moment
$M_{x,\omega}$	[Nm]	Torsional moment from restrained warping
M_x	[Nm]	Torsional moment around x-axis
$M_{y,gl}$	[Nm]	Bending moment around global y-axis
$M_{y,Rd}$	[Nm]	Strong axis bending moment design resistance
$M_{y,z}$	[Nm]	Bending moment around y- and z-axes
M_ω	[Nm]	The so called bi-moment, related to warping
N	[N]	Axial compression force
$N_{b,Rd}$	[Nm]	Column design resistance for axial load with regards to flexural buckling
N_{cr}	[N]	Critical column buckling force
N_{Ed}	[N]	Applied axial load in column
N_{Rd}	[N]	Column axial load design resistance
N_y	[N]	Axial compression force resulting in yielding
P_{base}	[N]	Initial applied load in a linear buckling analysis
$P_{cr,FEM}$	[N]	Critical load according to FEM linear buckling analysis
S	[ ]	Stress stiffness matrix
W_{el}	[m^3]	Elastic section modulus
W_{pl}	[m^3]	Plastic section modulus
b	[m]	Flange width
b_s	[m]	Equivalent flange width for simplified channel cross-section
e_0	[m]	Max initial geometric bow imperfection
$e_{0,d}$	[m]	Max initial equivalent geometric bow imperfection
e_{SC}	[m]	Lateral distance between shear center and centre line of web
f_y	[$N/^2$]	Yield stress of steel
h	[m]	Total cross-section height
h_w	[m]	Height of web
h_s	[m]	Height between centre of of flanges
k_c	[ ]	Factor that depends on the shape of the moment diagram
k_w	[ ]	End rotational effective length factor
k_z	[ ]	End warping effective length factor
t_f	[m]	Flange thickness
t_w	[m]	Web thickness
u_x	[m]	Translation in x-direction
u_y	[m]	Translation in y-direction
u_z	[m]	Translation in z-direction
v	[m]	Lateral deflection of beam or column

v_0	[m]	Lateral deflection due to initial out-of-straightness
v_{max}	[m]	Lateral deflection due to initial imperfection and second order effects combined
x	[m]	Beam length direction
y	[m]	Lateral direction of beam
y_G	[m]	Lateral direction between the centre of gravity and the centreline of the web
z	[m]	Vertical direction of beam
z_a	[m]	Vertical coordinate for the point of load application
z_g	[m]	Vertical distance between point of load application and the shear centre
z_s	[m]	Vertical coordinate for the shear centre

1 Introduction

1.1 Background

As steel structures tend to be slender, a limiting factor in design is often the risk of various types of instability phenomena, known as buckling. Lateral-torsional buckling of steel beams is treated in the European standard EN-1993-1-1:2005 (hereafter Eurocode 3) in the following way: the theoretical elastic critical bending moment M_{cr} is needed to decide the normalized relative slenderness $\bar{\lambda}_{LT}$, which in combination with an imperfection factor α_{LT} gives the design bending moment reduction factor with regard to lateral-torsional buckling χ_{LT}.

Earlier versions of Eurocode 3 had a suggestion on how to calculate M_{cr}, which was removed in later versions. The approach was known as “the 3-factor formula” and produced reliable results for symmetric cross-sections such as I-beams. This is, however, not the case for channel sections, where the shear centre does not coincide with the vertical axis of the centre of gravity. The applied load will inevitably cause a torsional moment in the beam, which makes it difficult to predict M_{cr}.

For advanced loading cases, a modern approach is to utilize Finite Element Method (FEM) computer software in design. A disadvantage of this technique is that it can be very time consuming and hence not always economical. The designer may also lose some control over the calculation process which can make it more difficult to validate the results.

It has been noticed in an earlier Master’s thesis project at Reinertsen (Hauksson and Vilhjálmsson, 2014) that when dealing with non-symmetric channel sections some of the current engineering software differs significantly. At present, no simple way of checking the validity with hand calculations exists. The uncertainty might be handled by avoiding channel sections in longer spans, using lateral bracings or over-dimensioning the beam cross-section size to be on the safe side.

Scholars, such as (N. Trahair, 1998) has highlighted the need for additional research on other cross-sections than the already well known I-beams. Suggestions have already been made on how to improve the hand calculation procedure in Eurocode 3 for channel sections by (Snijder et al., 2008).

1.2 Aim and objectives

The overall purpose of this Master's thesis project was to gain further insight into the behaviour of lateral-torsional buckling of steel channel beams regarding the effects of slenderness, point of load application and cross-section size on deformations, stress patterns and load-carrying capacity.

1.3 Limitations

To avoid the risk of local buckling, only cross-sections in class 1 were considered. Standard UPE-sections 100, 160 and 220 were chosen, which implies that only beams with equal top and bottom flange size were studied. Laterally braced beams were not studied, nor continous beams or frames of structural members. The beams were not exposed to axial load.

The loading cases considered were end moment loading, point load in the middle of the span and linearly distributed load at top, middle and bottom web. The intermediate buckling region was of primary interest and therefore the study was limited to beams with slenderness values ($\bar{\lambda}_{LT}$) approximately between 0.6 and 1.7.

1.4 Method

Initially, a literature study on the theory behind various instability phenomena for steel beams was made, including how Eurocode 3 treats lateral-torsional buckling. The 3-factor formula that establishes the elastic critical moment M_{cr} was also studied. The present methods on how to deal with different loading conditions, end restraints and cross-section shapes when it comes to lateral-torsional buckling were assessed.

A parametric study was conducted where channel beams with different dimensions, lengths and load conditions were modelled and analysed in computer software ANSYS. The parametric study was performed in FE-software ANSYS with three chosen cross-sections: UPE100, UPE160 and UPE220. Load was applied through end moments, a point load in the beam mid section and finally distributed load in the top, the middle and the bottom of the web respectively.

The analyses were first made by performing a linear elastic buckling analysis. Then, the elastic critical buckling shape was used as an initial geometric imperfection for the collapse analysis, with a maximum lateral deflection of the beam length divided with 150. For the end moment load case an additional method was also used, where residual stresses were modelled in the beams and the maximum imperfection was L/1000. Eurocode 3 prescribes these two options for applying imperfections.

The end moment loading was used as a reference case to verify the validity of the model, as in this load case load eccentricity is avoided. The buckling curves plotted from the results of the analyses were therefore expected to resemble the general lateral-torsional buckling curves in Eurocode 3.

Thereafter point load and linearly distributed load were applied in collapse analyses, and the maximum load carrying capacity was plotted in buckling curve diagrams against beam slenderness $\bar{\lambda}_{LT}$.

To be able to analyse stress patterns the equivalent von Mises stress was extracted from three points in the mid-section of the beam for each load step, explained further in Section 7.1.2. The maximum deformation was also recorded.

Finally the results were compared to the study made by (Snijder et al., 2008).

2 Definitions

2.1 Coordinate system

The Cartesian coordinate system is used where the x-direction represents the length direction of the beam. When viewing the beam from the left, the z-axis is pointing down and the y-axis is pointing to the right, demonstrated in Figure 2.1. Due to the orientation of the cross-section, major axis bending will be about the y-axis and minor axis bending will be about the z-axis. When the channel beam is loaded with a vertical force or end moments (about the y-axis) then the strong axis will be the y-axis – major axis bending. The weak axis is referred to as the z-axis – minor axis bending.

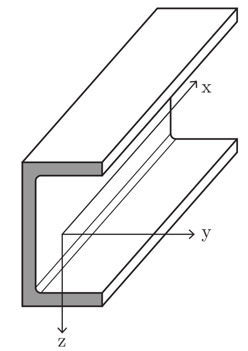

Figure 2.1: *Directions for the coordinate system*

2.2 Cross-section notation

The lengths and measurements of the cross-section are labelled according to the standard in Eurocode 3, see Figure 2.2.

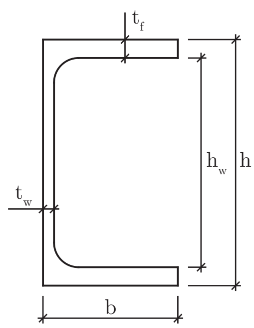

Figure 2.2: *Notation of the cross-section, following Eurocode 3 standard*

h = Total height of cross-section

h_w = Free height of the web between flanges

b = Width of flanges

t_w = Thickness of web

t_f = Thickness of flanges

2.2.1 Simplified cross-section in FE-model

Since most of the equations in this thesis are applied on a simplified channel cross-section that is the result of using shell elements in the FE-analysis, some additional notations are needed, shown in Figure 2.3.

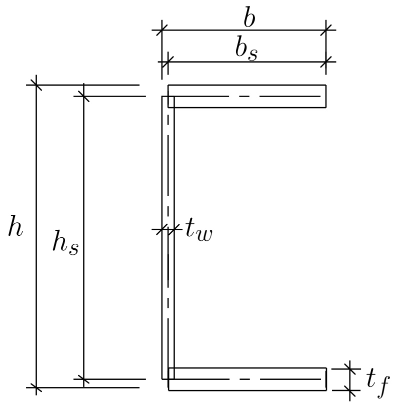

Figure 2.3: *Notations for simplified cross-section*

Additional cross-section labels are:

h_s = Finite element model web height

b_s = Finite element model flange width height

2.3 Centre of gravity, GC

The centre of gravity in a body of homogeneous material coincides with the geometric centre, known as the centroid (Lundh, 2000). The centre of gravity can figured as the point where the weight of an object is concentrated, as showed in Figure 2.4. The twisting moment caused by gravitation from the body is zero around this point.

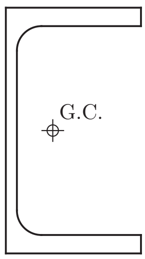

Figure 2.4: *The centre of gravity*

For a simplified channel section, the distance y_G from the web center line to the gravity centre is:

$$y_G = \frac{1}{A}\left(2t_f b_s \frac{b_s}{2}\right) \tag{2.1}$$

A is the cross-section area, $A = 2b_s t_f + h_s t_w$.

2.4 Shear centre, SC

If a structural element is transversally loaded in its shear centre, no twist occurs of the cross-section. If a torque is applied in the same point, no translation of the shear center takes place (Yoo and Lee, 2011).

This demonstrates that the sum of the shear stresses of one side of the point is equal to the shear stresses on the other side:

$$\sum \tau_{RightOfSC} = \sum \tau_{LeftOfSC}$$
$$\sum \tau_{TopOfSC} = \sum \tau_{BottomOfSC}$$

For a double symmetric cross-section the shear centre coincides with the gravity centre. For a single symmetric cross-section the shear centre will be located along the symmetry line, but not in the gravity centre.

In Figure 2.5, the cross-section for the I-beam is double symmetric which means that the shear centre will coincide with the gravity centre.

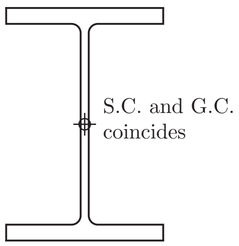

Figure 2.5: *Shear centre and gravity centre coincides in a double symmetric I-beam*

The channel beam, however, is symmetric about the y-axis but not about the z-axis which implies that the shear centre will coincide with the gravity centre in the z-direction but not in the y-direction. If such a beam is transversally loaded in the shear centre the beam would then bend in pure flexion and no twist is induced, see Figure 2.6.

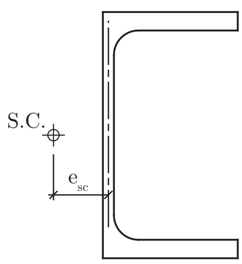

Figure 2.6: *Shear centre located outside of channel beam geometry*

The horizontal distance between the shear centre and the web centre line is calculated through the equation:

$$e_{SC} = \frac{b_s^2 h_s^2 t_f}{4I_y} \tag{2.2}$$

2.5 Degrees of freedom

2.5.1 Translation in x, y and z

The beam is able to move in the three principle axes x,y and z. The translation is depicted in Figures 2.7, 2.8 and 2.9.

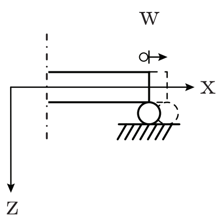

Figure 2.7: *Translation in the x-direction*

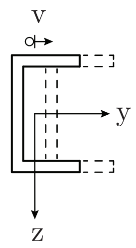

Figure 2.8: *Translation in the y-direction*

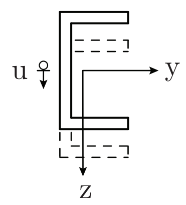

Figure 2.9: *Translation in the z-direction*

2.5.2 Rotation about x, y and z

The centre of rotation is defined in the gravity centre so that no additional translation is introduced. Major axis bending is rotation about the y-axis and minor axis bending is rotation about the z-axis. These rotations as well as rotation about the x-axis (torsion) are shown in Figures 2.10, 2.11 and 2.12.

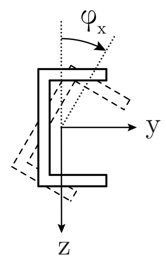

Figure 2.10: *Rotation about the x-axis (twisting of cross-section)*

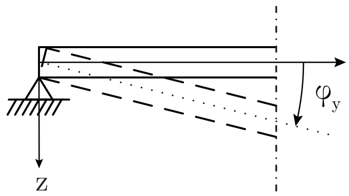

Figure 2.11: *Rotation about the y-axis, from major axis bending*

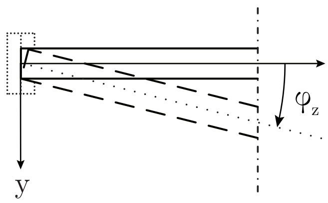

Figure 2.12: *Rotation about the z-axis, from minor axis bending*

2.6 Bending

Major axis bending of a beam can described by the simple formula:

$$M_y = -EIy\frac{\mathrm{d}^2u}{\mathrm{d}x^2} \tag{2.3}$$

The second moment of inertia I is defined as

$$I = \int\int z^2 dydz \tag{2.4}$$

For a channel beam with simplified cross-section, I_y is then defined as

$$I_y = \frac{2b_st_f^3 + t_wh_s^3}{12} + 2b_st_f\left(\frac{h_s}{2}\right)^2 \tag{2.5}$$

Minor axis bending is expressed as

$$M_z = -EI_z\frac{\mathrm{d}^2v}{\mathrm{d}x^2} \tag{2.6}$$

I_z is defined as

$$I_z = \frac{2t_fb_s^3 + h_st_w^3}{12} + 2b_st_f\left(\frac{b_s}{2} - y_G\right)^2 + h_st_wy_G^2 \tag{2.7}$$

2.7 Torsion

2.7.1 Pure torsion

When applying end torques to a prismatic beam with circular cross-section, as in Figure 2.13, the behaviour is described by uniform torsion (Höglund, 2006).

The correlation between torsional moment and the angle of twist can be described by Saint-Venant's torsion:

$$M_{x,SV} = GI_t \frac{\mathrm{d}\phi}{\mathrm{d}x} \tag{2.8}$$

where GI_t is the torsional stiffness

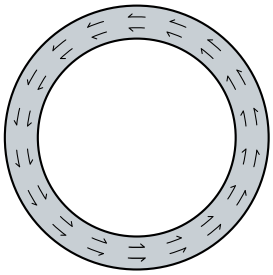

Figure 2.13: *Pure Saint-Venant torsion of a circular cross-section*

This equation implies that throughout the length of the beam the cross-section is rotated but remains plane and undistorted. The torsional moment of inertia I_t is defined as

$$I = \int_A r^2 dA \tag{2.9}$$

For rectangular thin elements within a cross-section I_t is simplified as $\frac{width \cdot height^3}{3}$. For a channel beam with simplified cross-section, I_t is therefore:

$$I_t = \frac{2b_s tf^3 + h_s tw^3}{3} \tag{2.10}$$

2.7.2 Warping

If a non-circular prismatic beam is exposed to torsional moment, however, the behaviour will differ. The beam will rotate about the x-axis but now also distort so that the cross-section no longer remains plane. For an I-beam or channel beam, this leads to the flanges distorting in opposite directions as can be seen in Figure 2.14.

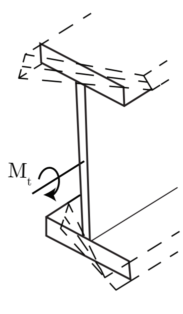

Figure 2.14: *Warping of flanges*

The warping restraint torsion is described by the following equation:

$$M_{x,w} = -EI_w \frac{\mathrm{d}^3\varphi}{\mathrm{d}x^3} \tag{2.11}$$

The warping constant I_w for a channel beam can be expressed by the following formula according to (Hoogenboom, 2003):

$$I_w = \frac{t_f b s^3 h s^2}{12} \cdot \frac{3b_s t f + 2h_s t w}{6b_s t f + h_s t w} \tag{2.12}$$

Bi-moment

The so called bi-moment is also known as warping moment and represents the distribution of longitudinal normal stresses resulting from restrained warping. For a double symmetric cross-section such as an I-beam, the bi-moment can be represented by a pair of equal and opposite bending moments in the flanges. For a channel beam the web also contributes. The bending moments in each cross-section subpart are multiplied with the distance to either of the "plastic neutral lines", extending from the gravity center. Thereby the bi-moment has the unity Nm^2. The resulting stress is given by

$$\sigma_{x,\omega} = \frac{M_\omega}{I_w}\omega \tag{2.13}$$

where ω is the sectorial coordinate, representing different locations on the cross-section. M_w is the applied bi-moment. Appendix C shows an example on how to calculate the sectorial coordinate ω and and the applied bi-moment M_ω.

$$M_\omega = -EI_w \frac{\mathrm{d}^2\varphi}{\mathrm{d}x^2} \tag{2.14}$$

2.7.3 Pure Saint-Venant torsion and warping restraint torsion combined

The torsional moment is resisted by the two components Saint-Venant torsion (pure twist of cross-section) and the warping restraint torsion:

$$M_{x,tot} = GI_t \frac{\mathrm{d}\phi}{\mathrm{d}x} - EI_w \frac{\mathrm{d}^3\varphi}{\mathrm{d}x^3} \tag{2.15}$$

A beam loaded at mid span by a torsional moment is shown in Figure 2.15 . At the supports, torsion is prevented but warping is freely allowed. At the middle of the beam length, warping is prohibited due to symmetry, but torsion is allowed.

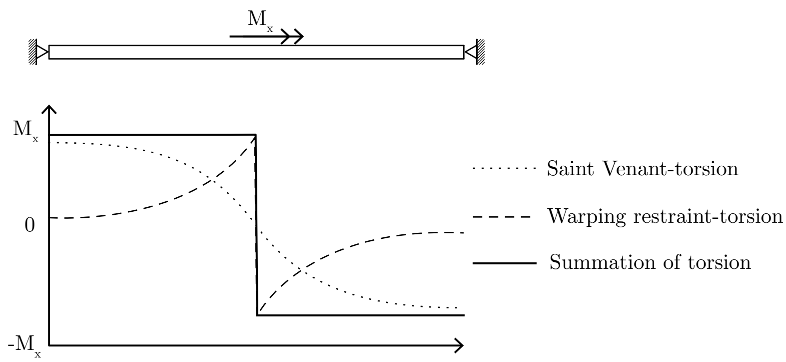

Figure 2.15: *Distribution of Saint-Venant torsion and warping torsion along beam*

2.8 Point of load application

The point of load application (PLA) is defined as the vertical distance from shear centre to the application of the load. Placing the load above the shear centre will increase the rotation of the cross-section due to the eccentricity that arises as soon as the cross-section starts to twist. In contrary, if the load is placed below the shear centre, the rotation of the cross-section will be counteracted by the load, demonstrated in Figure 2.16.

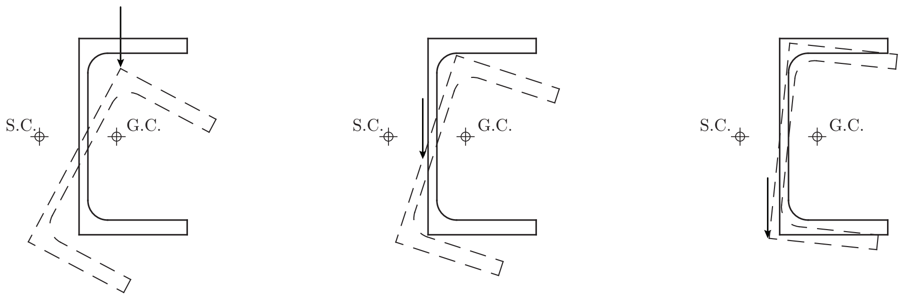

Figure 2.16: *Different points of load application*

If, however, the load is placed directly in the shear centre, the rotation will neither increase nor decrease. Beams with shear centres outside the physical geometry will behave like double symmetric beams when applying an imaginary load on a vertical axis through the shear centre. Applying real transversal loads on the structure will introduce an initial twisting of the cross-section due to the horizontal eccentricity.

2.9 Boundary conditions

To analyse lateral-torsional buckling for a single span beam that is simply supported on each end, a fork support is used. In a fork support, the translation in z and y is restrained at both ends and at one end the translation in x is locked. The rotation about the x-axis is prohibited due to the geometry of a fork support but rotations about the y- and z-axis are allowed. The fork support for each end is shown in Figure 2.17.

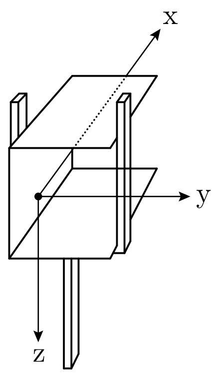

Figure 2.17: *Fork support*

3 Theoretical background to structural instability

It is claimed that the risk of buckling in general is the most important design consideration in many structural systems (Simitses and Hodges, 2006). Structural failure resulting from instability often lead to catastrophic consequences, and have commonly occured during erection (Galambos and Surovek, 2008). As an example of such failures a number of large steel box-girder bridges collapsed during a period around 1970:s.

Structural elements can be divided into four categories, depending on their relative dimensions (Simitses and Hodges, 2006):

1) Same magnitude in all three dimensions - compact solid elements such as a cube or a short cylinder, see Figure 3.1a.

2) One dimension is of smaller magnitude than the other two - plates, shells, see Figure 3.1b.

3) One of the dimensions is of larger magnitude than the other two, which are of equal size - thin beams and columns, see Figure 3.1c

4) All three dimensions are of different magnitudes - thin-walled beams with open cross-section, for example composite sections such as I-beams, see Figure 3.1d

The first category is not prone to instability but the other three are. In this thesis project, category 4 is of main interest.

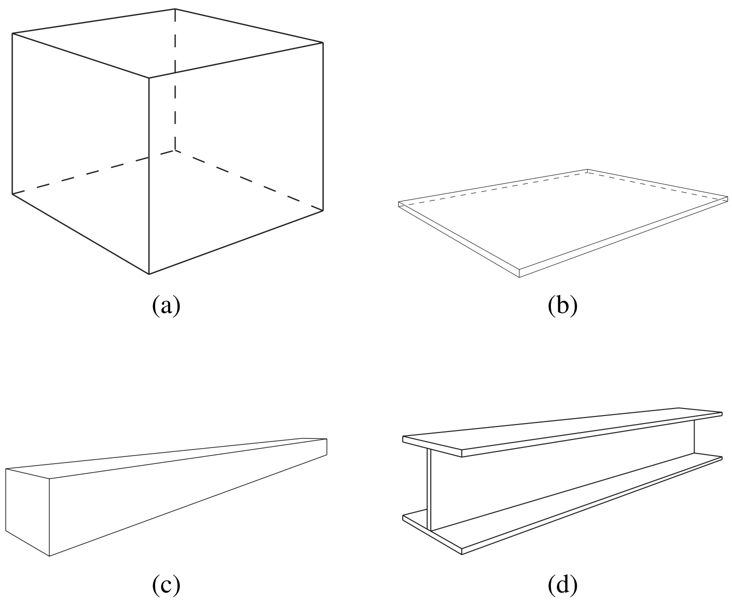

Figure 3.1: *Four categories of structural elements regarding their relative dimensions*

3.1 Principal states of stability

To describe the stability of a structural system, an often used concept is to refer to the equilibrium of a ball with different configurations as shown in Figure 3.2 (Yoo and Lee, 2011). Three main states can be distinguished in which the ball will respond differently to small disturbances.

Stable state
If the ball at position A is disturbed with a small force, and that force is later removed, the ball will return to its original position. This corresponds to the minimum energy of the system, and the ball is in a stable equilibrium.

Unstable state
The unstable state is when the ball is on the top, position B. If the ball at this position is slightly disturbed, it will increasingly move away from its original position. Therefore, the energy of the system is at its maximum when the ball is in position B.

Indifferent or neutral state
If the ball is in position C and is disturbed, there will be no change in the energy of the system. Thus, the ball can find a new equilibrium at any position and it will neither return to the original position nor continue to move increasingly.

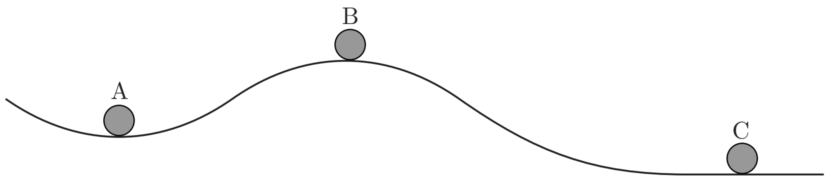

Figure 3.2: *Three principal states of stability*

3.2 Euler's theory of elastic column buckling

The first structural element analysed scientifically with regards to instability was the column, and was performed by Leonard Euler in 1757 (Timoshenko, 1983). When a column in compression reaches a critical load its behaviour passes from compression elastically (shortening) to bending laterally (i.e. global buckling). At that moment, a small increase in load gives a large increase in lateral deflection. When Euler calculated the critical load for columns the following assumptions were made (Pettersson, 1971):

- No residual stresses from the manufacturing process
- Perfectly straight column
- Load applied at the centre of the cross-section
- Elastic material response for both compression and tension (Hooke's law)
- Coplanar and quasistatically applied load
- Isotropic and homogeneous material

The derivation of the critical load N_{cr} starts by setting up a second order differential equation for a pinned-pinned column, where the load is applied axially (Salmon et al., 2008). The boundary conditions for this specific case imply that there are no movements at the supports.

$$EI\frac{\mathrm{d}^2y}{\mathrm{d}x^2}+M_z=0 \tag{3.1}$$

$$y(0)=y(L)=0 \tag{3.2}$$

According to Figure 3.3 the bending moment, M_z, can be substituted with $M_z = N \cdot y(x)$ and hence:

$$EI\frac{\mathrm{d}^2y}{\mathrm{d}x^2}+N\cdot y(x)=0 \tag{3.3}$$

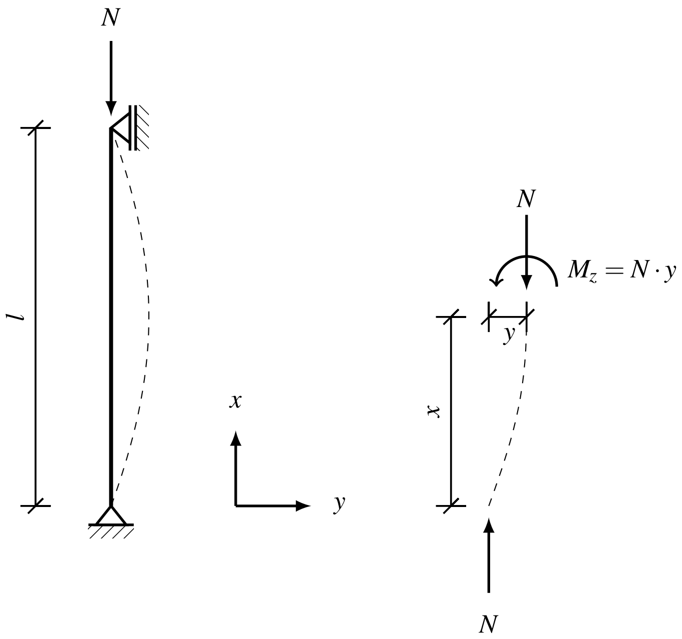

Figure 3.3: *Bending moment introduced due to second order effects*

By dividing all terms with EI and introducing $k^2 = N/EI$ Equation (3.3) can be rewritten into:

$$\frac{\mathrm{d}^2y}{\mathrm{d}x^2}+k^2y(x)=0 \tag{3.4}$$

The general solution to this differential equation is given on the form:

$$y(x)=A\sin(kx)+B\cos(kx) \tag{3.5}$$

By inserting the boundary condition $y(0) = 0$, B can be solved:

$$A\sin(0k)+B\cos(0k)=0 \quad \Rightarrow \quad B=0 \tag{3.6}$$

Continue solving the differential equation by using the other boundary condition, $y(L) = 0$:

$$A\sin(kL) = 0 \quad \Rightarrow \quad \begin{cases} A = 0 & \text{No deflection (trivial)} \\ kL = 0 & \text{No applied load} \\ kL = n\pi,\ (n = 1,2\dots) & \text{Buckling occurs} \end{cases} \tag{3.7}$$

The critical force is then solved for by inserting $k = \sqrt{N/EI}$ into the third term in Equation (3.7)

$$\sqrt{\frac{N}{EI}}L = n\pi \quad \Leftrightarrow \quad N = \frac{n^2\pi^2 EI}{L^2} \tag{3.8}$$

The buckling mode of interest is related to the lowest value of N which corresponds to $n = 1$. This force is usually called the critical buckling force:

$$N_{cr} = \frac{\pi^2 EI}{L^2} \tag{3.9}$$

Below in Figure 3.4 the buckling force is plotted against column slenderness to produce an elastic critical buckling curve for columns according to Euler's theory. The dashed line shows the force N_y that would result in yielding of the entire cross-section.

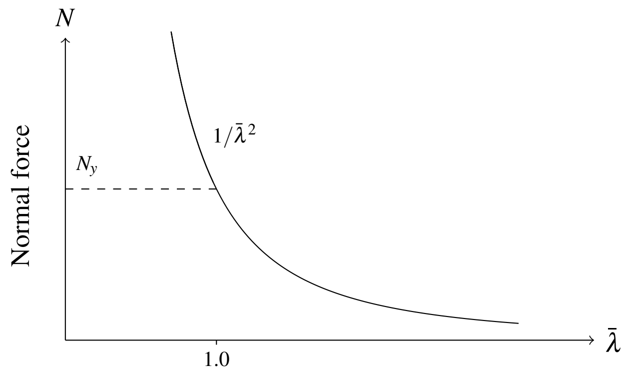

Figure 3.4: *Elastic buckling curve according to Euler's theory*

A column that buckles according to Euler's theory follows the theory of stability. For $N < N_{cr}$, the system is in the stable state, and the column only deforms axially. For $N > N_{cr}$ the system is in the unstable state, where a small increase in load results in a large increase in lateral deflection.

For structural systems it is usually of interest to find the critical load that leads to the unstable state. At this load, the system can find equilibrium for both a completely straight and slightly bent shape (Galambos and Surovek, 2008). This is explained further in Section 4.1.1.

3.3 Real columns with imperfections

The theoretical Euler buckling is also known as bifurcation type buckling. In Figure 3.5 the compression load is plotted against lateral deflection. Initially the increased load does not result in lateral deflection, but at the critical level N_{cr}, there is a sharp turn, thereby the name bifurcation buckling (Yoo and Lee, 2011).

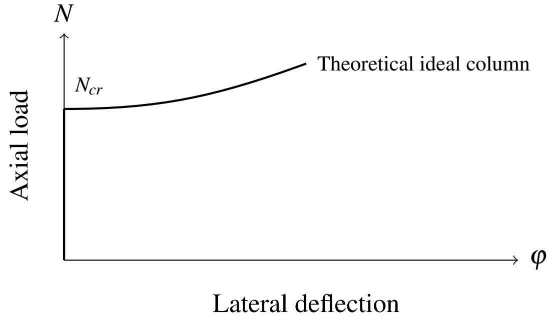

Figure 3.5: *Buckling behaviour of an ideal column*

In reality, initial geometric imperfections, residual stresses and load eccentricity will lead to a behaviour that could be described as deflection-amplification type buckling. At first, a small deflection leads to increased stresses due to a second order moment, which increases the deflection and so on. The principal load-deflection curve of a real column (or beam) will resemble the curves in Figure 3.6.

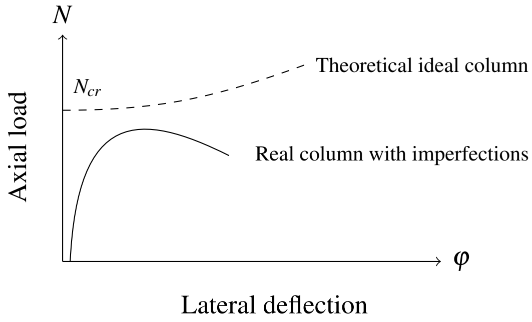

Figure 3.6: *Buckling behaviour of real and ideal column*

3.3.1 Effect of initial geometric imperfections

No production method leads to perfectly straight structural members, and therefore second order effects are introduced when axial loads are applied on a column. The initial geometric imperfection is assumed to have a bow shape, seen in Figure 3.7 below, and a common manufacturing limit for the maximum initial deflection is L/1000, but depends on the type of cross-section (Galambos, 1998).

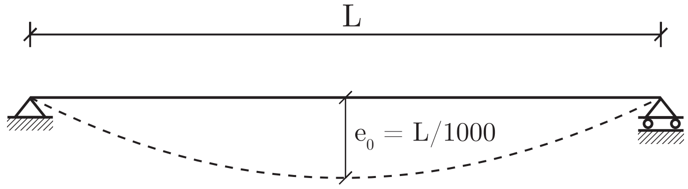

Figure 3.7: *Inititally assumed geometric out-of-straightness*

3.3.2 Effect of residual stresses

When hot-rolled or welded sections are manufactured, subsequent uneven cooling lead to residual stresses in the metal. The difference in stress is higher in more stocky cross-sections, and steel class and cooling temperature are also of some importance (Galambos, 1998).

Cold-formed sections exhibit residual stresses due to plastic deformations during bending, but not of the same magnitude as hot-rolled or welded sections (Höglund, 2006).

Without residual stresses, the loading of a beam would result in a symmetric stress distribution in the cross-section. When taking this effect into account, however, a certain part such as the outer edge of a flange, might yield much earlier than expected. Residual stresses and stresses from applied loads are added through superposition resulting in the actual stress level, as illustrated in Figure 3.8.

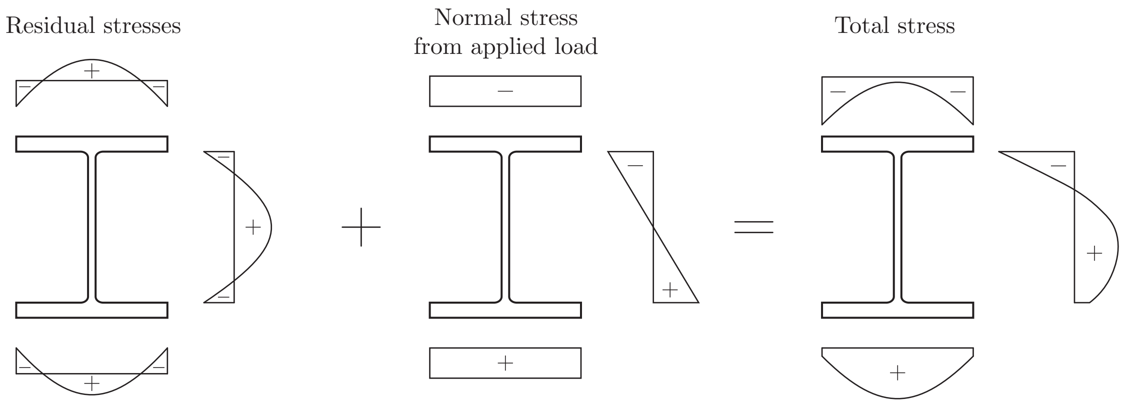

Figure 3.8: *Combined effect of residual stresses to the left and normal stresses caused by bending moment from applied load in the middle*

3.3.3 Ayrton-Perry formulation for buckling of real columns

In 1886, Ayrton and Perry further developed Euler's theoretical column buckling theory by taking into consideration the yield strength of the material as well as an initial geometric imperfection. Thereby a formulation of the failure load was established for columns, but the magnitude of the initial imperfection was not decided (Brown, 2016). Later, in 1925, Robertson made further contributions by determining actual imperfection values with the support from experiments. Therefore initial geometric imperfections, residual stresses and unintended load eccentricity was automatically implemented. His curve, which became known as the Perry-Robertson curve, had an elastic failure criterion where the column failed when the outer most fibre in the cross-section at the critical part of the column reached yielding.

The starting point of the Ayrton-Perry formulation is to model residual stresses, geometric imperfections and unintended load eccentricity as an "equivalent geometric imperfection" in the form of a single bow with a maximum deflection of $e_{0,d}$ (Boissonnade et al., 2006):

$$v_0(x) = e_{0,d} \sin \frac{\pi x}{L} \tag{3.10}$$

The additional deflection due to the axial load can also be represented by a sinusoidal function:

$$v(x) = A\sin\frac{\pi x}{L} \tag{3.11}$$

The differential equation for the deflected shape can be written as:

$$v'' + \frac{N_{Ed}}{EI}(v_0 + v) = 0 \tag{3.12}$$

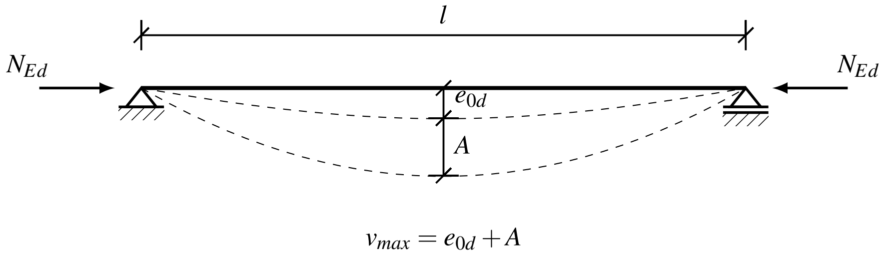

Figure 3.9: *Eccentricity due to second order effects*

By inserting Equations (3.10) and (3.11) into Equation (3.12), the amplitude A can be solved:

$$-\frac{\pi^2}{L^2}A\sin\frac{\pi x}{L} + \frac{N_{Ed}}{EI}\sin\frac{\pi x}{L}\left(e_{0,d} + A\right) = 0 \tag{3.13}$$

$$\sin\frac{\pi x}{L}\left(\frac{N_{Ed}}{EI}e_{0,d} + \frac{N_{Ed}}{EI}A - \frac{\pi^2}{L^2}A\right) = 0 \tag{3.14}$$

$$A = \frac{N_{Ed}}{N_{cr} - N_{Ed}}e_{0,d}, \quad \text{where} \quad N_{cr} = \frac{\pi^2 EI}{L^2} \tag{3.15}$$

The total deflection, v_{max} is the sum of the initial maximum deflection and deflection due to axial load $(A + e_{0,d})$, see Figure 3.9. Hence:

$$\begin{aligned} v_{max} =& \frac{N_{Ed}}{N_{cr} - N_{Ed}}e_{0,d} + \frac{N_{cr} - N_{Ed}}{N_{cr} - N_{Ed}}e_{0,d} \\ =& \frac{N_{cr}}{N_{cr} - N_{Ed}}e_{0,d} = \frac{1}{1 - N_{Ed}/N_{cr}}e_{0,d} \end{aligned} \tag{3.16}$$

A second-order in-plane control of an elastic column can be performed:

$$\frac{N_{Ed}}{N_{Rd}} + \frac{1}{1 - N_{Ed}/N_{cr}}\frac{N_{Ed}e_{0,d}}{M_{Rd}} \leq 1.0 \tag{3.17}$$

A collapse mechanism is formed when $N_{Ed} = N_{b,Rd} = \chi N_{Rd}$. By using the following relationships: $\bar{\lambda}^2 = \dfrac{N_{Rd}}{N_{Ed}}$, $N_{Rd} = Af_y/\gamma_{M1}$, $M_{Rd} = W_{el}f_y/\gamma_{M1}$, Equation (3.17) can be rewritten into:

$$\frac{\chi N_{Rd}}{N_{Rd}} + \frac{1}{1-\chi\bar{\lambda}^2} \frac{\chi \dfrac{Af_y}{\gamma_{M0}}}{\dfrac{W_{el}f_y}{\gamma_{M1}}} e_{0,d} \leq 1.0 \tag{3.18}$$

$$\chi + \frac{1}{1-\chi\bar{\lambda}^2} \frac{\chi A}{W_{el}} e_{0,d} \leq 1.0 \tag{3.19}$$

By introducing the generalised imperfection, $\eta = \dfrac{Ae_{0,d}}{W_{el}}$, we then have

$$\chi + \chi \frac{\eta}{1-\chi\bar{\lambda}^2} \leq 1.0 \tag{3.20}$$

Equation (3.20) can be solved and thus we have an expression for the reduction factor χ:

$$\chi = \frac{1}{\Phi + \sqrt{\Phi^2 - \bar{\lambda}^2}} \leq 1.0 \tag{3.21}$$

$$\Phi = 0.5[1 + \eta + \bar{\lambda}^2] \tag{3.22}$$

In Eurocode 3, the generalised imperfection is formulated as

$$\eta = \alpha(\bar{\lambda} - 0.2) \tag{3.23}$$

The imperfection factor α depends on the shape of cross-section, steel strength, around which axis the buckling occurs etc, and it takes residual stresses, out-of-straightness and load eccentricity into account. In Eurocode 3 there are five column buckling curves, shown in Figure 3.10, deriving from different values of α: a, a_0, b, c and d.

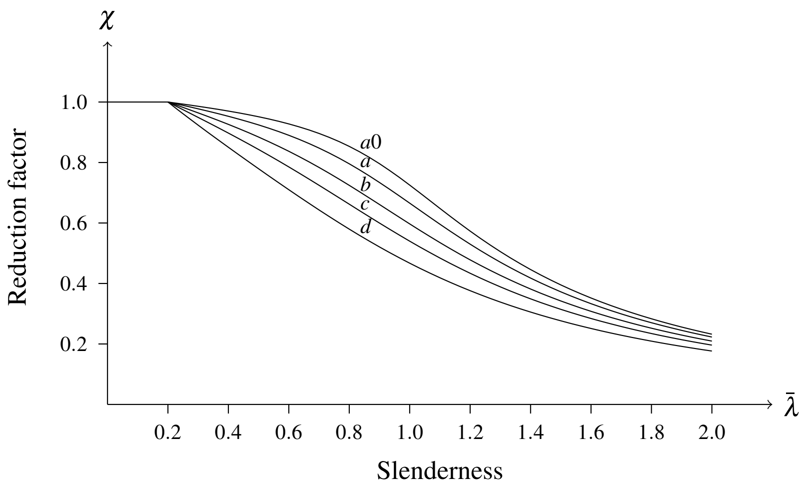

Figure 3.10: *Column buckling curves in Eurocode 3*

The value 0.2 in Equation (3.23) is the plastic limit, meaning that all columns with a lower slenderness are expected to develop full plastic cross-section capacity before failure.

3.3.4 Three principal buckling regions

The normalised slenderness $\bar{\lambda}$ of a beam or column is mainly depending on its length-to-thickness ratio. When plotting slenderness against buckling resistance three distinct regions can be distinguished in Figure 3.11 (Yoo and Lee, 2011).

Region 1 corresponds to stocky beams which fail through yielding of the whole cross-section. The phenomenon of buckling never takes place.

Region 3 corresponds to slender beams which fail in elastic buckling close to the predictions of Euler buckling theory.

Region 2 is called the intermediate region.

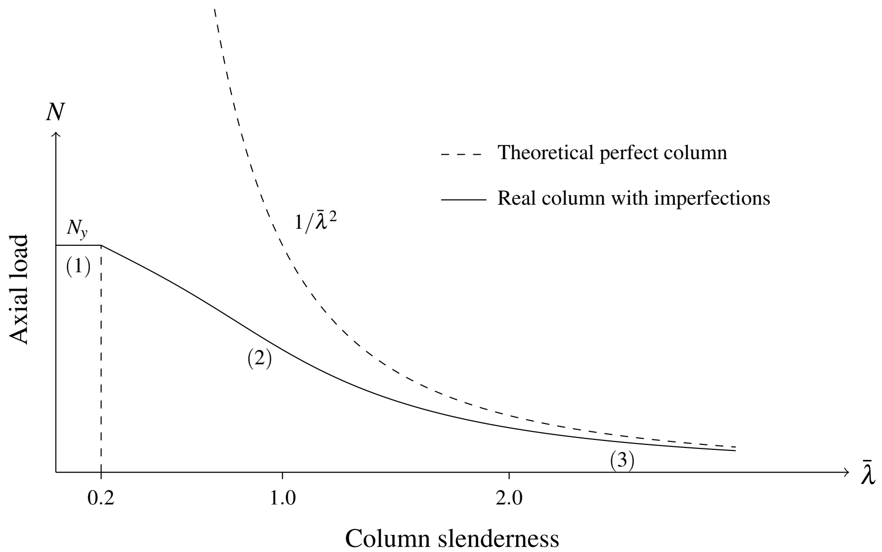

Figure 3.11: *Three buckling regions*

For increased understanding and to be able to interprete and analyse the results from the FE-analyses, a short explanation of other common instability phenomena (except lateral-torsional buckling) is given in the next section.

3.4 Other instability phenomena in beams and columns

3.4.1 Flexural buckling

Previous sections describing Euler's original elastic column buckling is an example of flexural buckling. This is the most common way in which a column buckles. No twisting takes place and deformation is two-dimensional so the response can be described as in-plane behaviour, as shown in Figure 3.12. In addition, a beam transversally loaded around its weak axis will buckle flexurally.

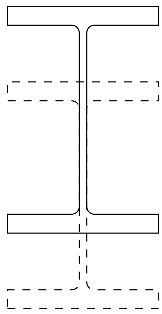

Figure 3.12: *Flexural buckling*

3.4.2 Torsional buckling

If a column or beam is subjected to a uniformly distributed axial torque, it might twist around its longitudinal axis without deflecting neither vertically nor laterally, as shown in Figure 3.13. This is referred to as torsional buckling. Already in 1855, the theory of uniform torsion was described by Saint-Venant (N. S. Trahair, 1993). At this time other instability phenomena were not described mathematically, except for column (flexural) buckling.

Torsional buckling can also occur without applied torque, with the conditions that the structural element is braced against flexural buckling or if it has a non-symmetric shape (Höglund, 2006).

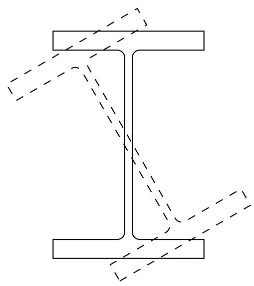

Figure 3.13: *Torsional buckling*

3.4.3 Local buckling

Local buckling can occur in a part of a cross-section, for example in the web or flange of an I-beam, if the part is slender enough (CEN, 2005). The structural member does not buckle globally, but several buckles might form next to each other in a certain region (Höglund, 2006).

The size of one buckle is usually about the width of the plate element, illustrated in Figure 3.14. If local buckling takes place, the cross-section stiffness is reduced and the risk of global buckling is increased (N. S. Trahair, 1993).

In general, the design philosophy is avoid local buckling in steel structures. This might not always be the best solution as the post-critical strength is not taken advantage of. Local buckling can in fact be the preferred failure mode in ultimate limit state in extreme loading cases (Seif and Schafer, 2010).

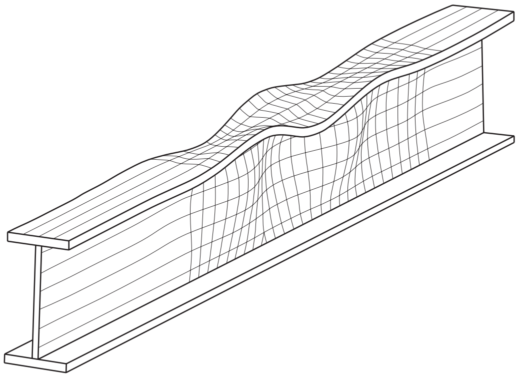

Figure 3.14: *Local buckling of web and top flange of I-beam*

3.4.4 Distortional buckling

This particular buckling mode can be described as something in between local buckling and global buckling (N. S. Trahair, 1993). The behaviour is more common in cross-sections with slender rather than stocky webs. For an I-beam, the section can for example be deformed in such a way that the bottom flange deflects laterally without significant twist, see Figure 3.15, if the top flange is braced laterally but not the bottom flange. This leads to reduced torsional stiffness (Samanta and Kumar, 2006).

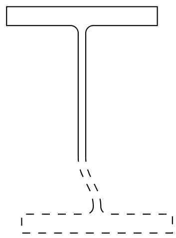

Figure 3.15: *Distortional buckling that could occur when the top flange is laterally braced while the bottom flange is not*

In a cold-formed lipped channel beam, flexural buckling of the lip and the flange it is attached to, might lead to distortional buckling, see Figure 3.16 (Höglund, 2006). Usually, there is no post-critical strength for this buckling mode. The buckles are formed with a length of three to eight times the element width.

Figure 3.16: *Distortional buckling of channel beam flanges*

3.4.5 Torsional flexural buckling

When some kind of asymmetry is involved, torsional flexural buckling can develop. Either one of the flanges is braced while the other is not, or the cross-section is of for example L-shape. The effect is simultaneous deflection and twist.

The resulting deformation pattern is similar to lateral-torsional buckling but the difference is that torsional flexural buckling is caused by axial compressive load and not by transversal load.

4 Lateral-torsional buckling

For a laterally unrestrained or insufficiently restrained beam, lateral-torsional buckling in particular is commonly the limiting factor in design (Hughes, 2009). Other conditions that need to be fulfilled for this effect to occur is that the cross-section must have significantly lower stiffness around the minor axis than the major axis, the load must be applied around the major axis and the cross-section need to have low torsional stiffness. Closed sections such as box-beams are therefore not prone to lateral-torsional buckling (Höglund, 2006).

In lateral-torsional buckling, the beam is loaded in the plane of its major axis until it buckles by a sudden simultaneous lateral deflection and twisting of the cross-section (Galambos and Surovek, 2008). As an example of this behaviour, consider a simply supported I-section beam. When loaded by a uniformly distributed load, the top flange is compressed whereas the bottom flange is tensioned. The compressed flange is prone to buckle as a strut but is partly restrained by the web in the vertical direction so it will instead buckle laterally. The tension flange however does not need to buckle and is, together with the web, partly restricting the lateral deformation of the compression flange. The imbalance in lateral deflection between the two flanges also lead to torsion of the cross-section. The resulting three-dimensionally bent shape can be seen in Figure 4.1.

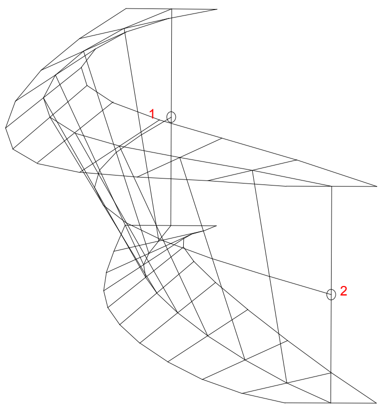

Figure 4.1: *Lateral-torsional buckling of I-beam*

The first work on lateral-torsional buckling was made in 1899 by Prandtl and Michell on thin, high cross-sections of rectangular shape (N. S. Trahair, 1993). A few years later, in 1905, Timoshenko included effects of warping, which made it possible to describe the torsion of I-section beams correctly. Other researchers such as Wagner made further contributions that eventually led to a general theory on lateral-torsional buckling which can be found in the textbooks by Timoshenko and others. Before the 1960s the assessment of lateral-torsional buckling required extensive calculations by hand, which was a clear limiting factor due to the time needed. The computer revolution made it possible to describe beam behaviour with various loading conditions and restraints in both isolated members and frames. With the use of the Finite Element Method for stuctural analysis, the need for scientific publications on the subject decreased.

In Chapter 3, the difference between theoretically perfect columns and real columns with imperfections was described. The same methodology will be used on lateral-torsional buckling the following sections, starting with elastic critical bending moment M_{cr}, moving on to the design of real beams in Eurocode 3 and then finishing with some methods for the design of channel beams specifically.

4.1 Elastic critical bending moment, M_{cr}

In Section 3.3.3 the critical load for column buckling N_{cr} was derived. By making the same assumptions (no material or geometric imperfections and so on), the elastic critical bending moment for lateral-torsional buckling, M_{cr}, can be described.

A number of methods to calculate the theoretical critical elastic buckling load of a beam are mentioned in (Simitses and Hodges, 2006). Analytical methods are not practical to use in design, since for every load case and boundary condition a new lengthy calculation procedure need to be performed. Therefore general expressions are used, such as the 3-factor formula which is described in Section 4.3.

Among the analytical methods are the equilibrium method, the dynamic method and the potential energy method. The potential energy method will be given a longer treatment in Section 4.1.1, since it is thereafter used to derive the expression for M_{cr} that the 3-factor formula is based on.

The equilibrium method is based on the fact that a beam or column remains straight until an equilibrium can exist in both the straight and the slightly bent shape. This is also called the bifurcation method. Mathematically the solution is derived from an Eigenvalue boundary problem.

The dynamic, or kinetic method, is a direct application of structural stability theory, which is described in Section 3.1. The equations of free vibrations of a system are studied to decide for what external load a small disturbance lead to a deviation of the equilibrium.

4.1.1 Potential energy method

The energy method is equivalent to the dynamic method for conservative systems, and can only be used for such systems, where the work performed by applied forces and reaction forces are independant on path, but dependant only on initial and final configurations.

An example of a conservative system is a ball subject to gravitational fields. It is irrelevant how the ball is moved, but the potential energy difference is dependant on initial and final height. An object subject to friction and moved along a surface is an example of an unconservative system. The work performed is not only dependant on the initial and final coordinates but on the path travelled.

Another example is shown in Figure 4.2 where a compressive load is applied at the free end of a column. If the load remains vertical it is a conservative stability problem, whereas if the load direction changes tangentially it is an unconservative system (Pettersson, 1971).

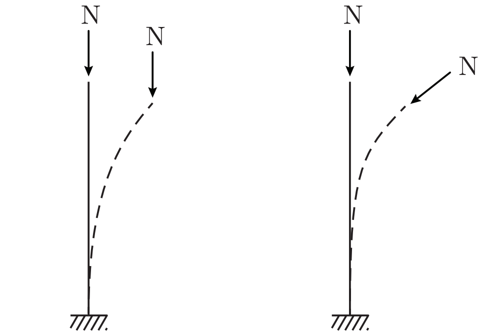

Figure 4.2: *An example of a conservative and an unconservative stability problem*

A structural element will find equilibrium in a position where the potential energy of the deflected shape is minimized, given that boundary conditions are fulfilled, according to (Höglund, 2006). The potential energy is expressed as having two parts, one with energy from external loads H_y and one from elastically stored internal energy in the deflected shape H_i.

$$H = H_y + H_i \tag{4.1}$$

It is useful to set the energy level for the straight position just before buckling as the energy zero level. Then the energy potential change ΔH is of interest:

$$\Delta H = H_{deflected} - H_{straight} \tag{4.2}$$

Since the work performed by applied loads is completely converted to elastic energy through deflection of the structure, it is true that for any equilibrium position:

$$H_y = -H_i \tag{4.3}$$
$$H_y + H_i = 0 \tag{4.4}$$

The potential energy at an equilibrium position is at its minimum, meaning that for the given loads and boundary conditions, any change in the shape of the beam will increase the potential energy as illustrated in Figure 4.3.

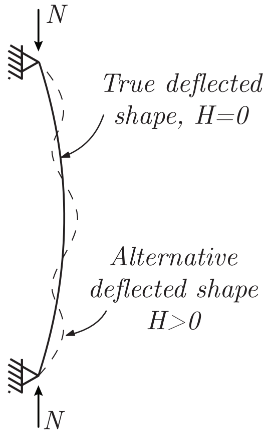

Figure 4.3: *Potential energy is at minimum in equilibrium positions*

For the special case of elastic buckling, the potential energy does not change, however, when the shape changes from straight to deflected at the critical buckling load, illustrated in Figure 4.4:

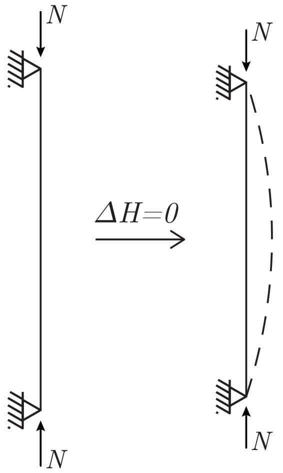

Figure 4.4: *Potential energy before and after buckling is equal*

$$\Delta H = 0 \tag{4.5}$$

To calculate the critical buckling load in this way, differential equations are set up that describe the energy in the system. The specific boundary and loading conditions are taken into account and then a deflected shape is assumed and the energy for the suggested shape can find a minimum.

This procedure is obviously not practical to use in structural design. The equations set up are only valid for the specific boundary and loading conditions, and extensive calculations are needed to obtain the solution. Following is a derivation through the potential energy method of M_{cr}, the elastic critical bending moment with regards to lateral-torsional buckling.

4.2 Derivation of M_{cr} through the potential energy method

To derive an expression for the critical elastic bending moment, the energy method described in the previous section can be used. The following derivation is based on the works of (Höglund, 2006) and (Galambos and Surovek, 2008).

Consider a single span, double symmetric beam with fork supports subjected to equal but opposite applied end moments. It should be noted that although the applied load is working around the y-axis, the deformed shape resulting from theoretical lateral-torsional buckling involves bending of the beam cross-section in the lateral direction (y-axis) and twist around the x-axis but major axis bending is actually not a part of the response.

Since a buckled beam will find the most energy efficient shape, the function for the total potential energy is at a local minimum for that specific shape. The total potential energy is obtained by adding the external work performed on the beam by the applied load and and the internally stored energy created by minor axis bending and twisting of the beam. By using calculus of variations and Euler-Poisson system of equations, it is possible to solve the differential equation that are derived, which is shown in detail in Section 4.2.4. The following assumptions are made:

- The material is linearly elastic, homogeneous and isotropic
- Angle of twist and deflections are small
- No local buckling or distortion of cross-section
- There are no residual stresses or initial out-of-straightness of the beam

It can be mentioned that different litterature uses different notations for warping and torsional stiffness, and therefore the following notations are equivalent:

Torsional stiffness: $GI_t = C = GK_v$
Warping stiffness: $EI_w = C_w = EK_w$

4.2.1 Elastically stored internal energy

Bending about weak axis

Work is defined as force multiplied by a distance in the same direction as the force. By combining the definition of stress ($\sigma = P/\mathrm{d}A$) and Hooke's law ($\sigma = E\varepsilon_y$) the force can be expressed as $P = \mathrm{d}AE\varepsilon_y$. The distance can be expressed by the Cauchy strain ($\Delta\mathrm{d}x = \varepsilon_y\mathrm{d}x$). For a beam subjected to a bending moment around the z-axis (M_z), the work, for an element in the infinitesimal part in the x-direction, is:

$$\mathrm{d}^2H_{(i,j)b,z} = \frac{1}{2}\underbrace{\mathrm{d}AE\varepsilon_y}_{force}\cdot\underbrace{\varepsilon_y\mathrm{d}x}_{direction} \tag{4.6}$$

All elements in the x-direction summed up:

$$\mathrm{d}H_{ib,z} = \frac{1}{2}\mathrm{d}x\int_0^A E\varepsilon_y^2\,\mathrm{d}A \tag{4.7}$$

The previous equation can be rewritten by using $(\varepsilon_y = \sigma_x/A = -M_z y/EI_z)$

$$H_{ib,z} = \frac{\mathrm{d}x}{2}\frac{M_z^2}{EI_z^2}\int_0^A y^2\,\mathrm{d}A = \frac{1}{2}\frac{M_z^2}{EI_z}\mathrm{d}x \tag{4.8}$$

Integration along the beam gives

$$H_{ib,z} = \int_0^L \frac{M_z^2}{2EI_z}\,\mathrm{d}x \tag{4.9}$$

The fundamental Euler-Bernoulli beam equation states that

$$M_z = v''EI_z \tag{4.10}$$

M_z and v are here expressed in the local z cross-section direction, since the cross-section twist in lateral-torsional buckling. By inserting Equation (4.10) in Equation (4.9), the elastically stored energy from minor axis bending along the entire beam is then expressed as

$$H_{ib,z} = \int_0^L \frac{EI_z(v'')^2}{2}\mathrm{d}x \tag{4.11}$$

Saint-Venant torsion

The Saint-Venant torsion for an infinitely small part is expressed by the torsional stiffness GI_t multiplied by the angle of twist distributed along the part, as shown in Section 2.7:

$$T_{SV} = GI_t\frac{\mathrm{d}\varphi}{\mathrm{d}x} = GI_t\varphi' \tag{4.12}$$

The potential energy for an infinitesimal part of the beam is

$$\mathrm{d}H_{i,SV} = T_{SV}\frac{\mathrm{d}\varphi}{2} = \left\{\mathrm{d}\varphi = \frac{\mathrm{d}\varphi}{\mathrm{d}x}\mathrm{d}x = \varphi'\mathrm{d}x\right\} = \frac{1}{2}GI_t\left(\varphi'\right)^2\mathrm{d}x \tag{4.13}$$

Summarizing all the parts over the length of the beam yields

$$H_{i,SV} = \int_0^L \frac{GI_t(\varphi')^2}{2}\mathrm{d}x \tag{4.14}$$

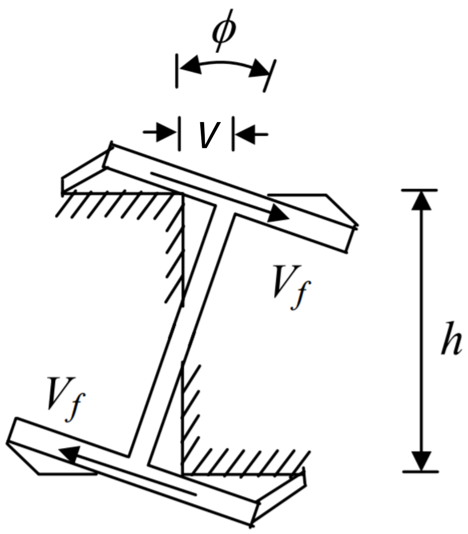

Figure 4.5: *Force couple in flanges creating warping torsion*

Warping torsion

The strain energy from warping comes from lateral bending of the flanges:

$$M = -EI_{z,flange}v'' \tag{4.15}$$

The relation between twist and lateral deflection of the flange centreline is $v = \frac{h_w + t_f}{2}\varphi$, illustrated in Figure 4.5.

Equation (4.15) can then be written

$$M = -EI_{z,flange}\frac{h_w + t_f}{2}\varphi'' \tag{4.16}$$

Calculating the force in the flanges by taking the derivative with respect to the moment gives

$$F = \frac{\mathrm{d}M}{\mathrm{d}x} = -EI_{z,flange}\frac{h_w + t_f}{2}\varphi''' \tag{4.17}$$

The moment of inertia about the z-axis can be approximated by the contribution from the flanges (ignoring the web): $I_z \approx 2I_{flange}$. Inserting this approximation into Equation (4.17):

$$F = -E\frac{I_z}{2}\frac{h_w + t_f}{2}\varphi''' \tag{4.18}$$

Torsion due to warping is calculated as:

$$T_w = F \cdot (h_w + t_f) = -\frac{EI_z(h_w + t_f)^2}{4}\varphi''' \tag{4.19}$$

Simplify Equation (4.19) by inserting $I_w = \frac{I_z\left(h_w + t_f\right)^2}{4}$:

$$T_w = -EI_w\varphi''' \tag{4.20}$$

The potential energy for an infinitesimal part is calculated in the same way as for Saint-Venant torsion:

$$\mathrm{d}H_{i,w} = T_w\frac{\mathrm{d}\varphi}{2} = -\frac{1}{2}EI_w\varphi'''\varphi'\mathrm{d}x \tag{4.21}$$

Calculate the total potential energy by integrating over the whole length of the beam

$$H_{i,w} = -\int_0^L \frac{EI_w\varphi'''\varphi'}{2}\mathrm{d}x \tag{4.22}$$

Perform integration by parts $(\int uv'\mathrm{d}x = uv - \int u'v\mathrm{d}x)$ where $\varphi''' = v'$ and $\varphi' = u$ to be able to rewrite the total potential energy:

$$H_{i,w} = -\int_0^L \frac{EI_w\varphi'''\varphi'}{2}\mathrm{d}x = -\frac{1}{2}\left[EI_w\varphi''\varphi'\right]_0^L - \left(-\int_0^L \frac{EI_w(\varphi'')^2}{2}\mathrm{d}x\right) \tag{4.23}$$

The first expression (after the equal sign) is equal to zero when a fork support is used, since $\varphi''(0) = \varphi''(L) = 0$ and hence

$$H_{i,w} = \int_0^L \frac{EI_w(\varphi'')^2}{2}\mathrm{d}x \tag{4.24}$$

Total potential energy for torsion

Total energy for torsion consists of Saint-Venant torsion and warping:

$$H_{i,t} = H_{i,SV} + H_{i,w} \tag{4.25}$$

Inserting Equations (4.14) and (4.24) into Equation (4.25) results in

$$H_{i,t} = \int_0^L \frac{GI_t(\varphi')^2}{2}\mathrm{d}x + \int_0^L \frac{EI_w(\varphi'')^2}{2}\mathrm{d}x \tag{4.26}$$

4.2.2 External energy: bending about weak axis

As explained earlier major axis bending is excluded from this derivation. The applied end moments work around the global y-axis but as soon as the beam starts to twist the applied bending moment M_y can be separated into cross-section components where the contribution to bending around the local cross-section z-axis is $M_y\phi$, as shown in Figure 4.6.

The potential energy from applied end moments is described by the following equation:

$$H_{y,M_y} = \int_0^L M_y\varphi v''\,\mathrm{d}x \tag{4.27}$$

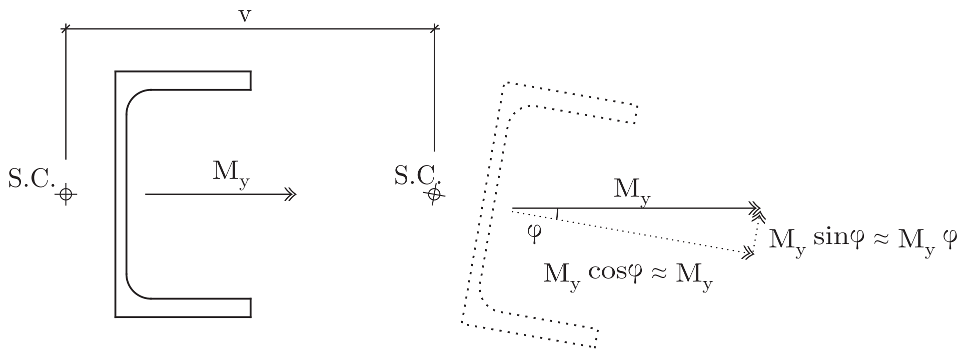

Figure 4.6: *Bending around global z-axis leading to local cross-section bending composants*

4.2.3 Calculus of variations and Euler-Poisson system of equations

Calculus of variations can be useful when needing to find extreme values to functions (Komzsik, 2014). A buckled beam will have such a shape that the potential energy is minimized, and therefore the method of calculus of variations can be used to find the load that is required for a beam to buckle elastically.

In calculus of variations a general functional that includes several functions with higher order derivatives can be desribed as:

$$F(y_1,...,y_m) = \int_0^L f(x, y_1, y_1', ..., y_1^{n_1}, ..., y_m, y_m', y_m^{(n_m)})\,\mathrm{d}x \tag{4.28}$$

According to (Komzsik, 2014), this leads to a system of equations:

$$\frac{\partial f}{\partial y_1} - \frac{\mathrm{d}}{\mathrm{d}x}\left(\frac{\partial f}{\partial y_1'}\right) + \frac{\mathrm{d}^2}{\mathrm{d}x^2}\left(\frac{\partial f}{\partial y_1''}\right) - ...(-1)^{n_1}\frac{\mathrm{d}^(\mathrm{n}_1)}{\mathrm{d}x^{n_1}}\frac{\partial f}{\partial y_1^{(n1)}} = 0 \tag{4.29}$$

$$\frac{\partial f}{\partial y_m} - \frac{\mathrm{d}}{\mathrm{d}x}\left(\frac{\partial f}{\partial y_m'}\right) + \frac{\mathrm{d}^2}{\mathrm{d}x^2}\left(\frac{\partial f}{\partial y_m''}\right) - ...(-1)^{n_m}\frac{\mathrm{d}^(\mathrm{n}_\mathrm{m})}{\mathrm{d}x^{n_m}}\frac{\partial f}{\partial y_m^{(n_m)}} = 0 \tag{4.30}$$

Calculus of variations does not find the maximum or minimum value to a function in itself, but it defines the differential equation(s) that the function must satisfy in order to have a stationary value (Yoo and Lee, 2011). The resulting differential equation(s) may be coupled or uncoupled and can be solved by inserting known boundary conditions.

4.2.4 Solving the differential equations for M_{cr}

The total energy from internal and external work is described as:

$$H = H_i + H_y = \int_0^L \frac{EI_z\,(v'')^2}{2}\,\mathrm{d}x + \int_0^L \frac{GI_t\,(\varphi')^2}{2}\,\mathrm{d}x + \int_0^L \frac{EI_w\,(\varphi'')^2}{2}\,\mathrm{d}x + \int_0^L M_y \varphi v''\,\mathrm{d}x \tag{4.31}$$

When using calculus of variations this can be expressed symbolically as:

$$F = \int_0^L f(v'', \varphi', \varphi'', \varphi''')\,\mathrm{d}x \tag{4.32}$$

So the functional is dependant on the second derivative of u and on the first three derivatives of φ:

$$f = \frac{EI_z\left(v''\right)^2}{2} + \frac{GI_t\left(\varphi'\right)^2}{2} + \frac{EI_w\left(\varphi''\right)^2}{2} + M_y\varphi v'' \tag{4.33}$$

The Euler-Poisson system of equations is then written:

$$\frac{\partial f}{\partial v} - \frac{\mathrm{d}}{\mathrm{d}x}\left(\frac{\partial f}{\partial v'}\right) + \frac{\mathrm{d}^2}{\mathrm{d}x^2}\left(\frac{\partial f}{\partial v''}\right) = 0 \tag{4.34}$$

$$\frac{\partial f}{\partial \varphi} - \frac{\mathrm{d}}{\mathrm{d}x}\left(\frac{\partial f}{\partial \varphi'}\right) + \frac{\mathrm{d}^2}{\mathrm{d}x^2}\left(\frac{\partial f}{\partial \varphi''}\right) - \frac{\mathrm{d}^3}{\mathrm{d}x^3}\left(\frac{\partial f}{\partial \varphi'''}\right) = 0 \tag{4.35}$$

Since v and v' is missing, Equation (4.34) can simply be written:

$$\frac{\mathrm{d}^2}{\mathrm{d}x^2}\left(\frac{\partial f}{\partial v''}\right) = 0 \tag{4.36}$$

and applied on Equation (4.33), Equation (4.36) is then described as:

$$EI_z v'''' + M_y\varphi'' = 0 \tag{4.37}$$

Equation (4.35) is treated the same way and leads to:

$$M_y v'' - GI_t\varphi'' + EI_w\varphi'''' = 0 \tag{4.38}$$

Integrating Equation (4.37) twice gives:

$$EI_z v'' + M_y\varphi = k_1 x + k_2 \tag{4.39}$$

The boundary conditions of a fork support imply that the curvature and the angle of twist at the supports is 0 leading to: $v''(0,L) = 0$ and $\varphi(0,L) = 0 \Rightarrow k_1 = 0$ and $k_2 = 0$

Therefore Equation (4.39) is simplified to

$$EI_z v'' + M_y\varphi = 0 \tag{4.40}$$

and further:

$$v'' = -\frac{M_y}{EI_z}\varphi \tag{4.41}$$

By inserting Equation (4.41) into Equation (4.38):

$$-\frac{{M_y}^2}{EI_z}\varphi - GI_t\varphi'' + EI_w\varphi'''' = 0 \tag{4.42}$$

The equations are now rewritten as to only depend on φ and its derivatives, as the rest of the terms are constants. A solution to the fourth order differential equation of φ is proposed on the form:

$$\varphi = A\sin\frac{j\varphi x}{L} \tag{4.43}$$

The fourth differential becomes:

$$\varphi'''' = A(\frac{j\varphi}{L})^2 \sin\frac{j\varphi x}{L} \tag{4.44}$$

By inserting Equation (4.44) into Equation (4.42):

$$A\sin\frac{j\varphi x}{L}\cdot\left[EI_w\left(\frac{j\pi}{L}\right)^4 + GI_t\left(\frac{j\pi}{L}\right)^2 - \frac{M_y^2}{EI_z}\right] = 0 \tag{4.45}$$

The trivial solution to $\left(A\sin\frac{j\varphi x}{L} = 0\right)$ is of no interest. Therefore the first factor is ignored, leaving $EI_w\left(\frac{j\pi}{L}\right)^4 + GI_t\left(\frac{j\pi}{L}\right)^2 - \frac{M_y^2}{EI_z} = 0$

$$\frac{M_y^2}{EI_z} = EI_w\left(\frac{j\pi}{L}\right)^4 + GI_t\left(\frac{j\pi}{L}\right)^2 \tag{4.46}$$

The smallest potential energy is reached when $j = 1$, which relates to the critical load $M_y = M_{cr}$:

$$\frac{M_{cr}^2}{EI_z} = \frac{\pi^4}{L^4}\left(EI_w + \frac{L^2GI_t}{\pi^2}\right) \tag{4.47}$$

Solving for M_{cr}:

$$M_{cr} = \sqrt{EI_z\frac{\pi^4}{L^4}\left(EI_w + \frac{L^2GI_t}{\pi^2}\right)} \tag{4.48}$$

Extend:

$$M_{cr} = \frac{\pi^2}{L^2}\sqrt{EI_z}\sqrt{EI_w + \frac{L^2GI_t}{\pi^2}}\cdot\frac{\sqrt{EI_z}}{\sqrt{EI_z}} \tag{4.49}$$

$$M_{cr} = \frac{\pi^2 EI_z}{L^2}\frac{\sqrt{EI_w + \frac{L^2GI_t}{\pi^2}}}{\sqrt{EI_z}} \tag{4.50}$$

$$M_{cr} = \frac{\pi^2 EI_z}{L^2}\sqrt{\frac{I_w}{I_z} + \frac{L^2GI_t}{\pi^2 EI_z}} \tag{4.51}$$

The expression that the 3-factor formula for elastic critical bending moment relies on is thereby reached.

4.3 The 3-factor formula for calculating M_{cr}

The previous section showed how to derive the elastic critical bending moment for a double-symmetrical I-beam, with the specific load of applied end moments and with fork end supports. However, Equation (4.51) has been extended to an analytical formula commonly known as the 3-factor formula, to incorporate also more load configurations, some single-symmetric cross-sections and end support conditions.

As of today, Eurocode 3 itself (CEN, 2005) gives no suggestion on how to calculate the elastic critical bending moment resistance, M_{cr}, for lateral-torsional buckling of beams. The earlier version of Eurocode 3 named ENV 1993-1-1:1992 had the 3-factor formula incorporated though, and the formula is now found in NCCI, non-contradictory complementary information to the Eurocodes, on which the following section is based on (Boissonnade et al., 2006) and (Bureau, 2006).

The formula contains a number of constants depending on material properties, cross-section parameters, load case, beam length and support conditions. The result is conservative and sometimes approximate (Boissonnade et al., 2006). An important fact to take into consideration is that the formula is only valid for major axis bending where the cross-section is uniform and symmetrical around the minor axis. It would therefore not be 100% accurate for channel beams. The formula is as follows:

$$M_{cr} = C_1 \frac{\pi^2 E I_z}{(k_z L)^2} \left(\sqrt{ (\frac{k_z}{k_w})^2 \frac{I_w}{I_z} + \frac{(k_z L)^2 G I_t}{\pi^2 E I_z} + (C_2 z_g - C_3 z_j)^2 } - (C_2 z_g - C_3 z_j) \right) \quad (4.52)$$

$C_1 =$ Coefficient depending on the shape of the moment diagram

$C_2 =$ Coefficient depending on the point of load application relative to the shear centre

$C_3 =$ Coefficient depending on the symmetry of the cross-section around the weak axis

$I_z =$ Moment of inertia around minor axis

$I_w =$ Warping constant

$I_t =$ Torsion constant

$k_z, k_w =$ Effective length factors that takes rotational and warping end restraints into account. They are usually set to 1.0 and are analogous to Euler buckling cases 2,3,4.

$z_g = z_a - z_s$

$z_a =$ Vertical coordinate for the point of load application

$z_s =$ Vertical coordinate for the shear center

$z_j = z_s - 0.5 \int_A (y^2 + z^2) \frac{z}{I_y} dA$

4.3.1 C_1-factor

The C_1-factor is mainly depending on moment distribution. It is not only the maximum bending moment in the beam that is of interest but how the bending moment is distributed along the beam. A uniform bending moment from applied end moment, which is the standard load case, gives the lowest value whereas a point load in mid span gives a higher value. C_1 is known for many standard load cases and can be found in handbooks such as (Boissonnade et al., 2006), some of these are presented in Table 4.1

Finite element results from (Kirby and Nethercot, 1979) show that C_1 does in fact also depend on a factor μ which depends on the length of the beam according to the following equation:

$$\mu = \frac{GI_t L^2}{EI_w} \tag{4.53}$$

The effect of μ on the C_1-value increases when the moment distribution is non-linear. Also the end restraint conditions affect C_1. If warping and bending is not allowed, and $k_z = k_w = 0.5$, it decreases.

C_1 for non-standard and combined load cases

When load cases are combined into a non-standard configuration, a table value for C_1 might not exist. It is then possible to use closed-form expressions to approximate it. The idea is to extract the exact bending moment at points along the beam, and then use these in a fixed formula that produces a value for C_1.

A simple formula was developed 1955 by (Salvadori, 1955) which is a good approximation for linear moment distributions, for example applied end moments.

$$C_1 = 1.75 - 1.05\Psi + 0.3\Psi^2 \leq 2.3 \tag{4.54}$$

Ψ is the fraction between the end moments at the two ends according to Figure 4.7.

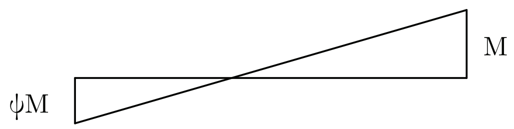

Figure 4.7: *Moment distribution for unequally applied end moments*

The contributions from (Serna et al., 2006) and (López et al., 2006) led to a formula for C_1 that also takes end warping and lateral restraint conditions into account through the coefficients k_w and k_z:

$$C_1 = \frac{\sqrt{\sqrt{k}A_1 + (\frac{1-\sqrt{k}}{2}A_2)^2(\frac{1-\sqrt{k}}{2}A_2)}}{A_1} \tag{4.55}$$

$$k = \sqrt{k_w k_z}$$

The A-factors take the shape of the moment diagram into account:

$$A_1 = \frac{M_{max}^2 + k(\alpha_1 M_1^2 + \alpha_2 M_2^2 + \alpha_3 M_3^2 + \alpha_4 M_4^2 + \alpha_5 M_5^2)}{(1 + \alpha_1 + \alpha_2 + \alpha_3 + \alpha_4 + \alpha_5)M_{max}^2} \tag{4.56}$$

$$A_2 = |\frac{M_1 + 2M_2 + 3M_3 + 2M_4 + M_5}{9M_{max}}| \tag{4.57}$$

The values for M_1-M_5 and M_{max} are decided according to Figure 4.8.

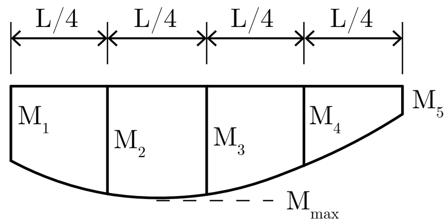

Figure 4.8: *Bending moment values from different parts of the beam*

The α-factors take end warping and lateral restraint conditions into account:

$$\alpha_1 = 1 - k_w$$

$$\alpha_2 = 5\frac{k_z^3}{k_w^2}$$

$$\alpha_3 = 5(\frac{1}{k_w} + \frac{1}{k_z})$$

$$\alpha_4 = 5\frac{k_w^3}{k_z^2}$$

$$\alpha_5 = 1 - k_z$$

4.3.2 C_2-factor

If a transversal load acts on a beam outside of the shear centre, the C_2-factor must be considered in the 3-factor formula. In reality this is often the case since it is physically impossible to load a beam inside of its actual geometry. For beams with open cross-section such as I-sections or channel sections, the load will typically act on the top or bottom flange.

A load above the shear centre, or on the top flange, will increase the twisting and therefore destabilize the beam, resulting in a lower value for the elastic critical bending moment M_{cr}. The opposite is true if the load is acts on the bottom flange, or under the shear centre. The beam is then stabilized against twisting and M_{cr} will be higher.

C_2 is linked to the vertical distance parameter z_j that describes the distance between the point of load application and the shear centre:

$$z_g = z_a - z_s$$

A rule of thumb is that z_g is negative if the load acts towards the shear centre, and positive if it acts away from the shear centre.

4.3.3 C_3-factor

A third C-factor is accounted for if the cross-section is assymetric about its major axis. It is not uncommon that I-beams have a larger top flange than bottom flange for example. C_3 is linked to the parameter z_j which is not as intuitive as z_g but is decided through the following formula:

$$z_j = z_s - 0.5 \int_A (y^2 + z^2) \frac{z}{I_y} dA \tag{4.58}$$

Since none of the beams studied in this thesis project have flanges of unequal size, the C_3-factor is also not used.

4.3.4 C-factors for some simple load cases

The C-factors are known approximately for basic loading cases such as simply supported and fixed beams with uniform or point load, as can be seen in Table 4.1.

Table 4.1: *C-factors for common load cases, from (Boissonnade et al., 2006)*

Loading and support conditions	Bending moment diagram	Values of k_z	Value of factors C_1	C_2	C_3
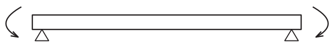		1.0	1.12	0.45	0.525
		0.5	0.97	0.36	0.478
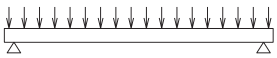		1.0	1.35	0.59	0.411
		0.5	1.05	0.48	0.338
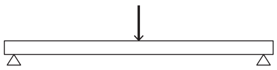	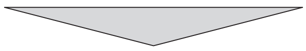	1.0	1.04	0.42	0.562
		0.5	0.95	0.31	0.539

4.3.5 End restraint coefficients k_w and k_z

End restraint coefficients k_w and k_z are equivalent to Euler buckling effective length factor L_{cr}/L, shown in Figure 4.9.

The factor k_w takes end warping conditions into account, and unless warping is prevented through special provisions, $k_w = 1.0$ (Bureau, 2006). End rotations about the z-axis are dealt with through k_z.

A beam with fork supports therefore has $k_w = k_z = 1.0$. If one end is fixed, these coefficients become 0.7 and if both ends are fixed they are 0.5.

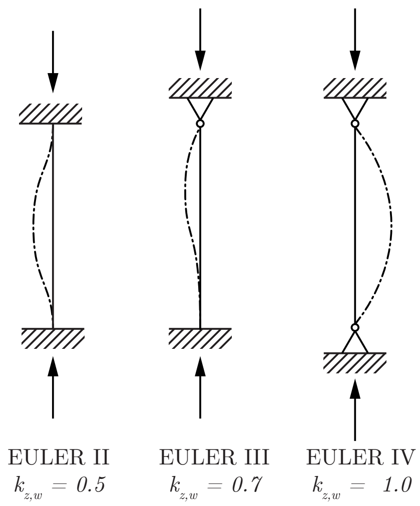

Figure 4.9: *Warping restraint coefficients k_w and k_z equivalent to Euler buckling lengths*

4.3.6 Simplified cases for M_{cr}

For the reference case, a doubly symmetric cross-section such as an I-beam, loaded with equally applied end moments and with fork supports, the terms with C-factors disappear in the formula, except for C_1 which becomes 1.0:

$$M_{cr,0} = \frac{\pi^2 EI_z}{L^2}\sqrt{\frac{I_w}{I_z} + \frac{L^2 GI_t}{\pi^2 EI_z}} \tag{4.59}$$

For the same beam loaded in its shear center, with either point load or linearly distributed load, the C_1-factor needs to be considered:

$$M_{cr} = C_1\frac{\pi^2 EI_z}{L^2}\sqrt{\frac{I_w}{I_z} + \frac{L^2 GI_t}{\pi^2 EI_z}} \tag{4.60}$$

If the beam is doubly symmetric but loaded along the vertical axis of the shear center, but not in the shear centre itself, the C_2-factor must be accounted for:

$$M_{cr} = C_1\frac{\pi^2 EI_z}{(k_z L)^2}(\sqrt{(\frac{k_z}{k_w})^2\frac{I_w}{I_z} + \frac{(k_z L)^2 GI_t}{\pi^2 EI_z} + (C_2 z_g)^2} - (C_2 z_g) \tag{4.61}$$

If the beam is loaded in its shear center but is singly symmetric, e.g. the top and bottom flanges are not equal, the C_3-term needs to be added:

$$M_{cr} = C_1\frac{\pi^2 EI_z}{(k_z L)^2}(\sqrt{(\frac{k_z}{k_w})^2\frac{I_w}{I_z} + \frac{(k_z L)^2 GI_t}{\pi^2 EI_z} - (C_3 z_j)^2 + (C_3 z_j)}) \tag{4.62}$$

4.4 Design methods in Eurocode 3

In Section 4.2 the elastic critical bending moment for equally applied end moments on a double symmetric cross-section with fork supports, M_{cr} was derived. The expression was then extended in Section 4.2 through the 3-factor formula, to allow for other load configurations and boundary conditions. As with column buckling it is possible to formulate an Ayrton-Perry expression to take residual stresses, initial geometric imperfection and unintended eccentric loading into account. The derivation is more advanced for lateral-torsional buckling, since it involves two degrees of freedom: lateral deflection v and twist φ. The initial imperfection v_0 and φ_0, relating to the first buckling Eigenmode of the beam, can be shown to have the following relation:

$$\frac{v_0}{\varphi_0} = \frac{M_{cr}}{N_{cr,z}} \tag{4.63}$$

where $N_{cr,z}$ is the elastic critical load for flexural buckling.

An Ayrton-Perry formulation for lateral-torsional buckling of beams can be found in its fullness in (Boissonnade et al., 2006), (Szalai and Papp, 2010) or (Taras and Greiner, 2010). The final end result is the same equation that was derived for column buckling in Section 3.3.3, but for beams the buckling reduction factor is instead labelled χ_{LT} and the generalized imperfection factor η_{LT}:

$$\chi_{LT} + \chi_{LT}\frac{\eta_{LT}}{1-\chi_{LT}\bar{\lambda}_{LT}^{2}} \leq 1.0 \tag{4.64}$$

The general imperfection for lateral-torsional buckling can be described as (Taras and Greiner, 2010):

$$\eta_{LT} = \frac{Ae_{0,d}}{W_{el}}\frac{\bar{\lambda}_{LT}^{2}}{\bar{\lambda}^{2}} \tag{4.65}$$

The first part is the generalized imperfection for columns η, but for η_{LT} the term $\frac{\bar{\lambda}_{LT}^{2}}{\bar{\lambda}^{2}}$ is also added.

In Eurocode 3, however, the generalized imperfection η_{LT} is still formulated in the same way as for the column buckling case:

$$\eta_{LT} = \alpha_{LT}(\bar{\lambda} - 0.2) \tag{4.66}$$

The so called buckling curves in Eurocode 3 were originally developed for flexural column buckling, but for simplicity a similar approach is applied for lateral-torsional buckling of beams (Taras and Greiner, 2010). There are two similar methods to calculate the buckling reduction factor χ_{LT}: the general case and an alternative procedure for rolled or equivalent welded sections, the former having a plastic limit of $\bar{\lambda}_{LT} = 0.4$ instead. There is also the possibility to use the general method for lateral and later-torsional method described in Section 4.4.4.

4.4.1 General case

According to Eurocode 3, beam bending moment capacity with regards to lateral torsional buckling is calculated the following way:

$$M_{b,Rd} = \chi_{LT} \frac{M_{y,Rd}}{\gamma_{M1}} \tag{4.67}$$

$M_{b,Rd}$ is the reduced buckling resistance capacity of a beam

$M_{y,Rd}$ is the cross-section bending moment resistance, and for a cross-section in class 1 this would be M_{pl}

γ_{M1} is a material partial factor, set to 1.0 in the latest Swedish version of Eurocode 3 (national parameter).

The buckling reduction factor χ_{LT} is decided through the following combination of equations:

$$\chi_{LT} = \frac{1}{\Phi_{LT} + \sqrt{\Phi_{LT}^2 - \bar{\lambda}_{LT}^2}} \leq 1.0 \tag{4.68}$$

where $\bar{\lambda}_{LT}$ is the non-dimensionless slenderness.

$$\Phi_{LT} = 0.5[1 + \alpha_{LT}(\bar{\lambda}_{LT} - 0.2) + \bar{\lambda}_{LT}^2] \tag{4.69}$$

$$\bar{\lambda}_{LT} = \sqrt{\frac{M_{pl}}{M_{cr}}} \tag{4.70}$$

The five buckling curves a_0, a, b, c and d come from the different values of the imperfection factor α_{LT} and give different reductions on the bending moment capacity. The imperfection factor depends on cross-section shape and whether it is a hot-rolled or welded section. The values of α_{LT} for the five buckling curves are the same as for column buckling, and are given in Table 4.2.

Table 4.2: *The imperfection factor α_{LT} and the corresponding buckling curves*

Buckling curve	a_0	a	b	c	d
Imperfection factor, α_{LT}	0.13	0.21	0.34	0.49	0.76

The general case only uses curves b,c and d, and the correct curves is decided from Table 4.3.

Figure 4.10 show the corresponding buckling curves.

Table 4.3: *Choice of buckling curve for general case*

Cross-section	Limits	Buckling curve
Rolled I-section	$h/b \leq 2$	b
	$h/b > 2$	c
Welded I-section	$h/b \leq 2$	c
	$h/b > 2$	d
Other		d

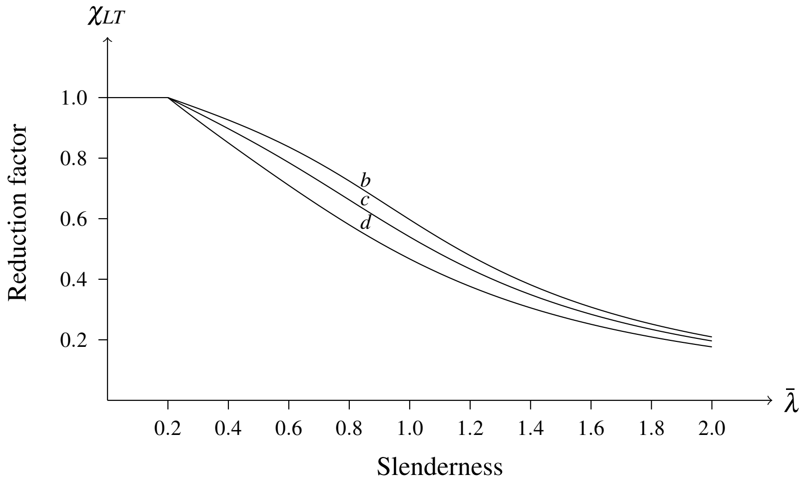

Figure 4.10: *General case buckling curves in Eurocode 3*

4.4.2 Alternative procedure for rolled sections or equivalent welded

Since the buckling curves for LT-buckling have not been as precise and well-defined as those for column buckling, extensive parametric simulations were carried out during a decade around 2000 using the GMNIA-technique (Geometrically and Materially Non-linear Imperfect Analyses). This method takes residual stresses, initial bow imperfection and material non-linearity into account, and represents reality well (Boissonnade et al., 2006).

The main focus was on I-sections, and here are some of the findings:

The study showed that the theoretical plateau-limit for $\bar{\lambda}_{LT}$ is about 0.25. Most codes already use a limit of 0.4 and therefore it was of interest to keep this number in design.

The studies resulted in a proposal of a slightly different way to calculate χ_{LT} using buckling curves. The procedure is as follows:

$$\chi_{LT} = \frac{1}{\Phi_{LT} + \sqrt{\Phi_{LT}^2 - \beta\bar{\lambda}_{LT}^2}} \leq 1.0 \tag{4.71}$$

$$\chi_{LT} \leq \frac{1}{\bar{\lambda}_{LT}^2} \tag{4.72}$$

$$\Phi_{LT} = 0.5[1 + \alpha_{LT}(\bar{\lambda}_{LT} - 0.4) + \beta\bar{\lambda}_{LT}^2] \tag{4.73}$$

$$\beta = 0.75$$

$$\bar{\lambda}_{LT} = \sqrt{\frac{M_{pl}}{M_{cr}}} \tag{4.74}$$

The buckling curve to use is decided through Table 4.4, and now the curve a is also available.

Table 4.4: *Choice of buckling curve for rolled or equivalent welded sections*

Cross-section	Limits	Buckling curve
Rolled I-section	$h/b \leq 2$	a
	$h/b > 2$	b
Welded I-section	$h/b \leq 2$	c
	$h/b > 2$	d
Other		d

The resulting buckling curves are illustrated in Figure 4.11.

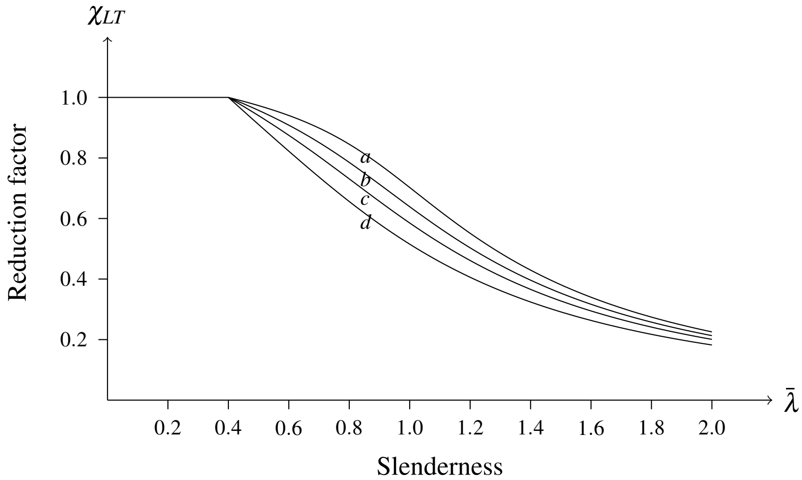

Figure 4.11: *Alternative procedure buckling curves in Eurocode 3*

Effect of moment distribution

To account for the moment distribution the following procedure is then followed:

$$\chi_{LT,mod} = \frac{\chi_{LT}}{f} \leq 1 \tag{4.75}$$

$$f = 1 - 0.5(1 - k_c)[1 - 2(\bar{\lambda}_{LT} - 0.8)^2] \leq 1 \tag{4.76}$$

The factor k_c depends on the moment diagram shape, see Figure 4.12.

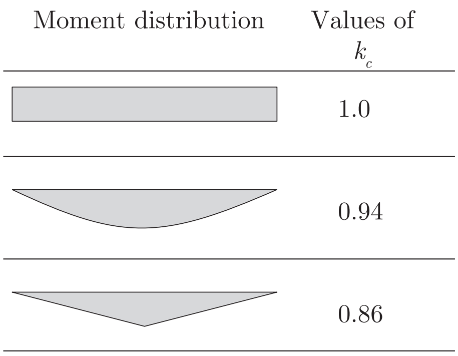

Figure 4.12: k_c *for some standard load cases*

For linear moment diagrams, $k_c = \dfrac{1}{1.33 - 0.33\Psi}$, and other cases can be found in graphs in Annex C in (Boissonnade et al., 2006).

4.4.3 Direct determination of $\bar{\lambda}_{LT}$ for simple cases

For certain cases there is no need to calculate M_{cr} to obtain $\bar{\lambda}_{LT}$. This is true for a beam subjected to transverse loads that acts through the shear center or if end moments are applied. Factor k_c takes the shape of the bending moment diagram into account and k_p the torsional stiffness of the cross-section. The formula is as follows: (Boissonnade et al., 2006)

$$\bar{\lambda}_{LT} = \bar{\lambda}_z k_p k_c \tag{4.77}$$

$$k_p = \frac{1}{[1 + \frac{1}{20}(\frac{\bar{\lambda}_z}{h/t_f})^2]^{0.25}} \tag{4.78}$$

h = the total height of the cross-section

t_f = the flange thickness

For rolled sections, k_p is reduced by factor 0.9.

4.4.4 The general method for lateral and lateral-torsional buckling combined

The general method, as described in Eurocode 3, for lateral and lateral-torsional buckling is particularly useful in combination with FE-analysis. The other methods mentioned here only deal with single members, but the general method can be used for both single members and whole frames. It can also deal with complex support conditions and non-uniform cross-sections.

The criterion to fulfill is:

$$\frac{\chi_{op}\alpha_{ult,k}}{\gamma_{M1}} \geq 1.0 \tag{4.79}$$

$\alpha_{ult,k}$ is the smallest load increase factor of the design loads to reach maximum capacity of the most critical section in the structure, but not considering lateral or lateral-torsional buckling.

χ_{op} is the reduction factor that takes into consideration lateral and lateral-torsional buckling, calculated from the slenderness factor $\bar{\lambda}_{op}$:

$$\bar{\lambda}_{op} = \sqrt{\frac{\alpha_{ult,k}}{\alpha_{cr,op}}} \tag{4.80}$$

$\alpha_{cr,op}$ is the smallest load increase factor of in-plane loads to cause elastic critical buckling in lateral or lateral-torsional buckling modes, but disregarding in-plane buckling.

χ_{op} is taken as the smallest of the two parameters χ and χ_{LT} according to Eurocode EN 1993-1-1 section 6.3.1 and 6.3.2. It is also possible to make an interpolation between these two values.

If $\alpha_{ult,k}$ is calculated through the following equation:

$$\frac{1}{\alpha_{ult,k}} = \frac{N_{Ed}}{N_{Rk}} + \frac{M_{y,Ed}}{M_{y,Rk}} \tag{4.81}$$

the resulting equation is (if the smallest of χ and χ_{LT} is taken):

$$\frac{N_{Ed}}{N_{Rk}/\gamma_{M1}} + \frac{M_{y,Ed}}{M_{y,Rk}/\gamma_{M1}} \leq \chi_{op} \tag{4.82}$$

If an interpolation is used then the equation instead looks like this:

$$\frac{N_{Ed}}{\chi N_{Rk}/\gamma_{M1}} + \frac{M_{y,Ed}}{\chi_{LT} M_{y,Rk}/\gamma_{M1}} \leq 1.0 \tag{4.83}$$

4.5 Design of channel beams

Lateral-torsional buckling of channel beams is not explicitly treated in Eurocode 3. The general method as presented in Section 4.4.4 could be used as it applies to all cross-sections and load cases.

When examining the research available on the design of channel beams, one realizes that there are few articles published on this matter. Some of them deal with lipped channel beams, which have stiffeners along the flange edges, and are therefore not applicable here. There is one relevant article in recent years found, however, published by (Snijder et al., 2008).

The article describes a number of possible design methods regarding lateral-torsional buckling of channel beams, then presents a new suggestion on a buckling curve for channel beams.

4.5.1 Modified κ_M-method

The method given in (DIN, 1990) is similar to Eurocode 3.

$$\frac{M}{\kappa_M M_{pl}} \leq 1.0 \tag{4.84}$$

M	is the design bending moment resistance of the cross-section.
M_{pl}	is the plastic bending moment resistance.
κ_M	is the buckling reduction factor, calculated differently than in Eurocode 3:

$$\kappa_M = (1 + \bar{\lambda}_M^5)^{-0.4} \tag{4.85}$$

The slenderness is, as in Eurocode 3, calculated in the following way:

$$\bar{\lambda}_M = \sqrt{\frac{M_{pl}}{M_{cr}}} \tag{4.86}$$

However, when dealing with channel beams an addition is made due to the torsional moment that arises:

$$\bar{\lambda}_{MT} = \bar{\lambda}_M + \bar{\lambda}_T \tag{4.87}$$

The added factor $\bar{\lambda}_T$ depends on the slenderness of the cross-section in the following way:

$$\bar{\lambda}_T = 1.11 - \bar{\lambda}_M \text{if } 0.5 \leq \bar{\lambda}_M < 0.75 \tag{4.88}$$

$$\bar{\lambda}_T = 0.69 - 0.44\bar{\lambda}_M \text{if } 0.75 \leq \bar{\lambda}_M < 1.14 \tag{4.89}$$

$$\bar{\lambda}_T = 0.19 \text{if } \bar{\lambda}_M \geq 1.14 \tag{4.90}$$

The resulting design curve is shown in Figure 4.13.

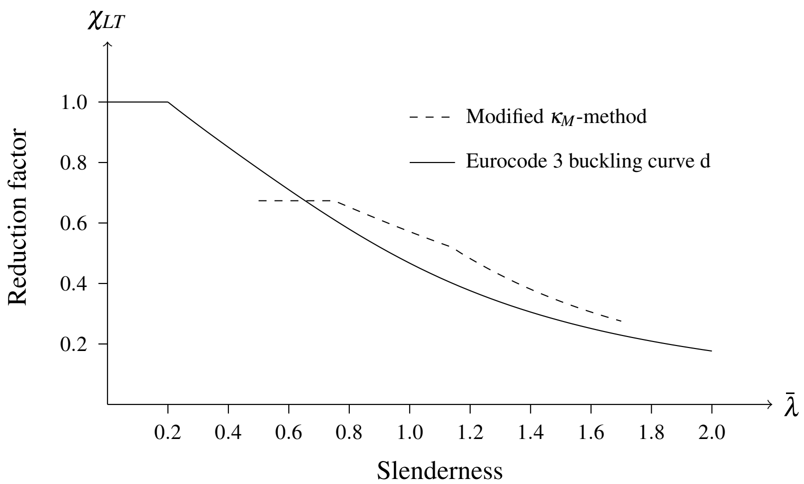

Figure 4.13: *Design curve for κ_M-method*

4.5.2 Modified χ_{LT}-method

By combining the Eurocode 3 equation for the reduction factor χ_{LT} and the added effect of torsion these equations are attained:

$$\chi_{LT} = \frac{1}{\Phi_{LT} + \sqrt{\Phi_{LT}^2 - \bar{\lambda}_{MT}^2}} \tag{4.91}$$

$$\Phi_{LT} = 0.5[1 + \alpha_{LT}(\bar{\lambda}_{MT} - 0.2) + \bar{\lambda}_{MT}^2] \tag{4.92}$$

Here $\bar{\lambda}_{MT}$ is the same as described in Equation (4.87).

The resulting design curve is presented in Figure 4.14

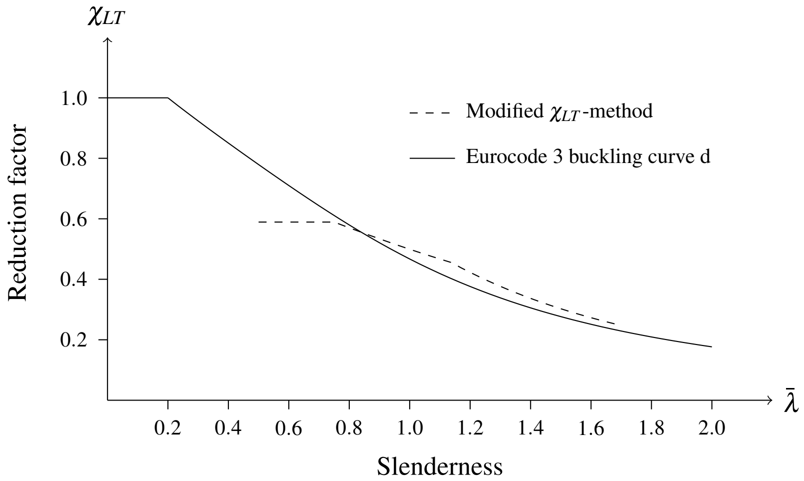

Figure 4.14: *Design curve for modified χ_{LT}-method*

4.5.3 Simplified design rule

A large investigation with both Finite Element Analyses and experimental analyses carried out in Germany led to a general design rule for combined bending and torsion on I- and channel section beams (Lindner and Glitsch, 2004).

$$\frac{M}{\chi_{LT} M_{pl,y}} + C_{mz}\frac{M_z}{M_{pl,z}} + k_{zw} k_w \alpha \frac{M_\omega}{M_{pl,\omega}} \leq 1.0 \tag{4.93}$$

Channel beams loaded at the web with a vertical load are not subjected to a bending moments around the z-axis, M_z is then 0 and the design rule is simplified:

$$\frac{M}{\chi_{LT} M_{pl}} + k_w \alpha \frac{M_\omega}{M_{pl,\omega}} \leq 1.0 \tag{4.94}$$

M is the design bending moment resistance of the cross-section. Solving for the design moment requires trial and error calculation and is explained further in Appendix C.

M_ω is the applied warping bi-moment.

$M_{pl,\omega}$ is the plastic bi-moment capacity.

k_w is a factor depending on the effect of the torsional moment:

$$k_w = 0.7 - 0.2\frac{M_\omega}{M_{pl,\omega}} \tag{4.95}$$

α is the amplification factor, according to the equation:

$$\alpha = \frac{1}{1 - \dfrac{M}{M_{cr}}} \tag{4.96}$$

This method does not result in a general buckling curve since it is load case and boundary condition dependant. The procedure in Appendix C has been followed to calculate the design curve for a UPE160-beam subjected to distributed load at the mid web, resulting in the design curve in Figure 4.15.

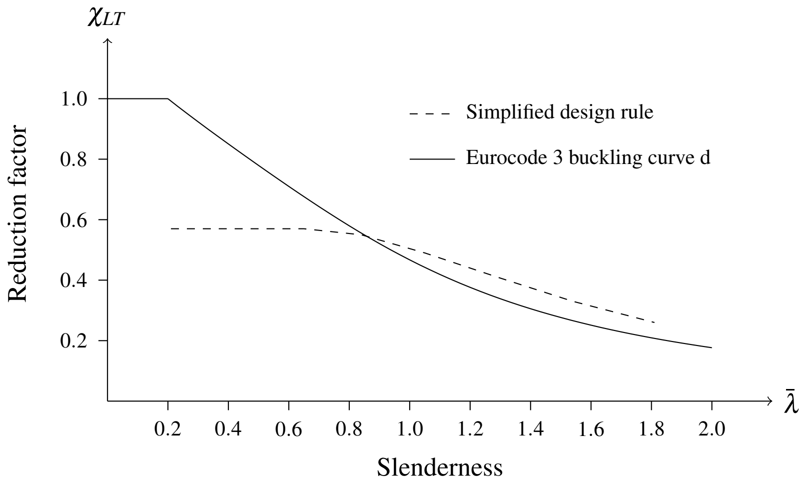

Figure 4.15: *Design curve for simplified design rule*

4.5.4 General method

The general method is possible to use for channel sections and has been described in Section 4.4.4.

4.5.5 Snijder design curve

A parametric study on channel beams was performed in 2008 by (Snijder et al., 2008). The article mentions briefly how the FE-model was set up with boundary conditions, load application and choice of elements.

From the results of the study, the researchers present a new suggestion to a buckling curve that could be used in accordance with Eurocode 3 but taking the torsional effect into account in the following way:

$$\chi_{LT} = \frac{1}{\Phi_{LT} + \sqrt{\Phi_{LT}^2 - \bar{\lambda}_{MT}^2}} \tag{4.97}$$

$$\Phi_{LT} = 0.5[1 + \alpha_{LT}(\bar{\lambda}_{MT} - 0.2) + \bar{\lambda}_{MT}^2] \tag{4.98}$$

Buckling curve a_0 is used:

$$\alpha_{LT} = 0.21 \tag{4.99}$$

$$\bar{\lambda}_{MT} = \bar{\lambda}_M + \bar{\lambda}_T \tag{4.100}$$

$$\bar{\lambda}_M = \sqrt{\frac{M_{pl}}{M_{cr}}} \tag{4.101}$$

The effect of torsion is considered by the added term $\bar{\lambda}_T$

$$\bar{\lambda}_T = 1.0 - \bar{\lambda}_M \text{ if } 0.5 \leq \bar{\lambda}_M < 0.8 \tag{4.102}$$

$$\bar{\lambda}_T = 0.43 - 0.29\bar{\lambda}_M \text{ if } 0.8 \leq \bar{\lambda}_M < 1.5 \tag{4.103}$$

$$\bar{\lambda}_T = 0 \text{ if } \bar{\lambda}_M \geq 1.5 \tag{4.104}$$

Figure 4.16 shows the suggested channel beam buckling curve plotted in a graph along with buckling curve d according to the general case in Eurocode 3.

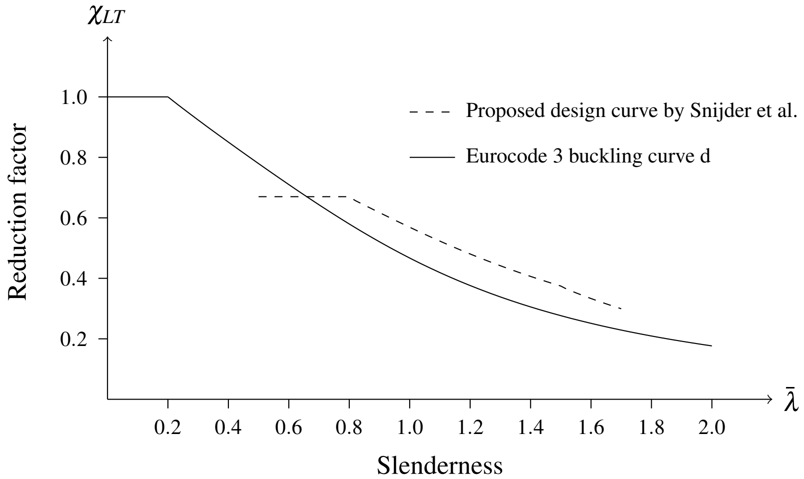

Figure 4.16: *Suggested channel beam design curve curve by (Snijder et al., 2008)*

5 Parametric study

A parametric study was performed on steel channel beams with strength class S355 and of UPE profile type. The chosen parameters were cross-section size, beam length and load case. It was deemed appropriate to use three different profiles, partly to evaluate the correctness of the modelling of boundary conditions: one of the smaller (UPE100), one of the larger (UPE220) and one in between (UPE160). Geometric properties for these are shown in Table 5.1.

Table 5.1: *Beam section properties for profiles UPE100, UPE160 and UPE220*

Section	**UPE100**	**UPE160**	**UPE220**
h_w(mm)	85	141	196
b_f(mm)	55	70	85
t_f(mm)	7.5	9.5	12
t_w(mm)	4.5	5.5	6.5
$I_y(\times 10^6\,\mathrm{m}^4)$	2.00	8.83	26.2
$I_z(\times 10^6\,\mathrm{m}^4)$	0.38	1.05	2.44
$I_w(\times 10^9\,\mathrm{m}^6)$	0.64	4.66	20.5
$I_t(\times 10^4\,\mathrm{m}^4)$	1.83	4.84	11.7

A number of different beam lengths were chosen for each load case, to create a spread of beam slenderness $\bar{\lambda}_{LT}$ approximately between 0.6 and 1.7. This is in the intermediate buckling region (although there is no clear definition for it) where the theory says that residual stresses and initial imperfections have the most influense. The effect of the shape of the moment diagram, i.e. the C_1-factor, in the 3-factor formula implies that the beam lengths for the end moment load case will be slightly shorter than for example those in the linearly distributed load case in order to have the same slenderness, if the maximum resulting bending moment is the same.

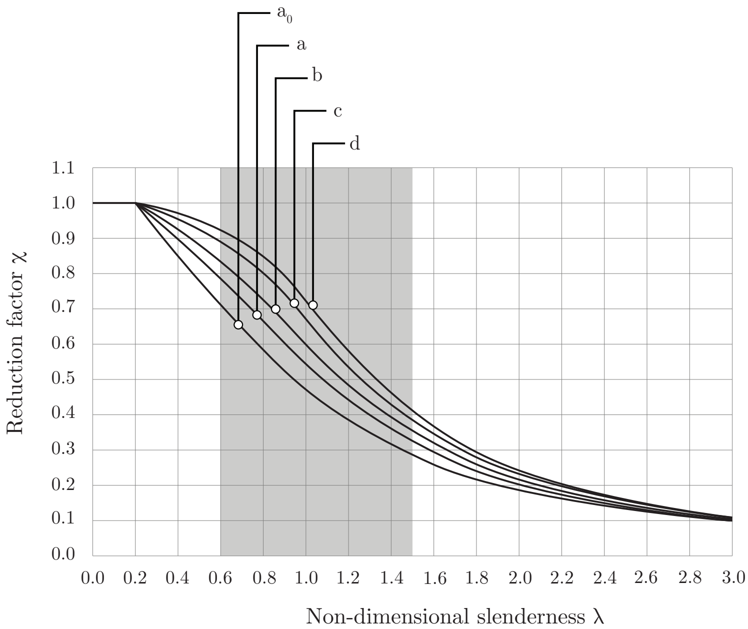

Figure 5.1: *Spread of $\bar{\lambda}_{LT}$-values in the parametric study*

5.1 Load cases

Three standard load cases were studied: end moment loading, uniformly distributed load and a point load in the mid span. The specifics are given under respective section below.

5.1.1 End moment loading

The load case that applies end moments to a channel beam, seen in Figure 5.2, is a good starting point since no load eccentricity is introduced in the beam. The results are therefore expected to follow ordinary buckling curves well. As mentioned earlier, the elastic critical moment from the 3-factor formula also uses this load case with fork supports as the reference case.

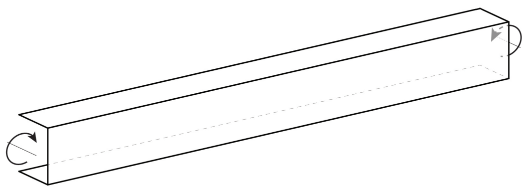

Figure 5.2: *Load case: Applied end moments*

For the lengths of analysed beams for the end moment load case, see Table 5.2.

5.1.2 Linearly distributed load at mid web: varying cross sections

For the mid web loading, the three cross-sections UPE100, UPE160 and UPE220 were compared. The load case is portrayed in Figure 5.3 and the chosen beam lengths can be found in Table 5.3.

Table 5.2: *Lengths of beams for load case applied end moments*

Profile	**Lengths** (mm) **Slenderness** , $\bar{\boldsymbol{\lambda}}_{LT}$				
UPE100	1000 0.59	1600 0.82	2300 1.02	3200 1.22	4700 1.49
UPE160	1200 0.60	1800 0.81	2500 1.02	3500 1.25	5000 1.53
UPE220	1400 0.59	2000 0.78	2800 1.00	4000 1.26	5500 1.51

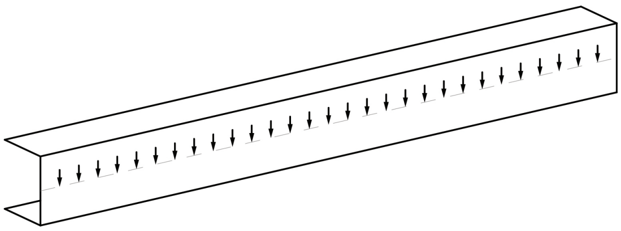

Figure 5.3: *Linearly distributed load: varying of cross-section*

Table 5.3: *Lengths of beams for linearly distributed load, varying of cross-section*

Profile	**Lengths** (mm) **Slenderness** , $\bar{\boldsymbol{\lambda}}_{LT}$				
UPE100	1200 0.64	1800 0.83	2600 1.03	3600 1.23	5200 1.49
UPE160	1400 0.64	2000 0.83	2800 1.03	4000 1.28	5500 1.52
UPE220	1600 0.62	2200 0.79	3000 0.99	4200 1.22	6000 1.50

5.1.3 Linearly distributed load: varying of point of load application

To study the effect of point of load application, the beam cross-section size does not need to be varied. Therefore only UPE160 beams with different lengths were loaded at top of web and bottom of web, see fig Figure 5.4 and Table 5.4. The linearly distributed load case at mid web with UPE160 from last section is also used as results.

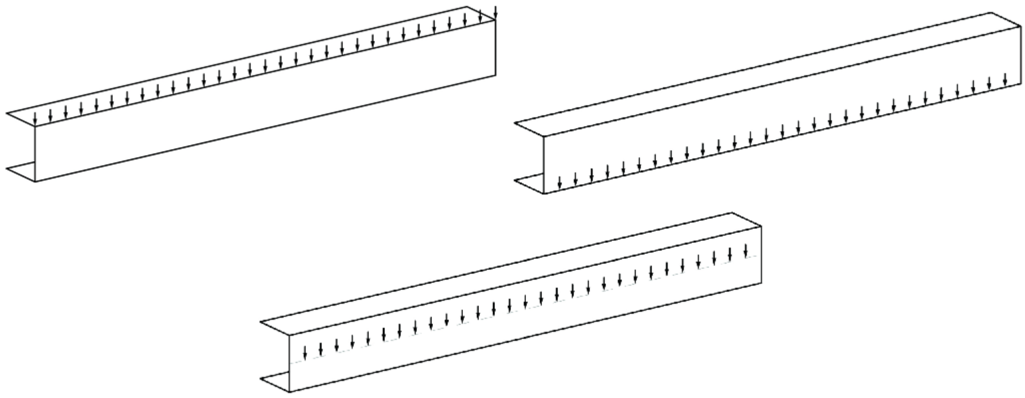

Figure 5.4: *Linearly distributed load: Varying point of load application*

It was decided to use the same lengths on the beams regardless of point of load application. The beams that would have a slenderness, $\bar{\lambda}_{LT}$, under 0.6 or above 1.7 were however not analysed, which means that the beams with lengths 2000, 2800, 4000 and 5500 mm were analysed for all points of load applications. Beam lengths of 1400 mm were analysed for top web and mid web loading and 7500 mm were analysed only for bottom web loading.

Table 5.4: *Lengths of beams for linearly distributed load, varying of PLA*

Profile	**Lengths** (mm) **Slenderness** , $\bar{\boldsymbol{\lambda}}_{LT}$				
Top web	1400 0.77	2000 0.97	2800 1.17	4000 1.40	5500 1.63	
Mid web	1400 0.64	2000 0.83	2800 1.03	4000 1.28	5500 1.52	
Bottom web		2000 0.71	2800 0.91	4000 1.16	5500 1.42	7500 1.70

5.1.4 Point load

For the point load, a single series of UPE160 beams were analysed. The load is applied in the middle of the web in mid span, see Figure 5.5. The chosen beam lengths can be found in Table 5.5.

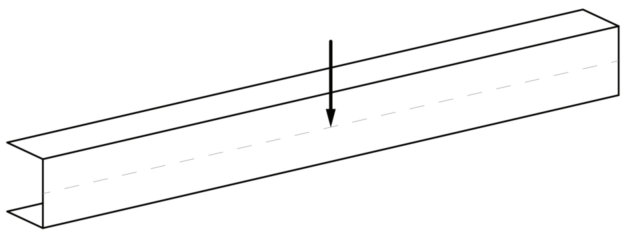

Figure 5.5: *Load case: point load*

Table 5.5: *Lengths of beams for point load*

Profile	Lengths (mm) Slenderness , $\bar{\lambda}_{LT}$				
UPE100	1400 0.65	2000 0.81	2800 0.98	4000 1.18	5500 1.40
UPE160	1800 0.70	2500 0.87	3600 1.09	4800 1.29	6000 1.45
UPE220	1400 0.67	2000 0.79	2800 0.99	4000 1.23	5500 1.54

5.2 Boundary conditions

The beams were modeled with the boundary conditions known as fork supports which allows warping, see Section 2.9 and Figure 5.6. The method used to accomplish fork support behaviour in the FE-model is described in Section 6.3.3.

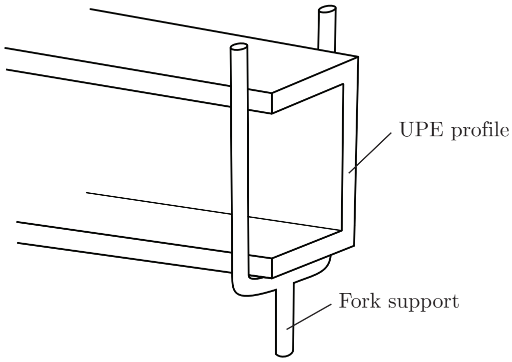

Figure 5.6: *Fork support. Adopted from Höglund, (2006).*

5.3 Two methods of GMNIA

The most advanced method to determine the buckling strength capacity of steel beams is through a Geometrically and Materially Non-lInear Analysis which includes imperfections (Schneider, 2006). The shape of the failing buckling mode for the structure is first generated and then applied in a second analysis as an initial geometric imperfection.

Eurocode 3 states that one of two methods might be used in design:

- An equivalent geometric initial imperfection is applied to the beam, and the maximum deflection is set to the length of the beam divided by a certain number, which depends on the cross-section. According to Table 5.6, from Eurocode 3 (1993-1-1 section 5.3.2), a channel beam would fall under buckling curve d and so the magnitude of the geometric imperfection is set to L/150. This is to account for initial bow imperfection, residual stresses and unintended load eccentricity.

Table 5.6: *Equivalent geometric imperfection according to Eurocode 3*

Buckling curve	**Equivalent geometric imperfection**
a_0	$L/350$
a	$L/300$
b	$L/250$
c	$L/200$
d	$L/150$

- An initial imperfection with maximum deflection of the length divided by 1000 is applied, and the effect of residual stresses is explicitly taken into account. The value L/1000 is taken from the fact that this is a common manifacturing tolerance limit for unintended initial out-of-straightness for structural members.

The two methods are described in table format in Table 5.7.

Table 5.7: *Two different methods to apply GMNIA according to Eurocode 3*

Method	**Initial imperfection**	**Residual stresses**
Method one	$L/150$	Not included
Method two	$L/1000$	Included

In this study, the method that uses an equivalent bow imperfection of L/150 will mainly be used, but the application of residual stresses is performed as a comparison for the same series of beams for the end moment load case on UPE160.

6 Finite Element Model

6.1 General overview of FEM-program ANSYS

ANSYS, Inc. is a company in the USA that develops computer-aided engineering software (CAE) which gives the user the ability to analyse and simulate different situations concerning electronics, fluid dynamics and structural analysis. The software is centered on an instance called Workbench where the simulation is set up in a tree-like manner, where different components are dropped to the canvas and interconnected to other components. Different parameters can be initialized in each component and controlled on a global scale in Workbench. In Engineering Data, which is present in each of the analysis components, the material is specified and can also be viewed in Workbench. A simple example for a structural analysis is set-up in Figure 6.1. The first box presents the geometry and the second is the analysis to be performed.

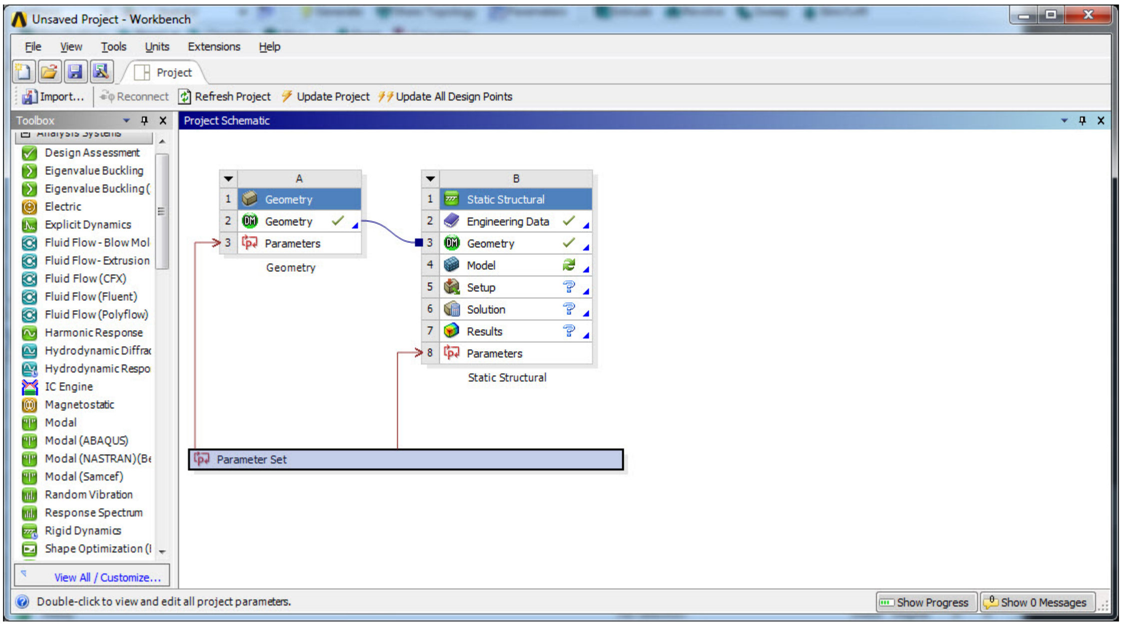

Figure 6.1: *Graphic overview of Workbench in ANSYS*

The parameters that are created can be viewed and controlled in Workbench, see Figure 6.2. In the top right corner Table of Design Points is placed where rows can be added to extend the simulation.

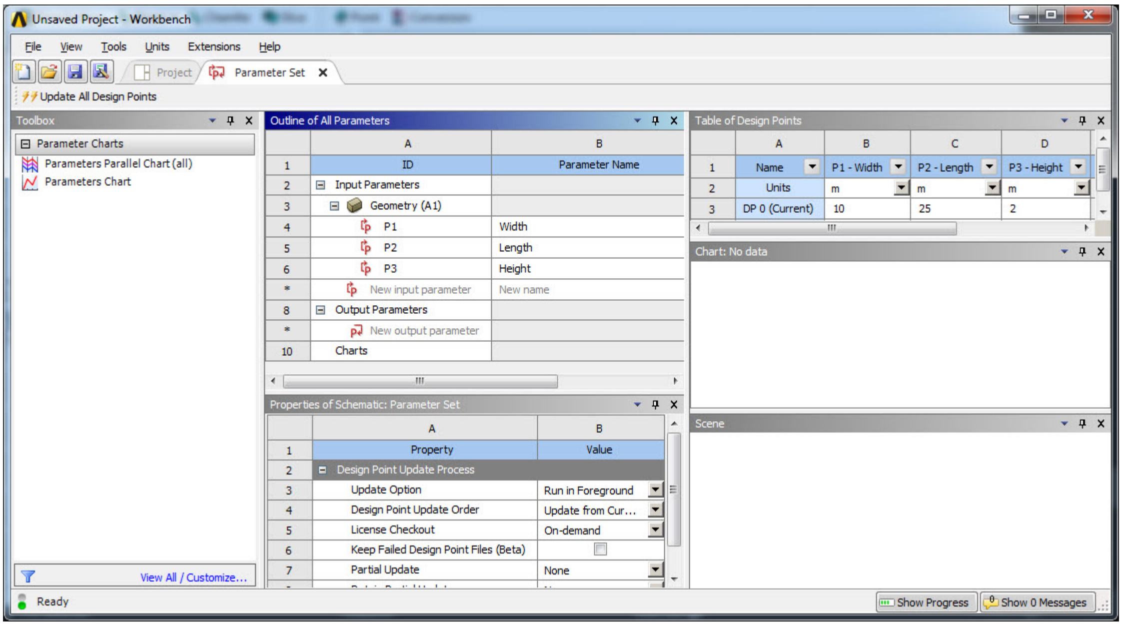

Figure 6.2: *Control of analysis parameters*

The geometry is either defined in a built-in instance called DesignModeler, see Figure 6.3, or externally in a program such as SolidWorks by Autodesk. In DesignModeler parameters can be initialized such as the length, width and height of structural components and these can be externally controlled in Workbench.

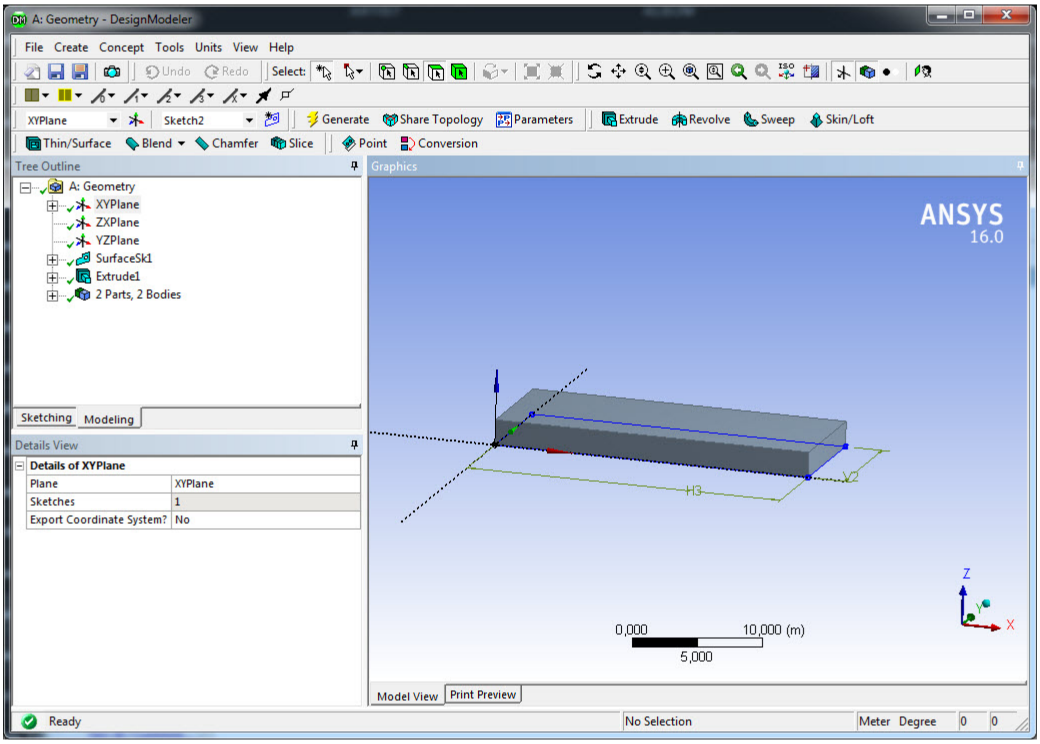

Figure 6.3: *Building geometry in DesignModeler*

When it comes to the analysis itself, all is controlled in yet another instance called Mechanical, see Figure 6.4, which adapts to the specific analysis component chosen in Workbench. Here, the geometry is imported from the previously defined geometry component. In the model, the user has the ability to define the density of the Finite Element mesh and what type of element to use. In ANSYS there exists many different element types for 1D, 2D and 3D geometry and the elements are chosen according to the best fit to the analysis.

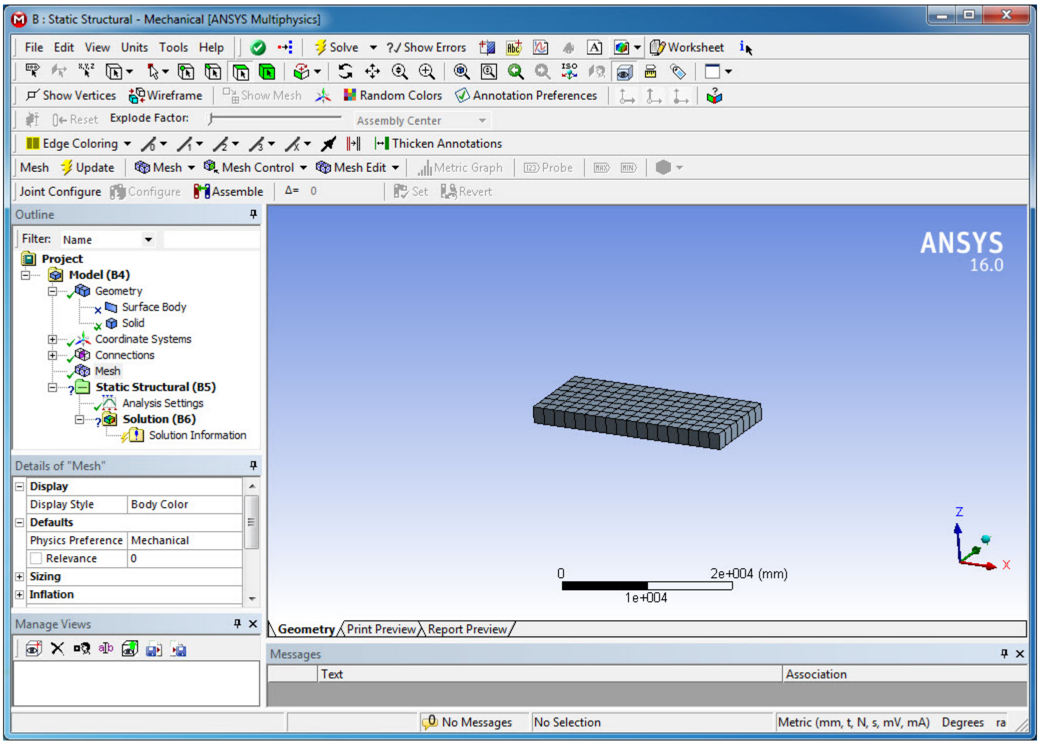

Figure 6.4: *Analysis specifics performed in Mechanical*

6.2 Schematic description of Finite Element analysis steps

The FE-analysis was made in two steps. The first step is to perform a linear Eigenvalue buckling analysis where the first buckling mode is found, and that shape is then used as a geometric imperfection for consequent collapse analysis. Geometry, elements, meshing and boundary conditions are the same for both analyses, but linear buckling is performed with linear elastic material whereas the collapse analysis is made with a bi-linear material simulating an elastic-plastic stress-strain curve with low strain hardening. This is explained further in Section 6.3.2. Figure 6.5 shows a schematic figure of the analysis setup steps.

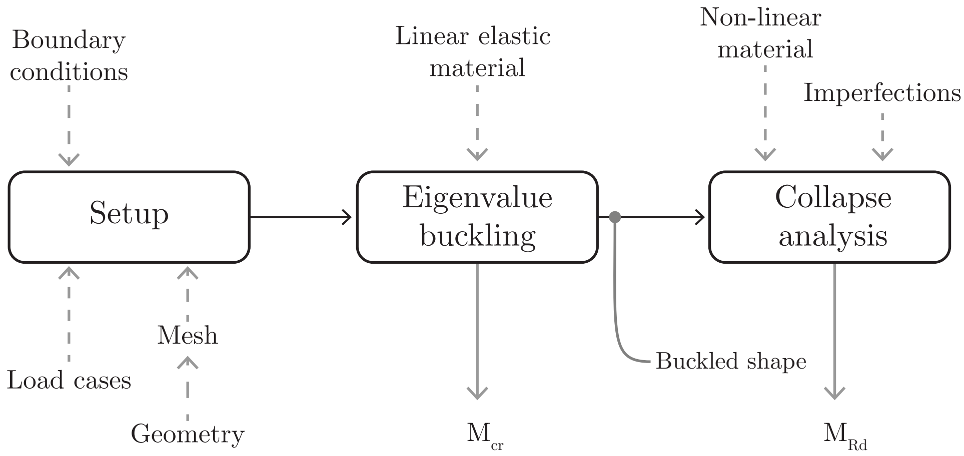

Figure 6.5: *Schematic figure showing the setup in ANSYS*

6.3 Analysis setup

6.3.1 Geometry and choice of elements

The Finite Element structure was built with ANSYS shell elements "SHELL181", which is a 4-node element with 6 degrees of freedom for each node. These include translational dof in x,y, and z-direction as well as rotational dof around the x,y and z-axes. This shell element is suitable for non-linear applications with large strain and large rotation. Shell elements are good to use for slender structures, where the stress doesn't vary much through the thickness of a material, which is the case for the cross-sections considered (Snijder et al., 2008).

At the supports additional stiff beam elements were added, see comment in Section 6.3.3.

The beam geometry was split in half at the x-midpoint and along the web at the y-midpoint, see image below. In this way the load can be placed directly at the nodes created by the geometry, which is shown in Figure 6.6.

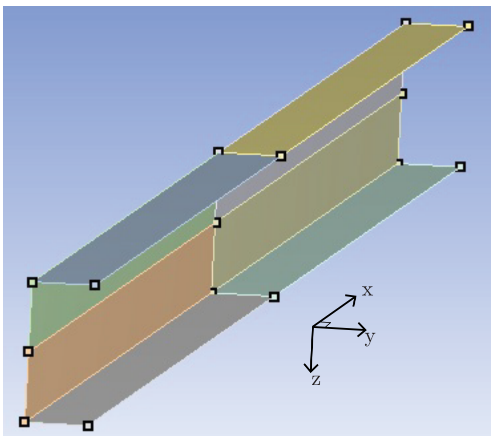

Figure 6.6: *Geometry of a beam built with shell elements*

6.3.2 Material model and properties

Steel with a yield strength of 355 MPa was used in the parametric study. A bilinear material model was used for the collapse analysis, shown on the right in Figure 6.7.

Young's modulus has been set to $E = 210$ GPa and the tangent modulus to $E_T = E/10000$. Eurocode 3 states that a tangent modulus of $E_T = E/10000$ or $E_T = E/100$ might be used, depending on if strain hardening effects are to be neglected or accounted for. The first alternative was chosen to rule out any unwanted effects of strain hardening. The stress levels therefore cannot reach much higher than the yield stress of 355 MPa.

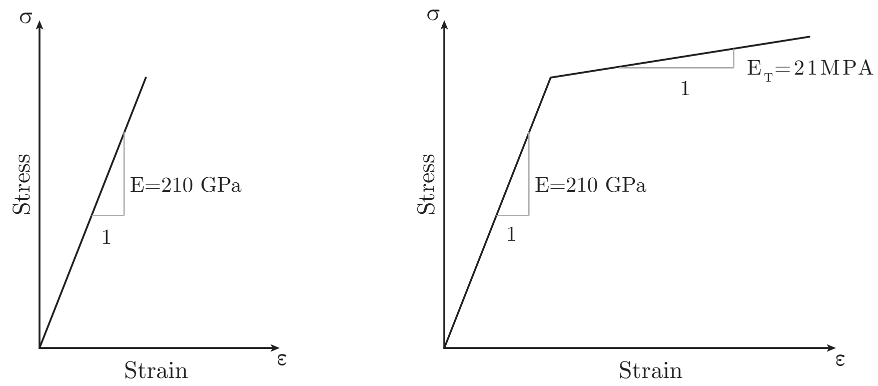

Figure 6.7: *Linear (left) and bilinear (right) material model for steel S355*

6.3.3 Applying boundary conditions

To set up fork support conditions, stiff beam elements as can be seen in Figure 6.8 were added along the edges of the cross-section. These elements allow the flanges to warp freely, and at the same time prevent the cross-section to distort locally. Unless these beam elements are used, the beam ends can distort. The beam elements are made of a very stiff material with Young's modulus $E = 10^{16}$ Pa. The width in global x-direction is 0.2 mm and in transverse direction (global y-direction for the web and global z-direction for the flanges) 5 mm.

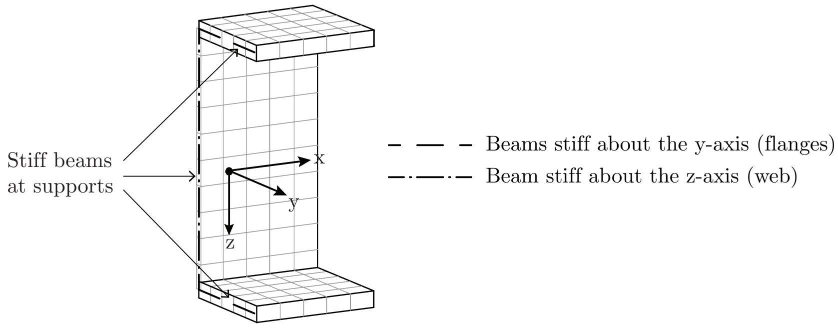

Figure 6.8: *Stiff beam elements along edges at supports*

The web midpoint was locked in x-,y- and z-directions for one support and y- and z-direction at the other. The beam has to be locked somewhere in the x-direction to avoid rigid body motion, but if both supports are fixed in the x-direction then the beam cannot shorten as it deflects vertically and laterally. The boundary conditions are shown graphically in Figure 6.9.

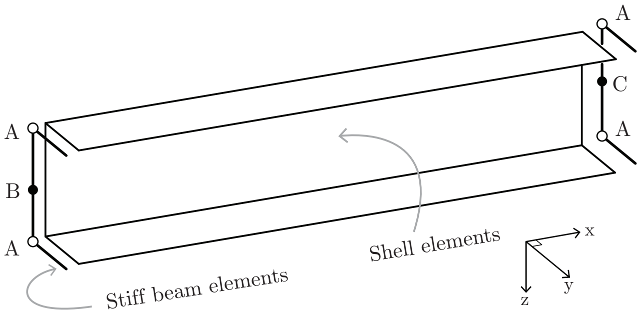

Points	X	Y	Z
A		✓	
B	✓	✓	✓
C		✓	✓

Figure 6.9: *Boundary conditions to resemble fork support*

6.3.4 Control of boundary conditions

To check the validity of the boundary conditions, the elastic critical eigenvalue buckling loads in terms of M_{cr} from the FE-analyses are compared to the value predicted by the 3-factor formula as explained in Section 4.3. The load case is applied end moments on UPE160 beams and the results are found in Table 6.1.

Table 6.1: *Comparison of elastic critical moment, 3-factor formula and FEM*

Beam length (mm)	$\boldsymbol{M_{cr,3\text{-}factor}}$ **(kNm)**	$\boldsymbol{M_{cr,FEM}}$ **(kNm)**	**Error (%)**
1200	121.76	115.77	4.9
1800	65.88	63.93	3.0
2500	42.44	41.38	2.5
3500	28.25	27.57	2.4
5000	18.96	18.50	2.5

The normal stresses in the x-direction are also examined. For a fork support with linearly distributed load, the normal stresses at the end of the beam are supposed to be zero as the beam is free to rotate around its y- and z-axes, and the flanges are free to warp. Some of these properties can be verified in Figure 6.10.

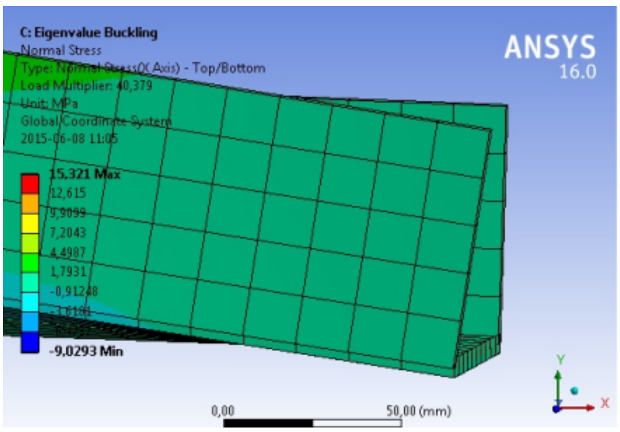

Figure 6.10: *Warping of flanges and visual examination of normal stresses*

6.3.5 Meshing

To create finite elements with close to quadratic shape and still keep the same mesh subdivision technique for the three cross-sections it was decided to divide the flanges into five subparts and the web into ten subparts. The properties for the three studied beam sections UPE100, UPE160 and UPE220 are found in Table 6.2. The term "size ratio" means the fraction between the lengths in the mesh elements two directions, and is displayed to show that the mesh elements are square or close to square.

Table 6.2: *Mesh element size description*

	Cross Section	UPE100	UPE160	UPE220
	Width, flange (mm)	52.75	67.25	81.75
	Height, web (mm)	92.5	150.5	208
Element size	Width, flange (mm)	10.55	13.45	16.35
	Height, web (mm)	9.25	15.05	20.8
	Length along beam (mm)	9.25	15.05	20.8
	Size ratio, flanges	0.88	1.12	1.27
	Size ratio, web	1.00	1.00	1.00

6.3.6 Mesh convergence

A more refined mesh would be ideal but given the total number of computer analyses to be made, the number of elements had to be limited somewhat. To study the effects of mesh size a number of analyses were made on a single cross-section with an increasingly more refined mesh according to the numbers in Table 6.3. The beam chosen was of cross-section UPE160 and with length of 3.5m.

Table 6.3: *Mesh convergence for linear buckling analysis*

Flange subdivision	Web subdivision	Total nr of elements	Buckling load multiplication factor, ANSYS
3	6	1680	4.54
4	8	2976	4.50
5	10	4660	4.47
6	12	6696	4.45
8	16	11904	4.43
10	20	18600	4.41
12	24	26784	4.40

With increased mesh density the buckling factor seems to converge at $\lambda = 4.40$. It was chosen to use 5 elements in the flanges and 10 elements in the web, since a denser mesh increased the time needed for the analyses beyond what was considered reasonable. The chosen mesh for this study resulted in $\lambda = 4.475$. This suggests that the results might be slightly unconservative (about 1.6 percent in this case).

6.4 Linear eigenvalue buckling

ANSYS formulates linear buckling problems through an Eigenvalue problem[1]:

$$([K] + \lambda_i [S]) \psi_i = 0$$

[K] = stiffness matrix

[S] = stress stiffness matrix

λ_i = ith eigenvalue, load multiplication factor

ψ_i = ith eigenvector, displacements

Only the buckling mode for the lowest critical load is of interest for this specific project. For a beam transversally loaded and with fork supports, the first buckling mode will be similar to the one seen in Figure 6.11, which is the lateral-torsional buckling load. The magnitude of the applied load P_{base} is set to a value lower than expected buckling load. The result of such analysis is a load multiplication factor λ that is multiplied with the applied load P_{base} to get the critical buckling load $P_{cr,FEM}$.

$$P_{cr,FEM} = \lambda \cdot P_{base}$$

Depending on the load case, the elastic critical bending moment $M_{cr,FEM}$ is then derived.

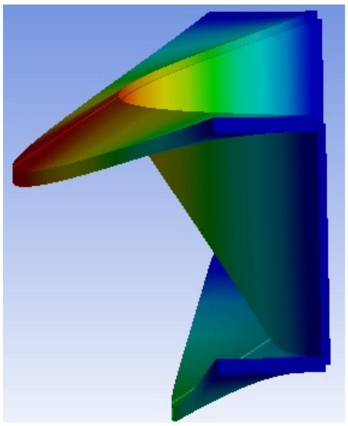

Figure 6.11: *Shape of buckled beam from ANSYS linear eigenvalue buckling analysis*

6.5 Collapse analysis

6.5.1 Modelling of residual stresses

Table values of residual stresses for many I-sections exist but this is not the case for channel sections. The residual stresses were therefore modelled from the suggestion of (Snijder et al., 2008) as can be seen in Figure 6.12. Positive numbers represent tension and negative numbers compression.

[1]ANSYS help manual

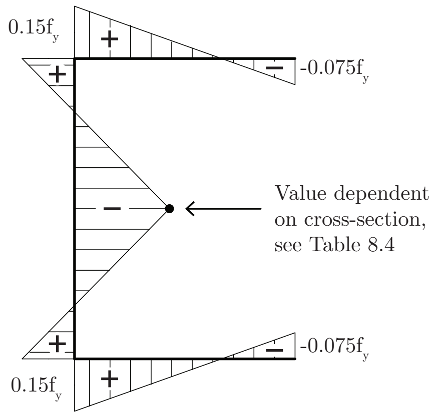

Figure 6.12: *Residual stresses in a channel section*

Where flanges and web meet, the stress is set to $0.15 \cdot f_y$ and at the ends of the flanges to $-0.075 \cdot f_y$. To create force equilibrium in the cross-section the value in the middle of the web is adjusted according to the specific profile, see Table 6.4.

Table 6.4: *Maximum compression value from residual stresses in middle of web*

Profile	**Max compression stress, web**
UPE100	$-0.293 \cdot f_y$
UPE160	$-0.266 \cdot f_y$
UPE220	$-0.209 \cdot f_y$

In order to apply residual stresses into each shell element, the command "INISTATE" in ANSYS was used, and the code with explanation is found in Appendix F. "INISTATE" means "initial state" and is given as start value before the actual analysis start. Note that the stress is applied equally over the integration points in one element, which means that there will be a clear difference in applied stress between adjacent elements, creating the stair pattern in Figure 6.13.

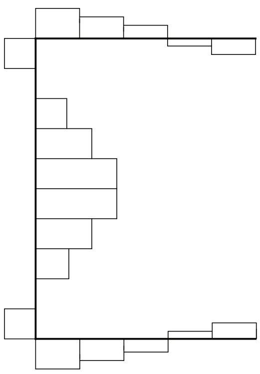

Figure 6.13: *Actual application of residual stresses in each shell element*

The resulting normal stress levels as shown in the 3d-model in ANSYS is shown in Figure 6.14.

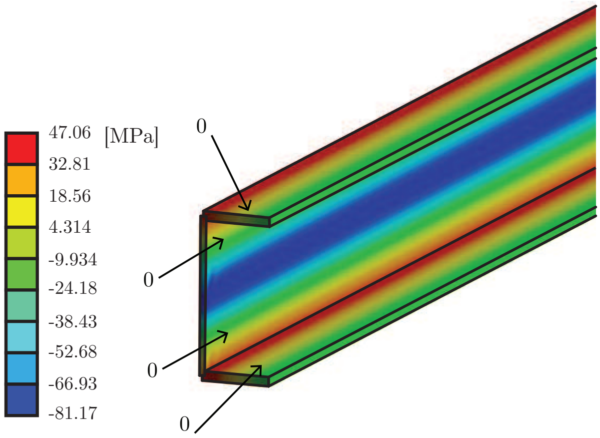

Figure 6.14: *Resulting normal stresses from application of residual stresses*

6.5.2 Load increment in collapse analysis

For end moments and linearly distributed load, the load was applied with maximum 200 increments until the FE-analysis could not reach convergence anymore. The maximum load was set to a reasonable value in relation to expected load-carrying capacity for the specific beam and load case. To verify that the number of increments was sufficient enough, the steps were increased five times to maximum 1000 increments and it was noted that the final results were very similar, differing with maximum 0.5 %.

For the point load case, instead a displacement-controlled analysis was made. In this analysis type, the point where the force is supposed to act was deflected step-wise downwards, meaning negative global z-direction. The deformation is set to act in the z-direction, but the point is free to move in x- and y-direction. A fictituous support is therefore placed at the point of load application, and the reaction force can be evaluated by the FEM-program. When applying a point force through displacement-controlled increments, post-buckling behaviour can be studied and a force-deflection curve can be plotted. For a force-controlled analysis it is not possible to study post-buckling behaviour, since the finite element software cannot find convergence when it increases the load above the maximum load carrying capacity of the beam.

6.5.3 Yield criterion

The finite element model relies on the von Mises yield criterion, where the equivalent stress is calculated as:

$$\sigma_{VM} = \sqrt{\frac{(\sigma_1-\sigma_2)^2+(\sigma_2-\sigma_3)^2+(\sigma_3-\sigma_1)^2}{2}}$$

$\sigma_{1,2,3}$ are the principal stresses, and yielding occurs when $\sigma_{VM} = f_y = 355MPa$.

6.5.4 Integration method

Full Newton-Raphson integration method as shown in Figure 6.15 was used, which is the standard method to solve nonlinear problems in ANSYS. Five integration points were used through the shell thickness in each element, which was considered enough.

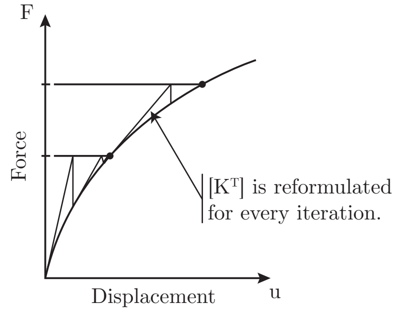

Figure 6.15: *Full Newton-Raphson integration method*

7 Results and discussion

7.1 Outline of result and discussion

Each load case is presented under its own section in the following order: end moments, point load, distributed load at mid web and finally distributed load with varying of point of load application. Each section is divided into two subsections: one for elastic buckling and load-carrying capacity and one for deformation and stress results.

Under each section a discussion follows since it would be difficult to refer to all the result graphs otherwise than where they are presented. In the last section a final discussion is made on the most crucial issues, aswell as a comparison to the design curve created by (Snijder et al., 2008).

7.1.1 Elastic critical bending moments and load-carrying capacity

The elastic critical bending moments and the ultimate load-carrying capacities for each beam and load case are extracted from the FE-analyses and presented in Appendix D. The reduction factor χ_{LT} is calculated from the ultimate bending resistance, M_{Rd}, and then plotted against beam slenderness, $\bar{\lambda}_{LT}$. These plots are combined with the existing buckling curves in Eurocode 3.

7.1.2 Deformation and stresses

It would be far too comprehensive to present graphs of stresses and deformation for each FE-analysis made in the parametric study. Therefore, only a few examples under each load case have been chosen to highlight certain observations and conclusions.

Deformation and stresses are plotted against applied load to be able to study their interdependance. The term "Max deformation" in the graphs mean the resultant deformation in x-, y- and z-axis combined. The stress levels are evaluated for three points in the beam, described in Figure 7.1. These three specific points were chosen since it was noted that yielding in the beam first occurred in any of these three points.

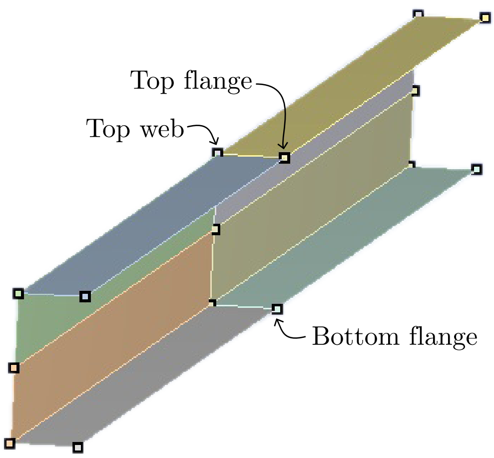

Figure 7.1: *Stress extracted from three result points at the beam mid section*

Finally the true scale deformation and stress levels from the final load step before failure of the beams from the FE-analyses are shown. The von-Mises stress criterion has been used as a tool to determine which parts of the beam that have reached yielding at failure, and these regions are shown with the darkest colour, while areas with lower stress levels are lighter.

7.2 Load case: Applied end moments

The load case with applied end moments was performed on all three cross-sections UPE100, UPE160 and UPE220 with slenderness values approximately between 0.6 and 1.7. The end moment load case is used as a reference case for the analyses since it does not involve load eccentricity. If the finite element model is correct then these results should be in agreement with the shape of the buckling curves found in Eurocode 3.

The first sections below describe the results from analyses performed with GMNIA-method 1, which uses an initial maximum geometric imperfection of the beam length divided by 150. Finally a comparison is made with a series of UPE160 beams with various lengths but now performed with GMNIA-method 2 (geometric imperfection are modelled using L/1000 and residual stresses are considered by applying initial stresses in each shell element).

7.2.1 Elastic critical buckling and load-carrying capacity

The ultimate load-carrying capacity from the FE-analysis are plotted against the buckling curves in Eurocode 3, see Figure 7.2. It was expected that due to the lack of load eccentricity, the results would be similar to that of a beam with an I-section. For the stockiest beams the results are along buckling curve b (third line from the top), however for the slender beams the reduction is above buckling curve a_0 (top line). A rolled I-section with h/b > 1.2 with slender flanges and web is approximated by buckling curve a, which is quite similar to the given results.

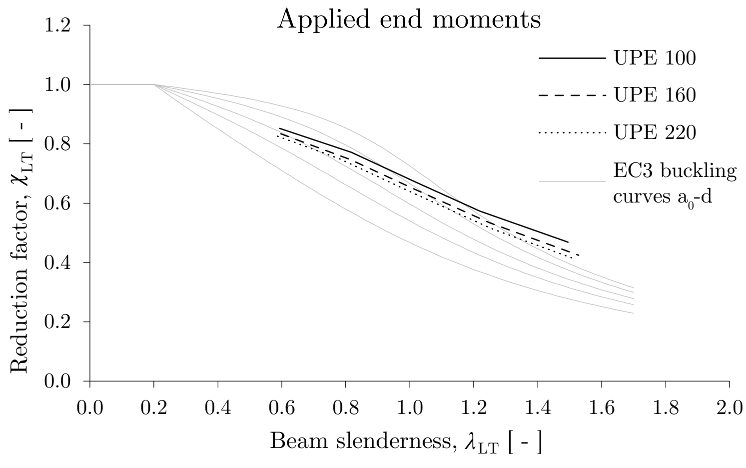

Figure 7.2: *Buckling curves from end moment loading.*

The stiff beam elements that are used to model fork supports, seem to give the beam an added, unintended stiffness also in the lateral direction. This can be noted by studying the three curves from UPE100, UPE160 and UPE220 in Figure 7.2. The smallest cross-section (UPE100) results in a curve with the highest reduction factor, and the largest cross-section (UPE220) results in a curve with the lowest reduction factor curve. A possible explanation for this is that since the stiff beam elements along the edges of the end of the beam are of the same width and thickness, the stiffening effect is greater the smaller the cross-section is. However, the difference in load-carrying capacity according to the buckling curves in Figure 7.2 between UPE100, UPE160 and UPE220 is quite small which was taken as a sign towards that the boundary conditions of a fork support were modeled in a satisfactory manner. The stocky beams seem to approach full plastic cross-section capacity and the slender beams seem to approach elastic buckling.

In Appendix D, the elastic critical bending moment calculated by the FE-analysis in the end moment series ($M_{cr,FEM}$) is compared to the theoretical value given by the 3-factor formula ($M_{cr,3ff}$). For stocky beams with $\bar{\lambda}_{LT} \sim 0.6$, the difference is about 5 % while for slender beams with $\bar{\lambda}_{LT} \sim 1.5$, the difference is smaller at around around 3 %. It seems that the boundary conditions were modelled in a satisfactory manner.

7.2.2 Stresses and deformation

The deformation patterns for the end moment load case follow expected behaviour. All beams deflect into shapes that are typical to what is expected for beams failing in lateral-torsional buckling, such as the one in Figure 7.3 below (deformations are magnified).

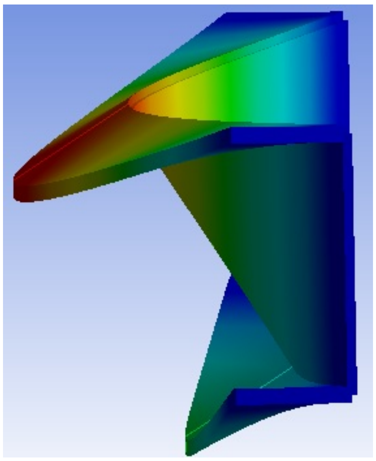

Figure 7.3: *Shape of elastic buckling for end moment load case*

Stresses and deformation are shown in Figure 7.4 for the shortest UPE220 beam. For the stocky beam with length 1400 mm the stresses increase linearly until close to failure. The deformation curve is also linear up to the point where the top web yields. The linearity is due to the small deformations which limits second order effects, and the fact that yielding does not occur until about 70 % of max load. The graph also shows that the stresses in the outer edge of the top flange remain low throughout the whole loading history.

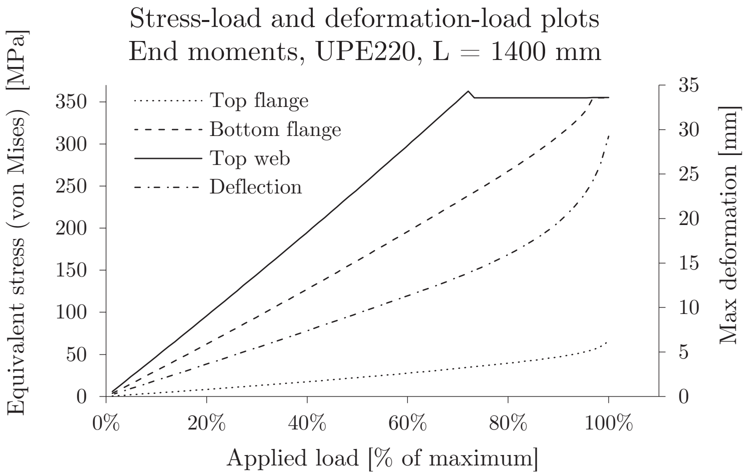

Figure 7.4: *Equivalent stress in probe points for UPE220 L1400 at failure.*

The stress pattern in Figure 7.5 show that there is yielding along the whole beam in the areas where the web and the flanges are connected. The entire bottom flange also yields at the beam mid section. The angle of twist at failure is only a few degrees and it is difficult to distinguish if the bottom flange has deformed laterally at all. Since the top flange deflects laterally, it also displays a minor axis bending pattern, which added to the major axis bending creates stresses close to zero at the outer edge of the top flange.

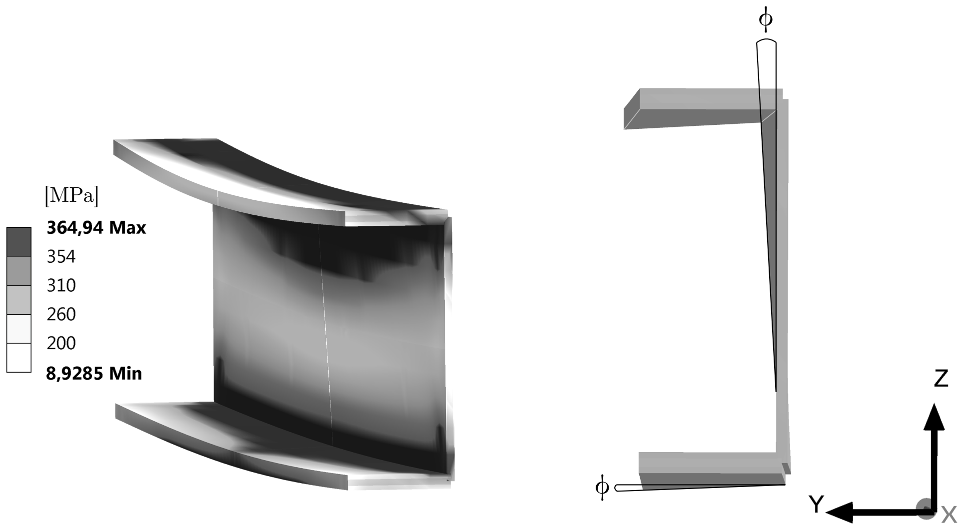

Figure 7.5: *Stresses and deformation for UPE220 L1400 at failure.*

The results for the beam with length 5500 mm, see Figure 7.6, are presented. Both stresses and deformation increase linearly up to about 35-40 % of max load, and the bottom flange yields first, at around 85 % of max load. The other two result points reach yielding shortly after that.

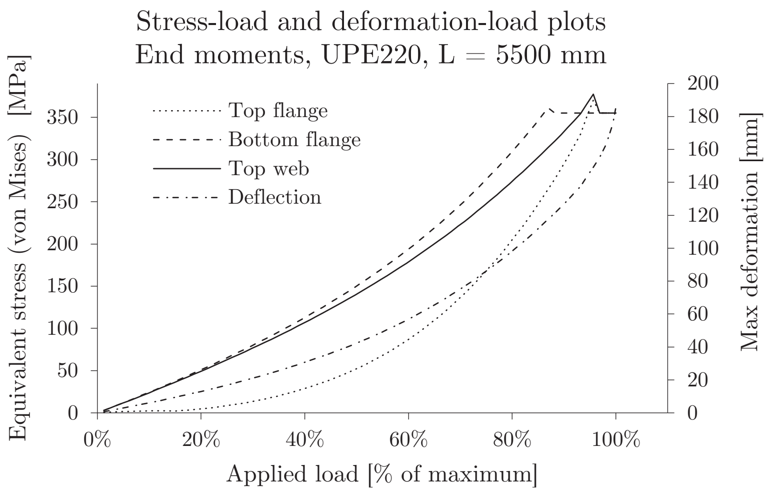

Figure 7.6: *Equivalent stress in probe points for UPE220 L5500*

The fact that all three result points reach yielding does not imply that the whole cross-section yields. The result points are the extremes, and the stress is in both compression and in tension, which means that in between them are areas with zero stress, as can be seen in the stress pattern at failure in Figure 7.7.

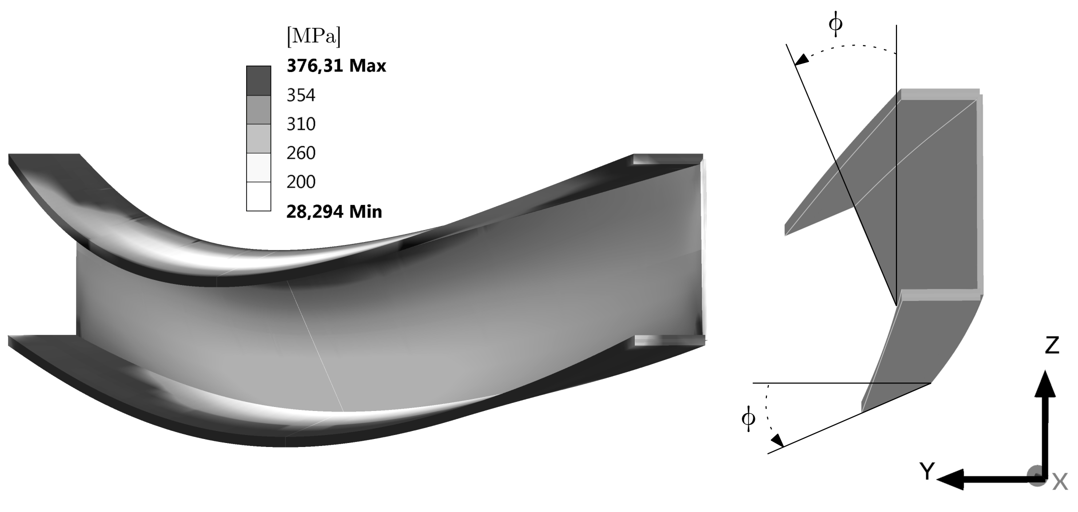

Figure 7.7: *Stresses and deformation for UPE220 L5500*

Unlike for stockier beams, the largest yielding zones are now located at the supports where the entire flanges yield a few decimeters from the beam ends. Also the bottom flange deflects laterally. When viewing the beam shape and stress levels at failure, one can draw the conclusion that minor axis bending is the defining action in the mid section, whereas major axis bending is so at the supports. At the supports the stress levels in the flanges are equal: the entire top flange is in compression and the entire bottom flange is in tension. For the middle section of the beam, and especially the top flange, the outer edge is in tension while the inner edge is in compression.

It can also be said that no significant difference in behaviour between the three studied cross-sections was noticed for the end moment load case.

7.2.3 Comparison of load-carrying capacity between GMNIA-methods

For the UPE160 series of beams, both GMNIA-methods were used in analysis. The results from the comparison between the two methods of simulating imperfections in the beams are shown in Appendix D. The obtained buckling curves are presented in Figure 7.8, and the difference in load-carrying capacity is distinct. Analyses with GMNIA-method 2 result in a buckling curve about two "Eurocode 3 buckling curves" higher than with GMNIA-method 1. The difference is largest at a beam slenderness of approximately $\bar{\lambda}_{LT}$ = 1.0, and decreases as the slenderness increases or decreases from this value. This conclusion is in line with what is written in Section 3.3, that initial imperfections has greatest effect on the load-carrying capacity at an intermediate beam slenderness.

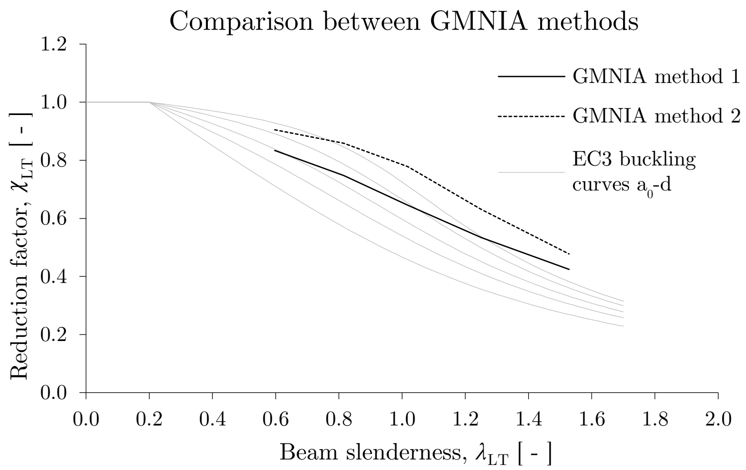

Figure 7.8: *Buckling curves from end moment loading.*

7.3 Load case: Point load

7.3.1 Elastic critical buckling and load-carrying capacity

The results are found in Appendix D. The elastic critical bending moment from the FE-analisis, $M_{cr,FEM}$, have a much lower value for the stocky beams than what is predicted by the 3-factor formula, $M_{cr,3ff}$. The difference for UPE160, L=1.6m, is 20.5 % ($\bar{\lambda}_{LT}$ = 0.64) and the beam with length 2200 mm ($\bar{\lambda}_{LT}$ = 0.81) is 10.8 %. The longest beam with length 6500 mm, however, only show 2.8 % difference. When looking at the buckling modes it seems that the linear buckling analysis displays a shape with local buckling for the shortest beams. In lateral-torsional buckling the beam cross-section should not deform but remain undistorted.

The buckling curve from the point load in the Finite Element analyses is shown in Figure 7.9. When studying the buckling curves it can be noted that the stockiest beam, UPE160 L=1600mm, resulted in a lower reduction factor than the second stockiest beam, UPE160 L=2200mm. The reason behind this unexpected behaviour is explained in Section 8.1.

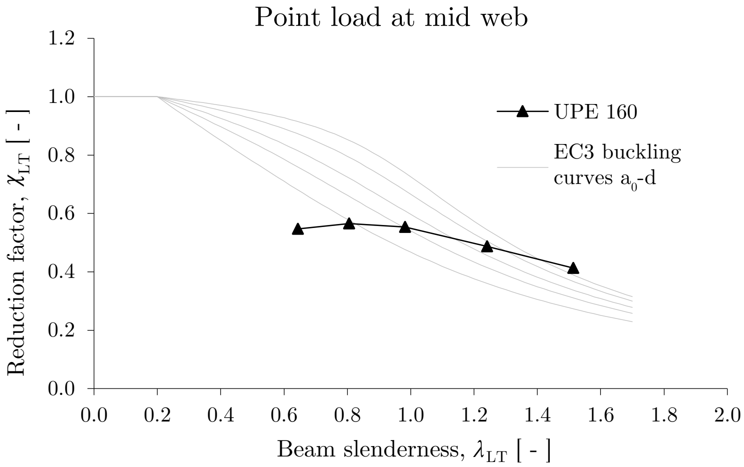

Figure 7.9: *Buckling curve from point load*

The stockiest beam has a slenderness of $\bar{\lambda}_{LT} = 0.64$ and a buckling reduction factor, χ_{LT}, of 0.547. Buckling curve d gives $\chi_{LT} = 0.683$ according to Eurocode 3. Hence the given results are 19.9 % lower than buckling curve d.

7.3.2 Stresses and deformation

Figure 7.10 show the stress distribution at failure for the shortest beam, with a length of 1600 mm. The ANSYS Finite Element results show that for the stockier beams, the concentrated point load makes the web deform and buckle locally, and the effect is more evident the stockier the beam is.

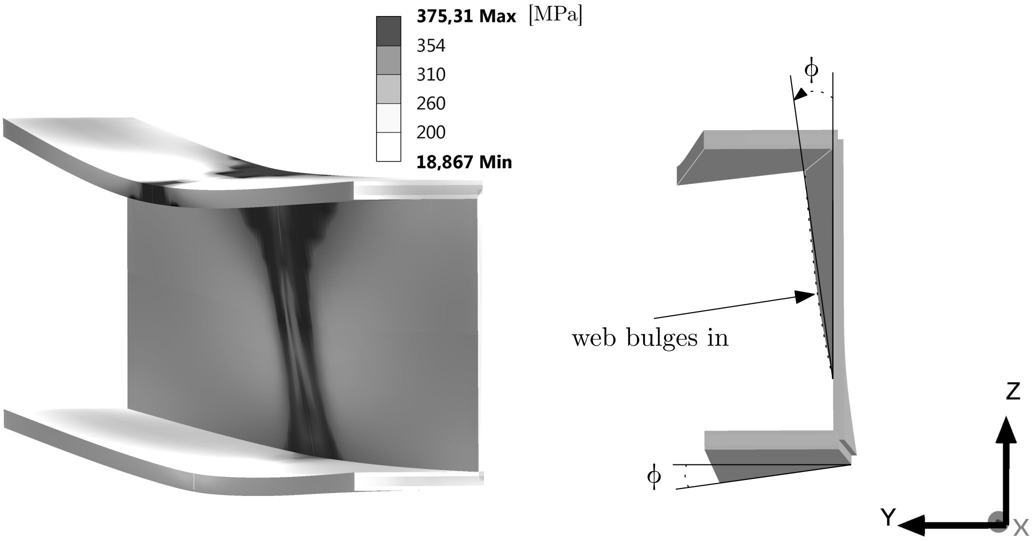

Figure 7.10: *Stresses and deformation for UPE160 L1600 at failure.*

It can be noticed from the stress pattern that major axis bending is the defining behaviour, since there is no lateral stress difference in the flanges. The mid beam cross-section yields almost entirely except for the bottom flange. The stresses are lower in large parts of the rest of the beam.

Compare the beam in Figure 7.10 with a slender beam in the end moment loading, as in Figure 7.11. In the point load case the bottom flange deflects in the opposite direction to the top flange. Hence the torsional effect of the load eccentricity is strong.

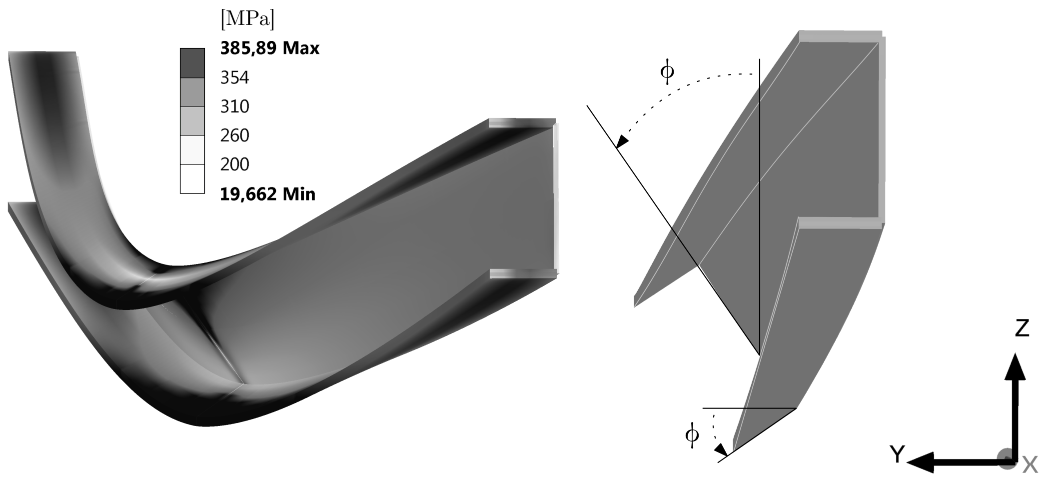

Figure 7.11: *Stresses and deformation for UPE160 L6500 at failure.*

Since the point load case is performed through a deflection-controlled load increment, the behaviour can be observed after maximum load-carrying capacity has been reached. The force-deflection curves are found in Appendix E and the stockiest beam (UPE160, L=1600mm) show a force-deflection curve that is almost bilinear with a steep angle up to the maximum load-carrying capacity and then a smaller angle on the slope after that. The explanation to the bi-linear behaviour, is that a stocky beam do not deflect or twist much so yielding of the entire cross-section occurs rapidly as second order effects are limited. The most slender beam has a load-deflection curve that has a "round" shape, which in this case at least partly depends on the fact that yielding in the cross-section occurs early. The yielding results in that the beam looses stiffness and deformations are magnified increasingly as load is added.

The force-deformation curves of beams with length 1600, 3000 and 6500 mm are normalized in Figure 7.12 by letting 100 % at the axes represent the point when maximum load-carrying capacity is reached.

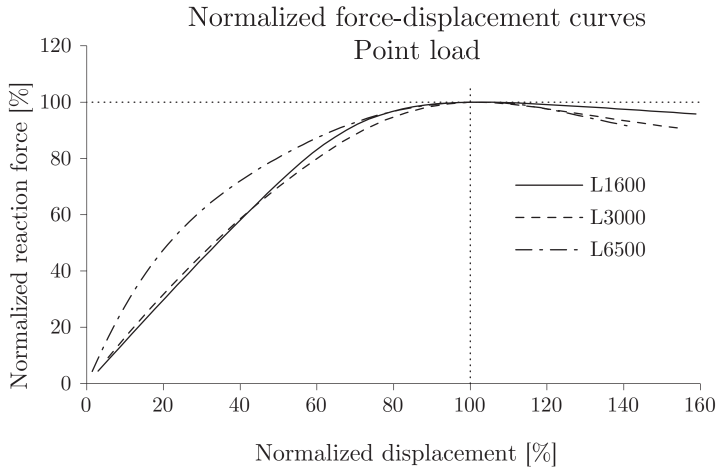

Figure 7.12: *Force-deflection curves from point load at mid web*

7.4 Load case: Linearly distributed load

7.4.1 Elastic critical buckling and load-carrying capacity

The elastic critical bending moments from the ANSYS FE-analyses follow the same patterns as in the case with end moment loading, which means that for more slender beams they differ only with a few percent to $M_{cr,3ff}$, given by the 3-factor formula. For the stockiest beams for each cross-section, however, the difference is 1.8 %, 4.9 %, and 9.1 % for UPE100, UPE160 and UPE220 respectively. The same effect was present for the end moment load case in that the stocky beams showed a greater spread in M_{cr} between the two methods, but the result did not differ significantly between the cross-sections.

When it comes to the ultimate load-carrying capacity, there is a similar outcome to notice. For the end moment load case, the buckling curves for the three cross-sections were very close, but that is not the case here. The discrepancy between the curves in Figure 7.13, representing the three cross-sections, is larger than what one could expect. At least for a double symmetric beam, the cross-section size should not effect the buckling curve. The explanation has to do with the normal stresses resulting from warping restrained torsion that comes from the load eccentricity. This effect is further discussed in Section 8.1 The UPE100 beam with length of 1200 mm has a slenderness of $\bar{\lambda}_{LT}$ = 0.64 and a buckling reduction factor, χ_{LT}, of 0.73. The UPE220 beam with length of 1600 mm has a slenderness of $\bar{\lambda}_{LT}$ = 0.62 and a buckling reduction factor, χ_{LT}, of 0.58. The UPE220 beam has a reduction factor approximately 20 % less than for the UPE100 beam.

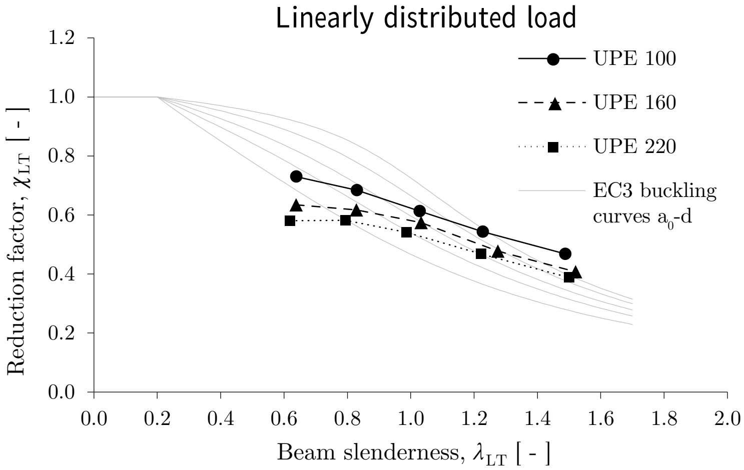

Figure 7.13: *Buckling curves from distributed load, varying cross-sections.*

7.4.2 Stresses and deformation

Figure 7.14 shows the final state of the UPE160 L1600 beam before failure. As in the case with point load, the flanges deflect in opposite directions. The areas with the lowest stress levels are located at the edges of the flanges and in the middle of the web height. Major axis bending of the flanges will create compression in the top flange and tension in the bottom flange. Minor axis bending is limited for such a short beam, but results in tension at the outer edge of the top flange and compression in the outer edge of the bottom flange (since it deflects and is bent the opposite direction of the top flange). The resulting stresses from major and minor axis bending therefore counteract each other in these areas. With the same reasoning, the opposite is true for the areas where flanges and web meet. Additionally, normal stresses from the warping restrained torsion should be added. The normal stress distribution from restrained warping is shown in Appendix C.

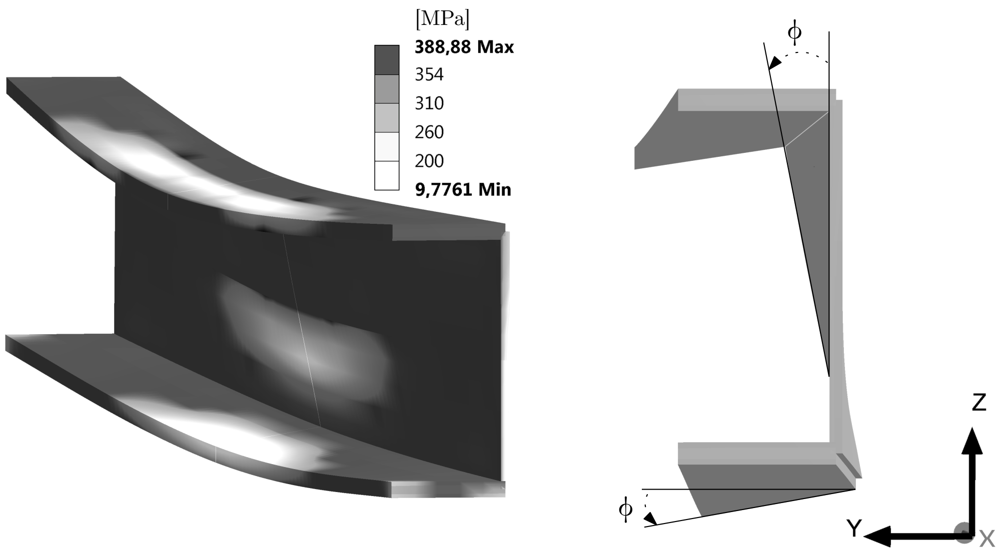

Figure 7.14: *Stresses and deformation for UPE160 L1600 at failure.*

Figure 7.15 show that the top of the web is where yielding starts. The deflection of the beam is linear up this point, which is at approximately 60 % of ultimate failure load. The load-deflection curve becomes more non-linear when the second yielding occurs in the top flange at about 80 % of max load. The stress in the outer part of the bottom flange stays at under 200 MPa until the very few last load steps when the stress approaches the yielding point and the beam deformation start to increase dramatically.

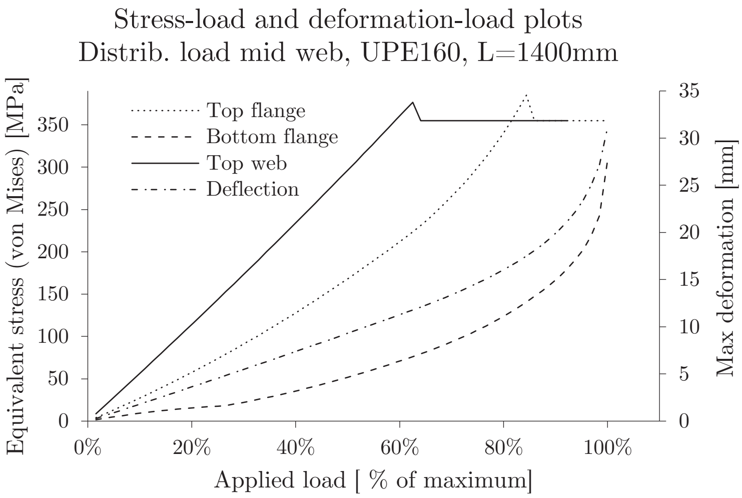

Figure 7.15: *Equivalent stress in probe points for UPE160 L1600*

The stress pattern for UPE160 L5500, shown in Figure 7.16, at failure is similar to the longest beam in the point load series, as seen in Figure 7.10, except that there is no stress concentration in the web at the mid section of the beam. The stress is high in both flanges near the supports and yielding is reached at the outer edges of the flanges.

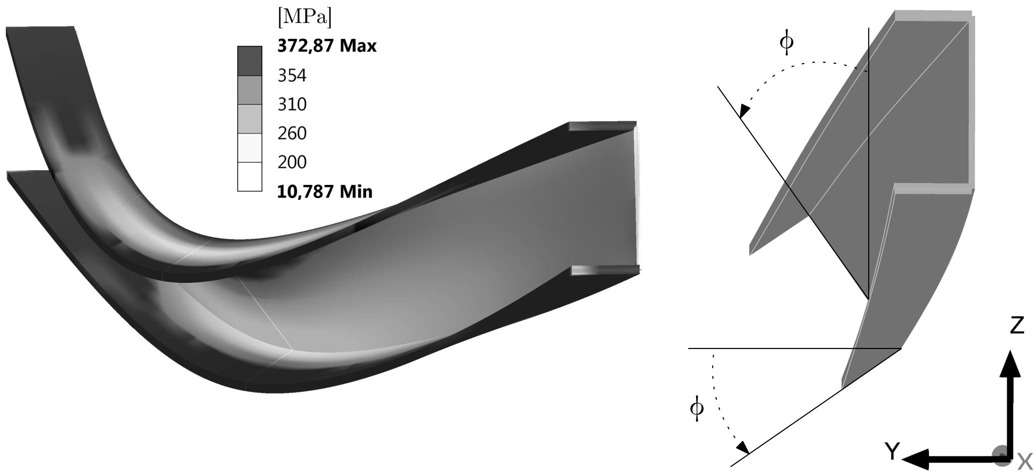

Figure 7.16: *Stresses and deformation for UPE160 L5500 at failure.*

The stress and deformation history for the most slender beam, see Figure 7.17, is more non-linear than for the stocky beam (L1600). Yielding first occurs at about 80 % of max load in the bottom flange, which is opposite behaviour compared to the previous stocky beam where the bottom flange had the lowest stress levels. Furthermore, the load-deflection plot deviates from linearity much earlier. The continually increasing deformation is a result of that the beam buckles in a linear elastic type buckling, since the deformation is non-linear even before the beam has yielded. It can also be noticed that the three displayed result points reach yielding close to each other.

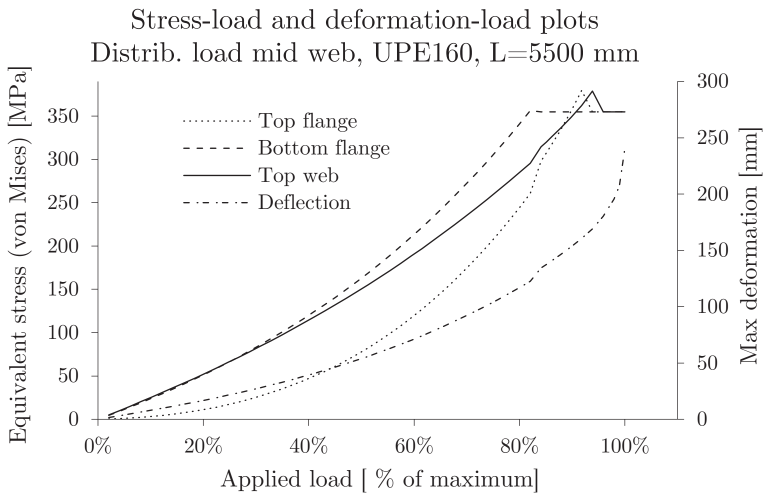

Figure 7.17: *Equivalent stress in probe points for UPE160 L5500*

7.5 Distributed load, varying point of load application

In the following section, a series of UPE160-beams are analysed with varying point of load application. The load is placed at the bottom of the web, middle of the web and top of the web. Note that the mid web series of beams is the same as presented in the results for the three cross-sections with distributed load.

7.5.1 Elastic critical buckling and load-carrying capacity

The elastic critical bending moments from ANSYS follow the same pattern as the other analyses with distributed load: for the stockiest beams the difference compared to the 3-factor formula is about 6 % and for the slender beams the difference is about 2 %. The results are found in Appendix D.

The buckling curves, as can be seen in Figure 7.18, show that the three cases (top web loading, mid web loading and bottom web loading) converge for slender beams, but diverge increasingly for stockier beams. The end moment loading series have been added for the UPE160-beam, to represent an imagined buckling curve for a channel beam loaded in its shear centre (since the end moment load case does not introduce torsional moment).

It is clear that without eccentricity (end moment load case), the beam reaches its highest capacity and after that bottom web loading, mid web loading and finally top web loading. This is also explanied through load eccentricity and warping restrained torsion in Section 8.1.

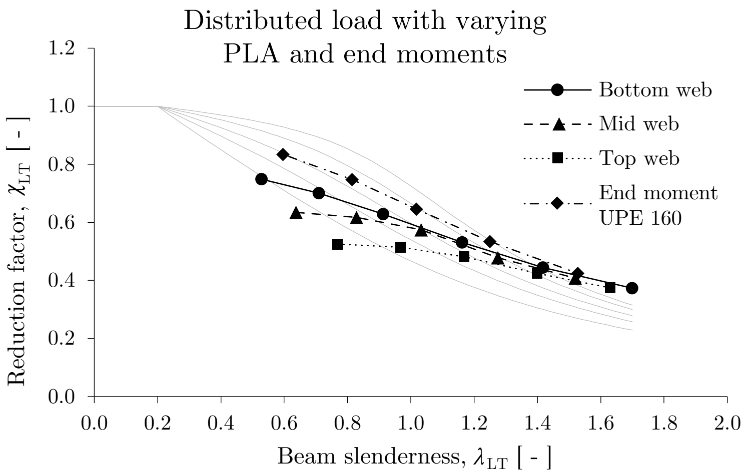

Figure 7.18: *Buckling curves from distributed load, varying PLA.*

Finally, the ultimate load-carrying capacity is compared between the three load cases for the same beam length in Table 7.1 below. For the stockiest beam with length 1400 mm, there is approximately 20 % higher capacity for lowering the point of load application (PLA) from top web to mid web or from mid web to bottom web. For the most slender beam with length 5500 mm, the difference is less, at about 9 %.

Table 7.1: *Load-carrying capacity for UPE160 beams depending on PLA*

Beam length (mm)	**Top web loading**	**Mid web loading**	**Bottom web loading**
1400	23.8	28.7	33.9
2000	23.3	27.9	31.7
2800	21.8	26.0	28.4
4000	19.2	21.6	24.0
5500	16.9	18.4	20.1

7.5.2 Stresses and deformation

Below are shown the final stress patterns for UPE160 length 2800 mm loaded at bottom web, mid web and top web respectively in Figures 7.19, 7.20 and 7.21. The angle of twist at failure increases as the load is moved from the bottom of the web to the top of the web. The angle is about twice as large for the top web loading compared to the bottom web loading, even though the beam with top web loading fail at a lower load than the the beam with bottom web loading.

It is noticed from the deformation pattern for the bottom flange, that for the bottom web loading, the bottom flange deflects in the same lateral direction as the top flange. When the beam is loaded at the mid web the bottom flange stays laterally undeflected but when loaded in the top, the flanges deflect in opposite directions as described in earlier load cases for stocky beams. This is expected, since the top web loading will increase the twisting moment due to load eccentricity more than the bottom web loading.

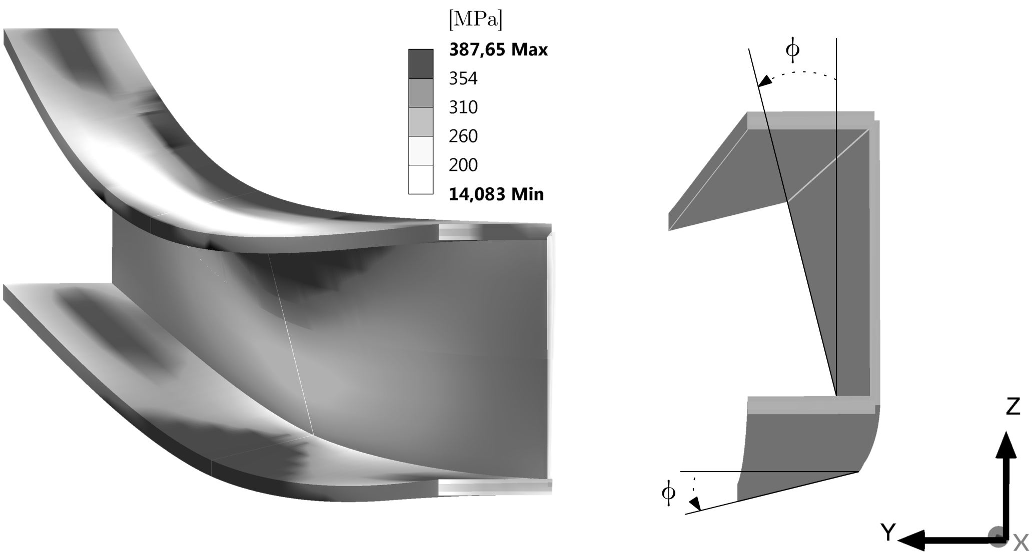

Figure 7.19: *Stresses and deformation for UPE160 L2800 at failure (bottom web loading).*

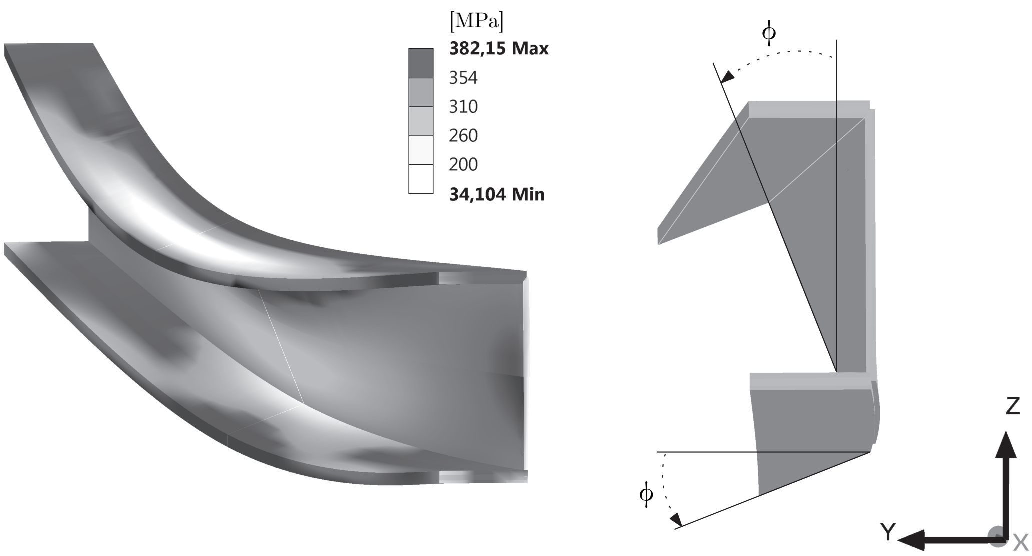

Figure 7.20: *Stresses and deformation for UPE160 L2800 at failure (mid web loading).*

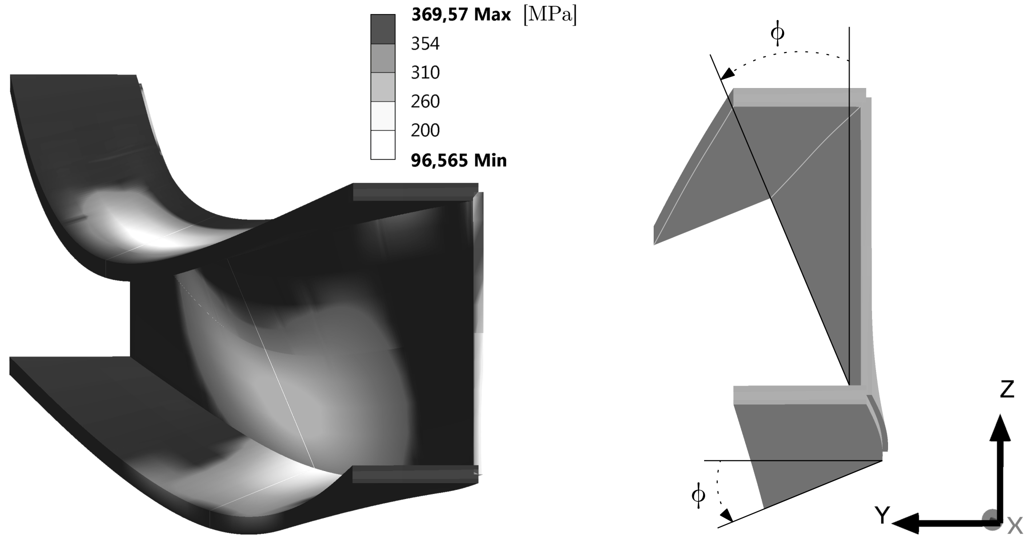

Figure 7.21: *Stresses and deformation for UPE160 L2800 at failure (top web loading).*

Stresses and deformation plotted against applied load for the three beams are shown in Figures 7.22, 7.23 and 7.24. For the bottom web loading, the behaviour of both deformation and stresses is mostly linear. The top web yields first at about 75 % and the load-stress curve is almost linear up to this point. The load-deformation curve also deviate from linearity at this load level.

When moving the load upwards from bottom web through mid web to top web, the outer edge of the bottom flange yields later and the outer edge of the top flange yields earlier. The top web yields first for all three cases at about 75 % of max load. When the load is located above the shear centre, it is more difficult to find a point where the beam behaviour changes from linear to nonlinear. The load-deformation curve start to deviate from linearity at 30 % of max load, and the increase in deformation is slightly less for the last few load steps than for the bottom web loading.

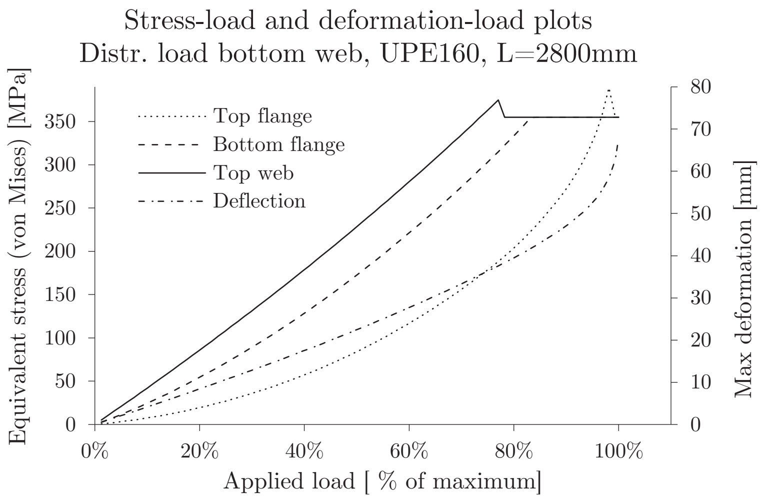

Figure 7.22: *Equivalent stress in probe points for UPE160 L2800, bottom web loading*

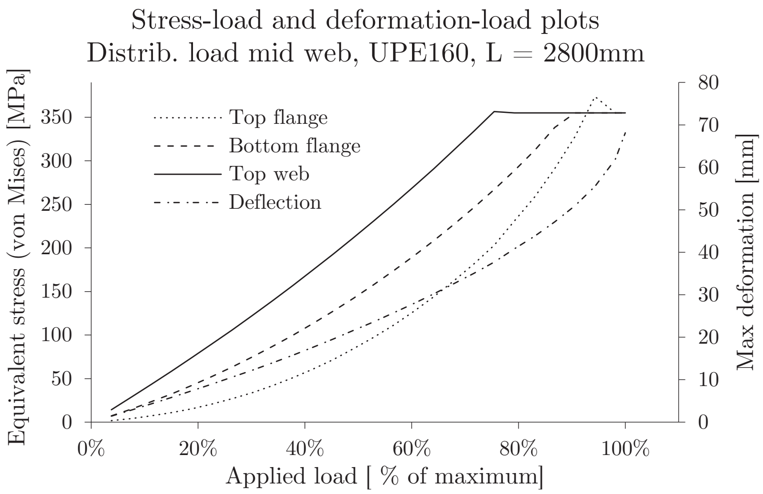

Figure 7.23: *Equivalent stress in probe points for UPE160 L2800, mid web loading*

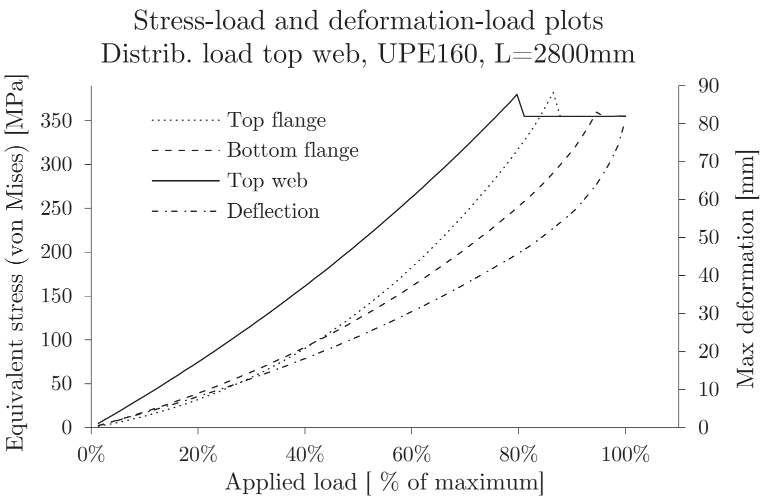

Figure 7.24: *Equivalent stress in probe points for UPE160 L2800, top web loading*

General conclusion from yielding patterns in result points

Table 7.2 shows the point of yielding for the outer edges of the top and bottom flange and the top part of the web. The top web result point reaches yielding first for all short beams regardless of point of load application for the disttributed load. In addition, the longer the beam is, yielding takes places at a greater load compared to the maximum applied load. However, for the outer edge of the bottom flange the opposite is true: for a longer and more slender beam, yielding will occur at a small load compared to the maximum value.

A fourth column has been added in the table to display "average yielding" of the three result points in the mid section of the beam. The result shows that beams with low slenderness have a higher post-yielding capacity than the more slender beams.

Table 7.2: *First yielding at result points*

	Beam length (mm)	Yielding starts at (% of max load) Top flange result point	Bottom flange result point	Top web result point	Average
Bottom web PLA	1400	86	98	56	80
	2000	96	91	65	84
	2800	99	85	75	86
	4000	96	81	85	88
	5500	94	80	90	88
	7500	90	80	95	88
Mid web PLA	1400	83	-	59	-
	2000	89	98	66	84
	2800	94	91	76	87
	4000	93	83	85	87
	5500	90	82	92	88
	7500	93	84	100	92
Top web PLA	1400	79	-	64	-
	2000	83	-	68	-
	2800	85	95	77	86
	4000	88	88	86	87
	5500	86	83	92	88

8 Discussion and analysis

8.1 The influence of warping stresses

It was generally observed from the results that when there is load eccentricity, beams with low slenderness failed for a load less than expected. The warping stresses will be investigated in order to explain this effect.

It is very difficult to analytically calculate the stresses in a second order plastic analysis. Therefore a first order elastic analysis is used, by studying the stress level in the outer edges of the flanges.

The stress from major axis bending is calculated as (here the full beam height h, rather than h_s, has been used):

$$\sigma_{x,My} = \frac{M_y}{I_y}\frac{h}{2} \tag{8.1}$$

Appendix C shows how to calculate the warping normal stress through Terrington's bi-moment:

$$\sigma_{x,\omega} = \frac{M_\omega}{M_{pl,\omega}}\omega_1 \tag{8.2}$$

If the elastic yield criterion is made so that

$$\sigma_{x,My} + \sigma_{x,\omega} = f_y \tag{8.3}$$

then an elastic first order yield criterion curve can be established. For the linearly distributed load cases in the FE-analyses it was noticed that for low slenderness values, the larger cross-sections resulted in a lower reduction factor χ than the smaller. Therefore the first order elastic yield curve is calculated for the the distributed load case for UPE100, UPE160 and UPE220 respectively. The result is shown in Figure 8.1.

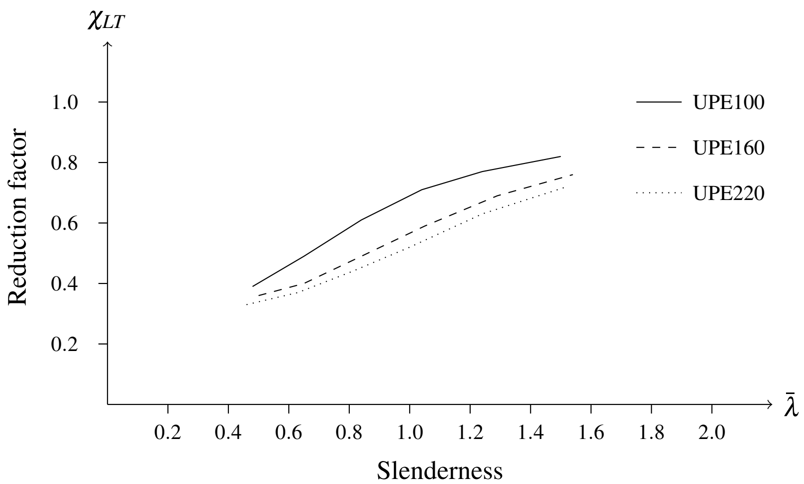

Figure 8.1: *First order elastic yield curve*

The first thing to notice is that the warping stresses are increasing with decreasing beam slenderness. For short beams a large part of the plastic cross-section capacity is utilized by warping normal stresses.

It can also be seen that the smaller cross-section UPE100 reaches yielding at a higher load level than the other two cross-sections. The first order elastic yield curve is not equivalent to the real non-linear behavior in a real beam, since it does not take into account increased second order twisting and deformation. For beams with low slenderness, however, the deformation and second order effects are small so it should be a fairly good indicator of the real effect. It is therefore reasonable to assume that the first order elastic yield lines confirm that when it comes to UPE-beams, the larger cross-sections have a lower load-carrying capacity at low slenderness values.

In Section 4.5.3, an example of the simplified design rule was made to show a buckling curve for linearly distributed load at mid web on a UPE160. Since this design rule implicitly takes warping normal stresses into account it would be interesting to add also the curves for UPE100 and UPE220, which is shown in Figure 8.2.

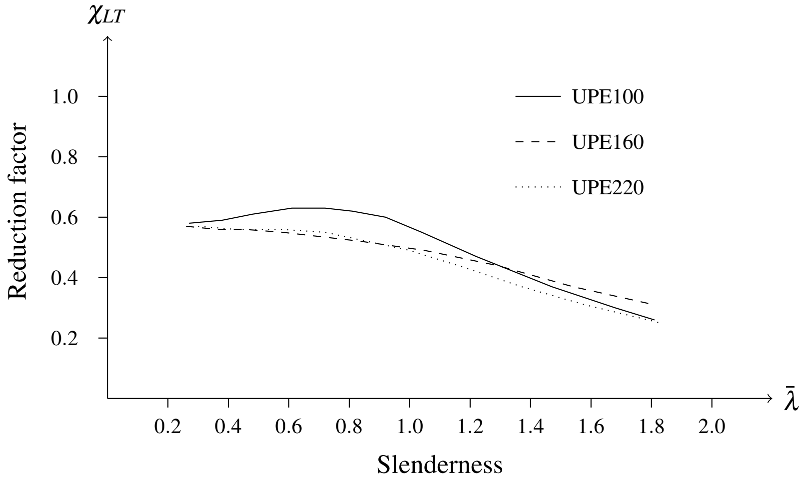

Figure 8.2: *Simplified design rule*

The simplified design rule seem to confirm that the smallest cross-section UPE100 should have a higher load-carrying capacity at low slenderness values than the other two cross-sections.

For the case of varying the point of load application the FE-results showed that for high slenderness, the three design curves converged but for low slenderness values the curves diverged increasingly. Also this can be explained through the influence of warping stresses.

For long beams the warping stresses are low, so the load-carrying capacity approaches elastic buckling regardless point of load applicatoin. For short beams, the warping stresses are much higher. From Terrington's formula for the bi-moment, it is clear that the (elastic) warping stresses are linearly depandant on the load eccentricity. Initially the eccentricity, e, is equal to the distance from the web centreline to the shear centre, e_{SC}, but as soon as the cross-section starts to twist, the distance changes. For the top web load application, the distance e increases and for the bottom web load application the load eccentricity actually decreases for increased twisting of the cross-section. The angle of twist at failure (and also the load eccentricity distance e) is significantly higher for the top web loading than the bottom web loading, thereby the normal stresses from restrained warping are also higher and the load-carrying capacity for top web loading is reduced.

8.2 Comparison with Snijder channel beam design curve

The simplified design rule does take normal stresses from warping implicitly into account, and it is therefore the most accurate design method. It is however not practical to use in design since it differs greatly from the existing procedure for lateral-torsional buckling in Eurocode 3. The fact that this buckling design curve depends on load case, boundary conditions and cross-section makes it impossible to establish one general design curve for all cases, which is preferred for simplicity.

The design curve by (Snijder et al., 2008) has therefore been chosen to serve as an example for comparison of the load-carrying capacity. There is no point comparing the end moment load case with channel beam design curves since it does not involve load eccentricity. The load-carrying capacity of the beams in Section 7.5 is plotted against the design curve proposed by (Snijder et al., 2008) in Figures 8.3 and 8.4.

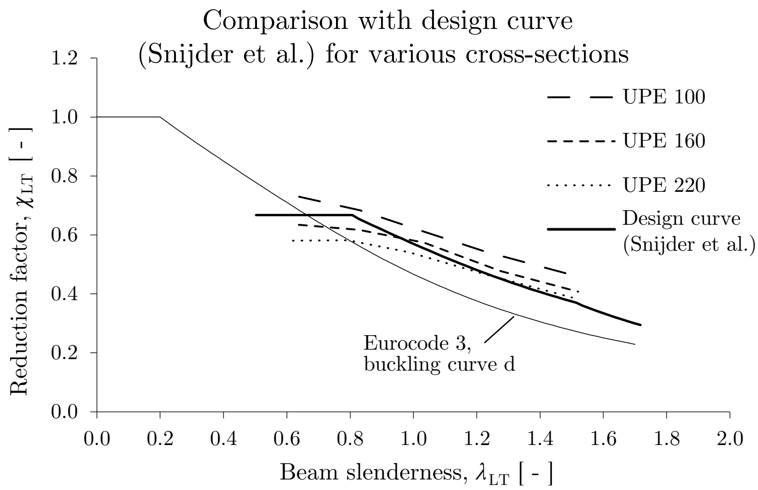

Figure 8.3: *Distributed load mid web, result comparison to Snijder et al. design curve*

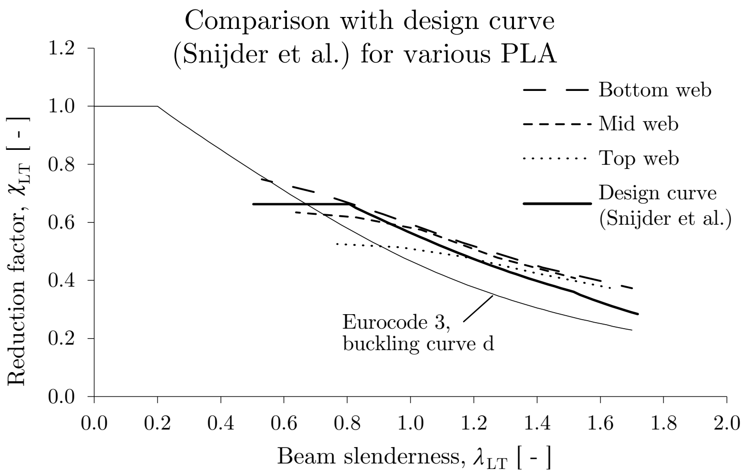

Figure 8.4: *Distributed load varying PLA, result comparison to Snijder et al. design curve*

In the study by (Snijder et al., 2008), an equivalent geometric imperfection of L/150 as well as L/1000 with residual stresses was used. The design curve is however based on the results from the second method of GMNIA. The results from this study are therefore not exactly equivalent. For the end moment load case, UPE160 L=2500mm ($\bar{\lambda}_{LT} = 1.03$), the difference between the two methods is 17 %. If one would assume that the difference in load-carrying capacity between the methods for other load cases is similar, then it seems the resulting buckling curves would end up "above" the proposed design curve.

Another explanation is found by the fact in the study by (Snijder et al., 2008), the beam studied were limited to the ratio of beam length divided by cross-section height between 15 and 40: $15 < L/h < 40$. For UPE160 the lower limit is at L=2400 mm, and the two shorter beams in this study are 1400 mm and 2000 mm long, which means they should not be compared to this design curve.

It seems that the effect of warping cannot be approximated through the beam slenderness. It might be that the length-height ratio L/h is more important to capture the load-carrying capacity reducing effect.

The shortest beams in the distributed load case at mid web were 1200 mm for UPE100, 1400 mm for UPE160 and 1600 mm for UPE220. The three beams have a very similar slenderness and are therefore comparable. The ratio L/h for the three cross-sections are 12 (UPE100), 8.75 (UPE160) and 7.27 (UPE220). This is interesting since the relation between the buckling curves for the low slenderness values in Figure 7.13 is very similar. UPE100 has a clearly higher buckling design curve than the other two, and the difference between UPE160 and UPE220 is not as large.

8.3 Structural engineering design considerations

It is obvious that the ordinary lateral-torsional buckling procedure in Eurocode 3, following buckling curve d for channel beams, is unconservative for beams with a low length-to-height ratio. The Snijder design curve seems to be a good way of taking the torsional effect into account, but it is only valid when L/h > 15. For shorter beams than that, perhaps the simplified design rule could be followed or extra caution be taken by reducing the reduction factor to 0.5. A clear proposal cannot be made here, since the studied beams were not in the slenderness range $\bar{\lambda}_{LT} < 0.6$.

8.4 Stress patterns

When comparing the stress pattern for the most slender and the stockiest beams in each load case series, it can be noticed that for the stocky beams the stress pattern differ clearly between the load cases whereas the slender beams show a similar stress pattern regardless of load case. The stocky beams for end moment, point load and distributed load case can be seen in Figures 7.4, 7.10 and 7.14 respectively. The slender beams for the same load cases are displayed in Figures 7.7, 7.11 and 7.16.

A probable explanation is that the more slender beams fail in a mode approaching elastic lateral-torsional buckling regardless of what type of load is applied, and a similar stress pattern is developed with the outer parts af the edges in tension and the top part of the web in compression. The stockier beams fail through yielding of almost the entire cross-section, but where the yielding areas are depend much more on the load case.

9 Conclusions

The most important conclusions from this master's thesis project are presented below:

- For stocky beams with eccentric loading ($\bar{\lambda}_{LT} \approx< 0.8$) the load-carrying capacity did not approach plastic strength. The bottom flange deflects laterally in the opposite direction to the top flange. The failure mode of these beams is related to the cross-section plastic capacity being reached from major axis bending and restrained warping effects combined.

- For eccentric loading the reduction factor χ increases when the cross-section size is smaller. The results also show that for beams with low slenderness the point of load application have a more significant effect than otherwise. Both of these observations can be explained through the effect of warping stresses.

- The Snijder channel beam design curve seems to be a good way of taking the torsional effect into account, but it does not claim to be valid for beams in the range L/h < 15. For these beams extra care should be taken, perhaps limiting the reduction factor χ to 0.5.

- Modelling the beams with residual stresses and a maximum initial imperfection of the beam length divided by 1000 results in a significantly higher capacity than if an equivalent geometric imperfection of L/150 is used. The difference is largest at $\bar{\lambda}_{LT}$=1.0 where the first method shows a 21 % higher load-carrying capacity for the end moment load case.

- Stress-deformation plots show that deformation is basically linear until yielding occurs for the stocky beams, but for slender beams deformation start to become unlinear at a much lower load. The behaviour of deformation and stress become more linear the stockier the beam is, and the lower below shear center the load is applied.

- For stocky beams ($\bar{\lambda}_{LT} \approx< 0.8$) yielding first occurs at the top of the web, but for slender beams the outer edge of the bottom flange yields first. Stocky beams have a much higher post-yielding capacity than slender beams.

References

Boissonnade, N. et al. (2006). *Rules for Member Stability in EN 1993-1-1: Background documentation and design guidelines*. ECCS European Convention for Constructional Steelwork.

Brown, D. (2016). "A Brief History of LTB". In: *New steel construction* 2, pp. 24–27.

Bureau, A. (2006). "NCCI: Elastic critical moment for lateral torsional buckling". In: *SN003a-EN-EU, Access Steel< project. access-steel. com/Content/Content. htm>[26.11. 06]*.

CEN (2005). *Eurocode 3: Design of Steel Structures. Part 1-1: General Rules and Rules for Buildings*. European Committee for Standardization. Brussels, Belgium.

DIN (1990). *DIN 18800-1:1990-11 Stahlbauten Bemessung und Konstruktion*. German Institute for Standardization.

Galambos, T. V. (1998). *Guide to stability design criteria for metal structures*. John Wiley & Sons.

Galambos, T. V. and A. E. Surovek (2008). *Structural stability of steel: concepts and applications for structural engineers*. John Wiley & Sons.

Hauksson, H. Þ. and J. B. Vilhjálmsson (2014). *Lateral-Torsional Buckling of Steel Beams with Open Cross Section*. Institutionen fÖr bygg- och miljÖteknik, Chalmers tekniska hÖgskola, no: 2014:28. GÖteborg, Sweden.

Höglund, T. (2006). "Att konstruera med stål, Läromedel för konstruktörer: Modul 6, Stabilitet för balkar och stänger". In:

Hoogenboom, P. (2003). *Theory of Elasticity: Exam Problems and Answers 1997-2003*. Delft University of Technology, Faculty of Civil Engineering, Geosciences, Mechanics, Materials, and Constructions, Section of Structural Mechanics.

Hughes, A. (2009). "Choice of lateral-torsional buckling curves-according to Eurocode 3 and the UK National Annex". In: *New steel construction* 17.1, pp. 32–34.

Kirby, P. and D. A. Nethercot (1979). *Design for structural stability*. Halsted Press.

Komzsik, L. (2014). *Applied calculus of variations for engineers*. CRC Press.

Lindner, J. and T. Glitsch (2004). "Vereinfachter Nachweis für I-und U-Träger–beansprucht durch doppelte Biegung und Torsion". In: *Stahlbau* 73.9, pp. 704–715.

López, A., D. J. Yong, and M. A. Serna (2006). "Lateral-torsional buckling of steel beams: A general expression for the moment gradient factor". In: *Proceedings of the International Colloquium on Stability and Ductility of Steel Structures*, pp. 6–8.

Lundh, H. (2000). *Grundläggande hållfasthetslära*. Institutionen för hållfasthetslära, Tekniska högsk.

Pettersson, O. (1971). "Knäckning". In: *Bulletines of Division of Structural Mechanics and Concrete Construction, Bulletin 24*.

Salmon, C. G., J. E. Johnson, and F. A. Malhas (2008). *STEEL STRUCTURES: DESIGN AND BEHAVIOUR (5th edition)*. Pearson.

Salvadori, M. G. (1955). "Lateral buckling of I-beams". In: *Transactions of the American Society of Civil Engineers* 120.1, pp. 1165–1177.

Samanta, A. and A. Kumar (2006). "Distortional buckling in monosymmetric I-beams". In: *Thin-walled structures* 44.1, pp. 51–56.

Schneider, W. (2006). "Stimulating equivalent geometric imperfections for the numerical buckling strength verification of axially compressed cylindrical steel shells". In: *Computational Mechanics* 37.6, pp. 530–536.

Seif, M. and B. W. Schafer (2010). “Local buckling of structural steel shapes”. In: *Journal of Constructional Steel Research* 66.10, pp. 1232–1247.

Serna, M. A. et al. (2006). “Equivalent uniform moment factors for lateral–torsional buckling of steel members”. In: *Journal of Constructional Steel Research* 62.6, pp. 566–580.

Simitses, G. J. and D. H. Hodges (2006). *Fundamentals of structural stability*. Burlington, USA: Butterworth-Heinemann.

Snijder, H. et al. (2008). “Design rules for lateral torsional buckling of channel sections subject to web loading”. In: *Stahlbau* 77.4, pp. 247–256.

Szalai, J. and F. Papp (2010). “On the theoretical background of the generalization of Ayrton–Perry type resistance formulas”. In: *Journal of Constructional Steel Research* 66.5, pp. 670–679.

Taras, A. and R. Greiner (2010). “New design curves for lateral–torsional bucklingÂ—Proposal based on a consistent derivation”. In: *Journal of Constructional Steel Research* 66.5, pp. 648–663.

Terrington, J. (1968). “Combined bending and torsion of beams and girders, Publication No. 31 (First Part)”. In: *British Construction Steelwork Association, London*.

Timoshenko, S. (1983). *History of strength of materials: with a brief account of the history of theory of elasticity and theory of structures*. Courier Corporation.

Trahair, N. S. (1993). *Flexural-torsional buckling of structures*. Vol. 6. CRC Press.

Trahair, N. (1998). “Multiple design curves for beam lateral buckling”. In: *Stability and ductility of steel structures, Pergamon*, pp. 13–26.

Yoo, C. H. and S. Lee (2011). *Stability of structures: principles and applications*. Elsevier.

Appendix A Cross-section geometry and material data

Cross-section geometry

Profile #	Dimensions for cross-sections: Total height (mm)	Height of web (mm)	Total width (mm)	Thickness of web (mm)	Thickness of flanges (mm)	Distance mid web to s.c. (mm)	Distance mid web to g.c. (mm)	Dimensions for FEM input: Height (mm)	Width (mm)	Area (mm)
UPE 100	100	85	55	4.5	7.5	22.4	17.28	92.5	52.75	1207.5
UPE 160	160	141	70	5.5	9.5	27.62	20.41	150.5	67.25	2105.5
UPE 220	220	196	85	6.5	12	33.21	24.2	208	81.75	3314

Cross-section constants

Profile #	I_y (mm^4)	I_z (mm^4)	I_t (mm^4)	I_w (mm^6)	W_{pl} (mm^3)	M_{pl} (kNm)
UPE 100	1.99E+06	3.74E+05	1.76E+04	5.68E+08	4.62E+04	16.41
UPE 160	8.81E+06	1.05E+06	4.68E+04	4.18E+09	1.27E+05	45.19
UPE 220	2.61E+07	2.43E+06	1.13E+05	1.84E+10	2.74E+05	97.39

Material parameters

Material	Yield strength (Pa)	Young's modulus (Pa)	Poissons's ratio (-)	Shear modulus (Pa)
Steel	3.55E+08	210E+09	0.3	81E+09

Variables for 3-factor-formula

Load case	C_1 (-)	C_2 (-)	C_3 (-)	k_z (-)	k_w (-)	z_j (mm)
Point load	1.35	0.59	0.411	1	1	0
Distributed load	1.12	0.45	0.525	1	1	0
End moments	1	1	1	1	1	0

Appendix B M_{cr} according to the 3-factor formula and χ_{LT} design calculation

The following example calculation is made for a 2000 mm long UPE160-beam with a uniformly distributed load. The load is acting vertically at the top of the web, in the centre of the top flange (point of load application). The calculation of elastic critical bending moment is based on "Rules for Member Stability in EN 1993-1-1, ECCS Technical Committee 8".

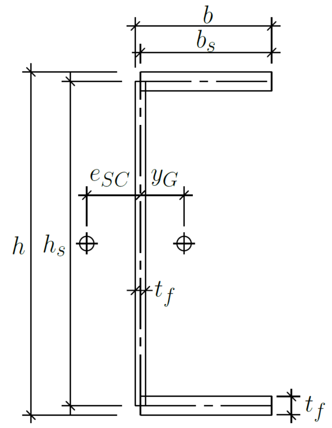

Geometry

Chosen profile (simplified cross-section) — UPE 160

Height — $h = 160\text{mm}$

Width — $b = 70\text{mm}$

Thickness, web — $t_w = 5.5\text{mm}$

Thickness, flanges — $t_f = 9.5\text{mm}$

FEM flange width — $b_s = b - \frac{t_w}{2} = 67.25 \cdot \text{mm}$

FEM web height — $h_s = h - t_f = 150.5 \cdot \text{mm}$

Beam length — $L = 2\text{m}$

Material

Young's modulus — $E = 210\text{GPa}$

Poisson's ratio — $\nu = 0.3$

Shear modulus — $G = \frac{E}{2 \cdot (1 + \nu)} = 80.77 \cdot \text{GPa}$

Partial safety factor, γ_{M1} — $\gamma_{M1} = 1.0$

Yield strength — $f_{yk} = 355\text{MPa}$

Geometric properties

Area, cross-section

$$A = t_w \cdot h_s + 2 \cdot (b_s \cdot t_f) = 2.11 \times 10^{-3} \text{m}^2$$

Vertical distance from the bottom of beam to the centre of gravity

$$z_G = \frac{1}{A}\left[b_s \cdot t_f \cdot \left(h_s - \frac{t_f}{2}\right) + h_s \cdot t_w \cdot \left(\frac{h_s}{2}\right) + b_s \cdot t_f \cdot \left(\frac{t_f}{2}\right)\right] = 75.25 \cdot \text{mm}$$

Horizontal distance from mid web to centre of gravity

$$y_G = \frac{1}{A}\left(2t_f \cdot b_s \cdot \frac{b_s}{2}\right) = 0.02\,\text{m}$$

Moment of inertia about the major axis (y-axis)

$$I_y = \frac{2 \cdot b_s \cdot t_f^3 + t_w \cdot h_s^3}{12} + 2 \cdot b_s \cdot t_f \cdot \left(\frac{h_s}{2}\right)^2 = 8.81 \times 10^6 \cdot \text{mm}^4$$

Moment of inertia about the minor axis (z-axis)

$$I_z = \frac{2 \cdot t_f \cdot b_s^3 + h_s \cdot t_w^3}{12} + 2 \cdot b_s \cdot t_f \cdot \left(\frac{b_s}{2} - y_G\right)^2 + h_s \cdot t_w \cdot y_G^2 = 1.05 \times 10^6 \cdot mm^4$$

Torsional moment of inertia

$$I_t = \frac{2 \cdot b_s \cdot t_f^3 + h_s \cdot t_w^3}{3} = 4.68 \times 10^4 \cdot mm^4$$

Warping moment of inertia (according to Hoogenbom)

$$I_w = \frac{t_f \cdot b_s^3 \cdot h_s^2}{12} \cdot \frac{3 \cdot b_s \cdot t_f + 2 \cdot h_s \cdot t_w}{6 \cdot b_s \cdot t_f + h_s \cdot t_w} = 4.18 \times 10^9 \cdot mm^6$$

Vertical distance from the shear centre to the bottom of the beam

$$z_{SC} = z_G = 75.25 \cdot mm$$

Vertical distance between the shear centre to the centre of gravity

$$z_s = z_{SC} - z_G = 0 \cdot mm$$

Horizontal distance from the shear centre to the centre of the web

$$e_{SC} = \frac{b_s^2 \cdot h_s^2 \cdot t_f}{4 \cdot I_y}$$

Elastic critical moment, according to (Boissonnade et al., 2006)

Factor, C_1: simply supported with a distrubuted load (C_1-factor accounts mainly for the moment distribution)

$$C_1 = 1.12$$

Factor, C_2: simply supported with a distrubuted load (C_2-factor accounts mainly for the point of load appl.)

$$C_2 = 0.45$$

Factor, C3: Channel shaped cross-section (C3-factor accounts for the cross-section asymmetry)

$$C_3 = 0.525$$

Factor, k_z: free to bend laterally at end supports

$$k_z = 1$$

Factor, k_z: free to warp at end supports

$$k_w = 1$$

Point of load application relative to the shear centre

$$z_g = 0.5 \cdot (h - t_f) = 75.25 \cdot mm$$

Degree of monosymmetry

$$z_j = 0mm$$

Elastic critical bending moment

$$M_{cr} = C_1 \cdot \frac{\pi^2 E \cdot I_z}{(k_z \cdot L)^2} \left[\sqrt{\left(\frac{k_z}{k_w}\right)^2 \cdot \frac{I_w}{I_z} + \frac{(k_z \cdot L)^2 \cdot G \cdot I_t}{\pi^2 \cdot E \cdot I_z} + (C_2 \cdot z_g - C_3 \cdot z_j)^2} - (C_2 \cdot z_g - C_3 \cdot z_j) \right]$$

$$M_{cr} = 46.344 \cdot kNm$$

Reduction factor, Eurocode EN-1993-1-1:2005

Ultimate design yield strength $f_{yd} = \frac{f_{yk}}{\gamma_{M1}} = 355 \cdot MPa$

Plastic section modulus $W_{pl.y} = \frac{t_w \cdot h_s^2}{4} + b_s \cdot h_s \cdot t_f = 1.27 \times 10^5 \cdot mm^3$

Plastic moment resistance $M_{pl.y} = W_{pl.y} \cdot f_{yk} = 45.19 \cdot kNm$

Beam slenderness $\lambda_{LT} = \sqrt{\frac{M_{pl.y}}{M_{cr}}} = 0.99$

Imperfection factor buckling curve d $\alpha_{LT} = 0.76$

Intermediate factor, ϕ_{LT} $\phi_{LT} = 0.5 \cdot \left[1 + \alpha_{LT} \cdot \left(\lambda_{LT} - 0.2\right) + \lambda_{LT}^2\right]$

Reduction factor for lateral-torsional buckling $\chi_{LT} = \frac{1}{\phi_{LT} + \sqrt{\phi_{LT}^2 - \lambda_{LT}^2}} = 0.47$

Design curve for channel beam according to (Snijder et al., 2008)

Beam slenderness $\lambda_M = \sqrt{\frac{M_{pl.y}}{M_{cr}}} = 0.99$

Torsional addition

$$\lambda_T = \begin{cases} \left(1 - \lambda_M\right) & \text{if} \quad 0.5 \le \lambda_M < 0.8 \\ \left(0.43 - 0.29 \cdot \lambda_M\right) & \text{if} \quad 0.8 \le \lambda_M < 1.5 \\ 0 & \text{if} \quad \lambda_M \ge 1.5 \end{cases}$$

Beam slenderness (torsional effects added) $\lambda_{MT} = \lambda_M + \lambda_T = 1.13$

Imperfection factor buckling curve a $\alpha_{LT} = 0.21$

Intermediate factor, ϕ_{LT} $\phi_{LT} = 0.5 \cdot \left[1 + \alpha_{LT} \cdot \left(\lambda_{MT} - 0.2\right) + \lambda_{MT}^2\right] = 1.24$

Reduction factor for lateral-torsional buckling $\chi_{LT.Snijder} = \frac{1}{\phi_{LT} + \sqrt{\phi_{LT}^2 - \lambda_{MT}^2}} = 0.57$

Appendix C Bi-moment and simplified design rule calculation

Terrington's applied bi-moment

In Section 2.7.2, the equation for bi-moment was explained shortly:

$$M_\omega = -EI_w \varphi''(x)$$

The first order angle of twist, φ, can be decided from tables where the torsional differential equation has been solved for different load cases and boundary conditions. Such tables can be found in (Terrington, 1968). For a beam with fork supports, and subjected to a distributed torsional load, the angle of twist can be described as:

$$\varphi(x) = \frac{qe_{SC}a^2}{GI_t}\left[\frac{L^2}{2a}\left(\frac{x}{L} - \frac{x^2}{L^2}\right) + cosh\left(\frac{x}{a}\right) - tanh\left(\frac{L}{2a}\right)sinh\left(\frac{x}{a}\right) - 1\right]$$

where $a = \sqrt{\dfrac{EI_w}{GI_t}}$, q = applied distributed load and e_{SC} is the load eccentricity. By deriving the former equation:

$$\varphi'(x) = \frac{qe_{SC}a^2}{GI_t}\left[\frac{L^2}{2a}\left(\frac{1}{L} - \frac{2x}{L^2}\right) + \frac{1}{a}sinh\left(\frac{x}{a}\right) - \frac{1}{a}tanh\left(\frac{L}{2a}\right)cosh\left(\frac{x}{a}\right)\right]$$

The equation is derived yet again:

$$\varphi''(x) = \frac{qe_{SC}a^2}{GI_t}\left[\frac{L^2}{2a}\left(-\frac{2}{L^2}\right) + \frac{1}{a^2}cosh\left(\frac{x}{a}\right) - \frac{1}{a^2}tanh\left(\frac{L}{2a}\right)sinh\left(\frac{x}{a}\right)\right]$$

Simplifying:

$$\varphi''(x) = \frac{qe_{SC}}{GI_t}\left[-1 + cosh\left(\frac{x}{a}\right) - tanh\left(\frac{L}{2a}\right)sinh\left(\frac{x}{a}\right)\right]$$

The mid part of beam has the highest load effect, therefore $x = \dfrac{L}{2}$ is inserted:

$$\varphi''(x = L/2) = \frac{qe_{SC}}{GI_t}\left[-1 + cosh\left(\frac{L}{2a}\right) - tanh\left(\frac{L}{2a}\right)sinh\left(\frac{L}{2a}\right)\right]$$

The bi-moment can now be expressed:

$$M_\omega = -EI_w\frac{qe_{SC}}{GI_t}\left[-1 + cosh\left(\frac{L}{2a}\right) - tanh\left(\frac{L}{2a}\right)sinh\left(\frac{L}{2a}\right)\right]$$

Warping normal stresses

For a channel section the sectorial coordinate is described by

$$\omega_i = -z_i(y_i + e_{SC})$$

For this specific case, the zero point for the y-coordinate is located at the web centreline. The sectorial coordinates at the four corner points are therefore:

$$\omega_1 = \frac{h_s(-b_s + e_{SC})}{2}$$

$$\omega_2 = \frac{h_s e_{SC}}{2}$$

$$\omega_3 = -\frac{h_s e_{SC}}{2}$$

$$\omega_4 = -\frac{h_s(-b_s + e_{SC})}{2}$$

The resulting stress is then:

$$\sigma_{x,\omega} = \frac{M_\omega}{I_w}\omega$$

Figure C.1 shows the location of the sectorial coordinates ω_{1-4}. The warping normal stress distribution will also have the same shape, since it is dependant linearly on ω.

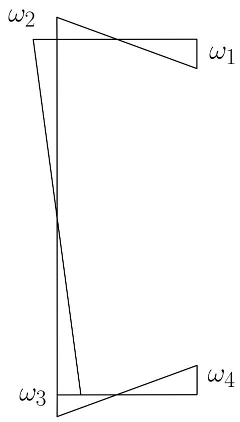

Figure C.1: *Plastic warping capacity*

Plastic warping capacity $M_{pl,\omega}$

The simplified design rule in Section 4.5.3 requires the plastic warping capacity to be known. The resulting moment from warping normal stresses around the horizontal symmetry line must be zero:

$$M_{pl,\omega,sl} = 0 = F_1\frac{h_s}{2} - F_2\frac{h_s}{2} - F_3\frac{h_s}{4}$$

$$F_1 = (b_s - b_{pl})t_f f_y$$

$$F_2 = b_{pl}t_f f_y$$

$$F_3 = \frac{h_s t_w f_y}{2}$$

The resulting forces are shown in Figure C.2.

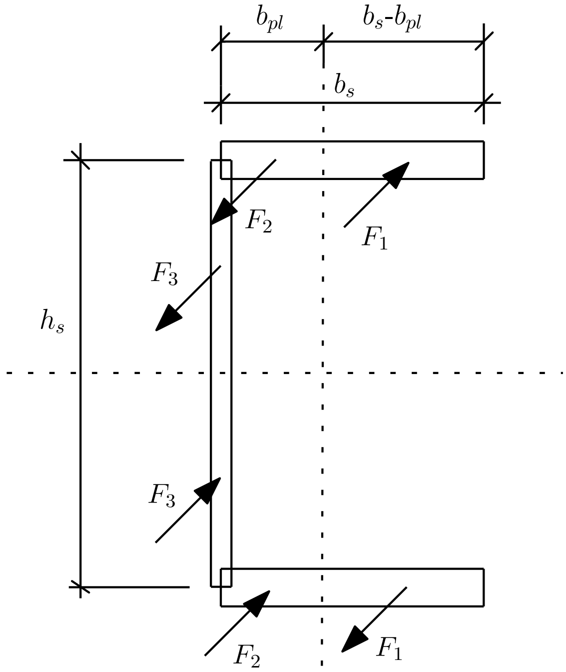

Figure C.2: *Plastic warping capacity*

By inserting the expressions for F_1, F_2 and F_3 in the former equation, the length b_{pl} can be decided:

$$b_{pl} = b_s\left(\frac{1}{2} - \frac{h_s tw}{8b_s t_f}\right)$$

The bending moment in the flanges are then multiplied with the distance to the horizontal symmetry line, and the bending moment in the web is multiplied with the distance to the vertical plastic line (b_{pl}):

$$M_{pl,\omega} = 2\frac{F_1(b_s - b_{pl})}{2}\frac{h_s}{2} + \frac{F_2 b_{pl}}{2} + \frac{2F_3 h_s}{2}b_{pl}$$

Simplified rule design calculation

The beam studied here has the same properties and load case as the one in Appendix B (UPE160 with length 2000mm and distributed load applied at the top of the web). χ_{LT} is calculated from buckling curve a however. Known properties are:

$$M_{pl,\omega}\text{= 0.89 kNm}^2$$

$$M_{pl,y}\text{= 45.19 kNm}$$

$$\chi_{LT} = 0.67$$

$$\lambda_{LT} = 0.99$$

$$M_{cr} = 46.34 \text{ kNm}$$

The simplified design rule requires trial and error calculation with an initial guess on the applied design load q since M, k_ω, α and M_ω depend on it. The load is iterated until:

$$\frac{M}{\chi_{LT} M_{pl,y}} + k_w \alpha \frac{M_\omega}{M_{pl,\omega}} \leq 1.0$$

This leads to a design load of $M = 17.2$ kNm. By changing the length of the beam and repeat the procedure a design curve can be established, which is shown in Figure 4.15

Appendix D FE-results for load carrying capacity

Applied end moments with method 1 (equivalent geometric imperfection L/150)

Profile	Length	Slender-ness, λ_{LT} [1]	Elastic critical buckling moment, 3-f-f	Ansys FEM-results: Elastic critical buckling moment	Ansys FEM-results: Bending moment capacity	Reduction factor χ_{LT}	Slenderness $\lambda_{LT,FEM}$ [2]	Difference in M_{cr} [3]
	(mm)	(-)	(kNm)	(kNm)	(kNm)	(-)	(-)	(%)
UPE 100	1000	0.604	44.91	42.72	14.00	0.853	0.620	4.9%
UPE 100	1600	0.829	23.89	23.24	12.68	0.773	0.840	2.7%
UPE 100	2300	1.028	15.54	15.14	11.04	0.673	1.041	2.6%
UPE 100	3200	1.233	10.80	10.50	9.42	0.574	1.250	2.8%
UPE 100	4700	1.509	7.20	6.98	7.70	0.469	1.534	3.1%
UPE 160	1200	0.609	121.76	115.77	37.72	0.835	0.625	4.9%
UPE 160	1800	0.828	65.88	63.93	33.81	0.748	0.841	3.0%
UPE 160	2500	1.032	42.44	41.38	29.20	0.646	1.045	2.5%
UPE 160	3500	1.265	28.25	27.57	24.15	0.534	1.280	2.4%
UPE 160	5000	1.544	18.96	18.50	19.20	0.425	1.563	2.5%
UPE 220	1400	0.599	271.57	256.95	80.50	0.827	0.616	5.4%
UPE 220	2000	0.782	153.60	147.90	73.00	0.750	0.811	3.7%
UPE 220	2800	0.998	94.99	92.10	62.40	0.641	1.028	3.0%
UPE 220	4000	1.255	60.31	58.62	50.10	0.514	1.289	2.8%
UPE 220	5500	1.513	41.67	40.54	40.25	0.413	1.550	2.7%

Applied end moments with method 2 (residual stresses and geometric imperfection L/1000)

Profile #	Length	Slender-ness, λ_{LT}	Elastic critical buckling moment, 3-f-f	Ansys FEM-results: Elastic critical buckling moment	Ansys FEM-results: Bending moment capacity	Reduction factor χ_{LT}	Slenderness $\lambda_{LT,FEM}$ [2]	Difference in M_{cr}
	(mm)	(-)	(kNm)	(kNm)	(kNm)	(-)	(-)	(%)
UPE 160	1200	0.597	121.76	115.77	40.94	0.906	0.625	4.9%
UPE 160	1800	0.815	65.88	63.93	38.87	0.860	0.841	3.0%
UPE 160	2500	1.108	42.44	41.38	35.20	0.779	1.045	2.5%
UPE 160	3500	1.250	28.25	27.57	28.53	0.631	1.280	2.4%
UPE 160	5000	1.528	18.96	18.50	21.60	0.478	1.563	2.5%

[1] Calculated from the 3-factor formula, $\lambda_{LT} = \sqrt{(M_{pl} / M_{cr})}$

[2] Calculated from FEM-results, $\lambda_{LT,FEM} = \sqrt{(M_{pl} / M_{cr,FEM})}$

Applied point load

Profile #	Length	Slenderness, λ_{LT}	Elastic critical buckling moment, 3-f-f	Ansys FEM-results: Elastic critical buckling load	Ansys FEM-results: Elastic critical buckling moment[1]	Ansys FEM-results: Max. load	Ansys FEM-results: Bending moment capacity[2]	Reduction factor χ_{LT}	Slenderness, $\lambda_{LT,FEM}$	Difference in M_{cr}[3]
	(mm)	(-)	(kNm)	(kN)	(kNm)	(kN)	(kNm)	(-)	(-)	(%)
UPE 160	1600	0.655	105.42	209.55	83.82	61.88	24.75	0.548	0.734	20.5%
UPE 160	2200	0.818	67.60	109.68	60.32	46.49	25.57	0.566	0.866	10.8%
UPE 160	3000	0.994	45.75	57.97	43.48	33.40	25.05	0.554	1.020	5.0%
UPE 160	4500	1.254	28.73	24.81	27.91	19.58	22.03	0.488	1.272	2.8%
UPE 160	6500	1.528	19.35	11.63	18.90	11.49	18.67	0.413	1.546	2.4%

[1] The elastic critical bending moment is calculated from the elastic critical buckling force ($M_{cr} = F_{cr} \cdot L/4$)

[2] The bending moment load carrying capacity is calculated from the max applied load ($M_{Rd} = F_{Rd} \cdot L/4$)

Distributed load applied at mid web.

				Ansys FEM-results						
Profile #	Length	Slenderness, λ_{LT}	Elastic critical buckling moment, 3-f-f	Elastic critical buckling load	Elastic critical buckling moment[1]	Max. load	Bending moment capacity[2]	Reduction factor χ_{LT}	Slenderness, $\lambda_{LT,FEM}$	Difference in M_{cr}[3]
	(mm)	(-)	(kNm)	(kN/m)	(kNm)	(kN/m)	(kNm)	(-)	(-)	(%)
UPE 100	1200	0.649	38.91	212.32	38.22	66.60	11.99	0.731	0.655	1.8%
UPE 100	1800	0.842	23.17	56.56	22.91	27.72	11.23	0.684	0.846	1.1%
UPE 100	2600	1.040	15.17	17.71	14.96	11.92	10.07	0.614	1.047	1.3%
UPE 100	3600	1.240	10.66	6.45	10.45	5.51	8.92	0.544	1.253	2.0%
UPE 100	5200	1.503	7.27	2.08	7.04	2.28	7.69	0.469	1.527	3.1%
UPE 160	1400	0.650	106.94	415.26	101.74	117.12	28.69	0.635	0.666	4.9%
UPE 160	2000	0.842	63.74	125.03	62.52	55.82	27.91	0.618	0.850	1.9%
UPE 160	2800	1.046	41.27	41.57	40.74	26.50	25.97	0.575	1.053	1.3%
UPE 160	4000	1.290	27.17	13.47	26.93	10.80	21.60	0.478	1.295	0.9%
UPE 160	5500	1.535	19.17	4.97	18.80	4.88	18.43	0.408	1.551	1.9%
UPE 220	1600	0.632	243.99	693.16	221.81	177.00	56.64	0.582	0.663	9.1%
UPE 220	2200	0.808	149.29	236.40	143.02	93.75	56.72	0.582	0.825	4.2%
UPE 220	3000	1.002	97.05	84.12	94.64	46.90	52.76	0.542	1.014	2.5%
UPE 220	4200	1.236	63.71	28.34	62.49	20.70	45.64	0.469	1.248	1.9%
UPE 220	6000	1.516	42.36	9.23	41.54	8.40	37.80	0.388	1.531	1.9%

[1] The elastic critical bending moment is calculated from the elastic critical buckling force ($M_{cr} = q_{cr} \cdot L^2 /8$)

[2] The bending moment load carrying capacity is calculated from the max applied load ($M_{Rd} = q_{Rd} \cdot L^2 /8$)

[3] The difference (expressed in %) between elastic critical moment according to FEM and the 3-factor-formula

Distributed load applied at bottom web.

Profile	Length	Slenderness, λ_{LT}	Elastic critical buckling moment, 3-f-f	Ansys FEM-results: Elastic critical buckling force	Ansys FEM-results: Elastic critical buckling moment[1]	Ansys FEM-results: Max. load	Ansys FEM-results: Bending moment capacity[2]	Reduction factor χ_{LT}	Slenderness, $\lambda_{LT,FEM}$	Difference in M_{cr}[3]
	(mm)	(-)	(kNm)	(kN/m)	(kNm)	(kN/m)	(kNm)	(-)	(-)	(%)
UPE 160	1400	0.536	157.13	599.00	146.76	138.17	33.85	0.749	0.555	6.6%
UPE 160	2000	0.718	87.67	171.18	85.59	63.36	31.68	0.701	0.727	2.4%
UPE 160	2800	0.922	53.14	53.63	52.56	28.98	28.40	0.628	0.927	1.1%
UPE 160	4000	1.173	32.82	16.25	32.49	12.00	24.00	0.531	1.179	1.0%
UPE 160	5500	1.430	22.09	5.75	21.75	5.31	20.08	0.444	1.441	1.6%
UPE 160	7500	1.714	15.37	2.14	15.02	2.40	16.88	0.373	1.734	2.3%

Distributed load applied at top web.

Profile	Length	Slenderness, λ_{LT}	Elastic critical buckling moment, 3-factor-formula	Ansys FEM-results: Elastic critical buckling force	Ansys FEM-results: Elastic critical buckling moment[1]	Ansys FEM-results: Max. load	Ansys FEM-results: Bending moment capacity[2]	Reduction factor		Difference in M_{cr}[3]
	(mm)	(-)	(kNm)	(kN/m)	(kNm)	(kN/m)	(kNm)	χ_{LT}		(%)
UPE 160	1400	0.788	72.78	278.92	68.34	96.99	23.76	0.526	0.813	6.1%
UPE 160	2000	0.987	46.34	89.40	44.70	46.50	23.25	0.514	1.005	3.5%
UPE 160	2800	1.187	32.05	31.87	31.23	22.20	21.76	0.481	1.203	2.6%
UPE 160	4000	1.417	22.49	10.99	21.98	9.60	19.20	0.425	1.434	2.3%
UPE 160	5500	1.648	16.63	4.29	16.22	4.48	16.92	0.374	1.669	2.5%

[1] The elastic critical bending moment is calculated from the elastic critical buckling force ($M_{cr} = q_{cr} \cdot L^2 / 8$)

[2] The bending moment load carrying capacity is calculated from the max applied load ($M_{Rd} = q_{Rd} \cdot L^2 / 8$)

Appendix E Load-deflection curves for point load

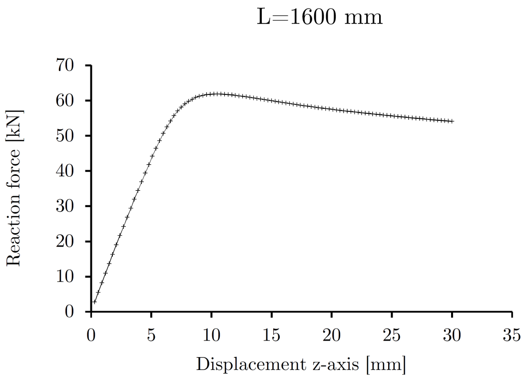

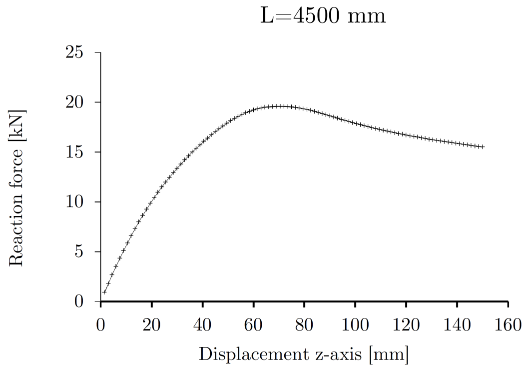

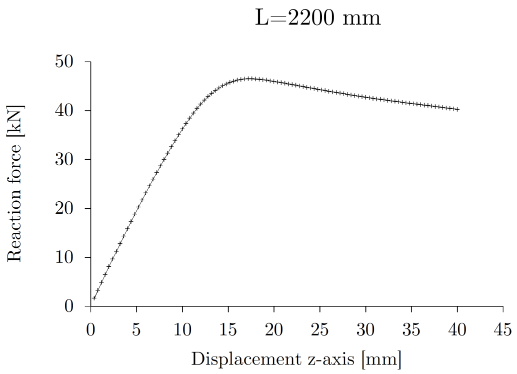

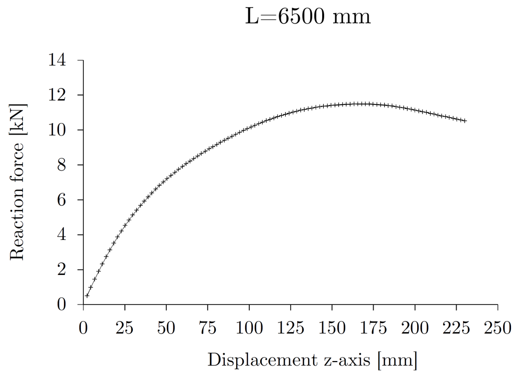

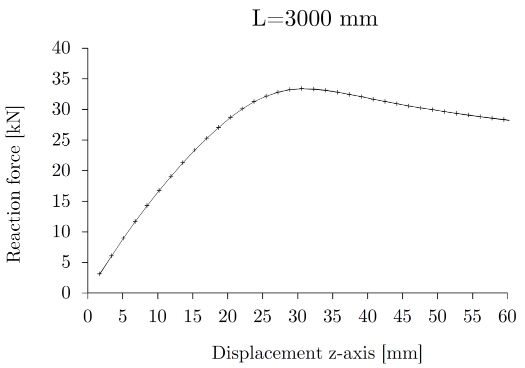

Appendix F Ansys code for applying residual stresses

```
/com ————————————————————————————————————————————
/com,  START
/com ————————————————————————————————————————————

!Input arguments
L=ARG1  !mm
NumDiv_B=ARG2  !-
NumDiv_H=ARG3  !-
B=ARG4  !mm
H=ARG5  !mm
fy=ARG6/1000000  !Pa
tf=ARG7  !mm
tw=ARG8  !mm

ee=1 !how many mm from ends of elements

amax=0.15*fy
bmax=-0.075*fy
cmax=0.15*fy
dmax=(-2*(amax+bmax)*B*tf/(H*tw)-cmax)

!Calculate element lengths
ElemLength_B=B/NumDiv_B
ElemLength_H=H/(NumDiv_H*2)

!WEB
*dim,f,array,NumDiv_H
*DO,i,1,NumDiv_H
        ii=NumDiv_H*2+1-i

        starti=(i-1)*ElemLength_H+ee
        stopi=i*ElemLength_H-ee
        startii=(ii-1)*ElemLength_H+ee
        stopii=ii*ElemLength_H-ee

        esel,s,cent,z,starti,stopi
        esel,a,cent,z,startii,stopii
        f(i)=cmax+(dmax-cmax)/(0.5*H)*(2*i-1)*ElemLength_H/2
        inistate,define,all,,,,f(i)
        !THINK ABOUT THE DIRECTIONS, ONE CAN CHANGE THE POS.
        OF f(i), LIKE 0,0,f(i) AND ALSO CHANGE THE SIGNS FOR
        amax,bmax,cmax,dmax
*ENDDO
```

```
!BOTH FLANGES
*dim,g,array,NumDiv_B
*DO,j,1,NumDiv_B

        startj=(j-1)*ElemLength_B+1
        stopj=j*ElemLength_B-1
        esel,s,cent,y,startj,stopj

        g(j)=amax+(bmax-amax)/B*(2*j-1)*ElemLength_B/2
        inistate,define,all,,,,g(j),0
        !THINK ABOUT THE DIRECTIONS, ONE CAN CHANGE THE POS.
        OF g(j), LIKE 0,0,g(j) AND ALSO CHANGE THE SIGNS FOR
        amax,bmax,cmax,dmax
*ENDDO

esel,all

/com ------------------------------------------------------------------
/com,   END
/com ------------------------------------------------------------------

!       elist
!       *status,f
```

Appendix G Ansys code for applying geometric imperfection

```
/prep7
length=ARG1

max_imp_factor=(length/150)
/com,%max_imp_factor%

upgeom,max_imp_factor,,,'%_wb_userfiles_dir(1)%buckledshape',rst,
/solu
```